TÉCNICO LISBOA

Development of a sensor for performance studies of the CFM56-3 engine

José Pedro Marinho Amorim Lopes

Thesis to obtain the Master of Science Degree in

Mechanical Engineering

Supervisors: Prof. João Eduardo de Barros Teixeira Borges
Eng. António Miguel de Abreu Ribeiro Henriques

Examination Committee

Chairperson: Prof. Carlos Frederico Neves Bettencourt da Silva
Supervisor: Prof. João Eduardo de Barros Teixeira Borges
Member of the Committee: Prof. André Calado Marta

November 2017

Para a minha avó, Maria Augusta Lopes Dias.

Acknowledgments

I would like to start by thanking TAP Maintenance & Engineering for the opportunity of doing this thesis in collaboration with them, more specifically to Chief Engineer António Ferreira.

To my supervisors, Professor Teixeira Borges and Engineer Miguel Henriques, for their guidance, availability, and belief in my capabilities.

To my friends and family, who were with me during this journey, especially to Marta Bruxelas, to my amazing uncles and to my study partners João Marques, Letícia Carvalho, Guilherme Sousa, Carlos Izidoro, Vicente Salgueiro and José Dias.

To all the staff that I worked with from TAP Maintenance & Engineering, engineers and technicians, thank you for all the help and hospitality. A special word to my two internship colleagues, Francisco Baptista and Tatiane Recrude.

Finally, the most important acknowledgement goes to my parents. Thank you for all your help, support and patience, through this master degree and this thesis. Without you this would not have been possible.

Resumo

O compressor de alta pressão é um dos principais focos quando se realiza manuntenção a um motor turbofan. Para estudar a performance deste componente é fundamental conhecer os valores de temperatura e pressão à sua entrada e saída. No contexto desta tese, foi desenvolvido e produzido um sensor capaz de medir estas variáveis para o motor CFM56-3, concretamente para a secção 25 que se posiciona antes do compressor de alta pressão. Com estes dados, e utilizando o software Gasturb™ cálculos de performance foram efectuados conduzindo a dois estudos.

O primeiro estudo é relacionado com a influência da folga do topo das pás na performance do compressor de alta pressão. O seu efeito em quatro parâmetros de performance, eficiência do compressor, razão de pressões, eficiência politrópica e caudal mássico corrigido, foi analisado. Para apresentar estes resultados recorreu-se à folga das pás adimensional. Estes apresentaram curvas com uma tendência incorrecta, levando à conclusão de que para estudar esta variável, uma abordagem que inclua mais elementos do compressor é necessária.

O segundo estudo, consistiu em analisar a influência de utilizar um sensor como o mencionado previamente, nos cálculos de performance de um compressor de alta pressão. O criador do Gasturb™ Joachim Kurzke e a CFM recomendam soluções alternativas para quando os valores da secção 25 não são conhecidos. Estas soluções são comparadas com os resultados obtidos com o sensor, calculando as quatro variáveis mencionadas acima e avaliando as suas diferenças. Os resultados conduziram a uma desconfiança em relação à correlação da CFM e suportam a necessidade de desenvolvimento de sensores semelhantes ao desenvolvido nesta tese.

Palavras-chave: Motor turbofan, Compressor de alta pressão, Sensor de temperatura, Sensor de pressão, Folga de topo da pá, Gasturb™

Abstract

The high pressure compressor is one of the main focus when performing maintenance to a turbofan engine. To study the performance of this component, it is important to know the temperature and pressure values at its entrance and exit. For this thesis, a sensor capable of measuring these variables for the CFM56-3 engine was developed and produced for station 25, the one before the high pressure compressor. With this data and using the Gasturb™ software, performance calculations were done which led to two studies.

The first study is related to the blade tip clearance influence on the performance of the high pressure compressor. Its effect on four performance parameters was analysed, the overall compressor efficiency, the pressure ratio, the polytropic efficiency and the corrected mass flow. To present the results the dimensionless tip clearance was used. The results obtained were erroneous, which led to the conclusion that to study this variable an approach which includes more variables of the compressor is necessary.

The second study performed, analysed the influence of having a sensor as the one previously mentioned, on the performance calculations of the high pressure compressor. The developer of Gasturb™ Joachim Kurzke, and CFM suggest alternative solutions when the thermodynamic values at station 25 are not measured. These solutions are compared with the results obtained using the sensor, by calculating the four variables aforementioned and evaluating their differences. The results led to some suspicion on the accuracy of the CFM correlation and support the development of similar sensors to properly study the high pressure compressor.

Keywords: Turbofan engine, High pressure compressor, Temperature sensor, pressure sensor, Blade tip clearance, Gasturb™

Contents

List of Tables

List of Figures

Nomenclature

Greek symbols

δ	Standard pressure coefficient
η^*	Polytropic efficiency
η_c	Overall compressor efficiency
γ	Heat capacity ratio
τ	Tip clearance-chord ratio
θ	Standard temperature coefficient

Roman symbols

c	Blade chord
C_{DS}	Coefficient of secondary drag
C_L	Coefficient of lift
c_p	Specific heat capacity at constant pressure
d	Dimensionless tip clearance
H_b	Blade Height
$\dot{m}$	Mass flow rate
$\dot{m}_{corrected}$	Corrected mass flow rate
N_1	Velocity of the low pressure spool
N_2	Velocity of the high pressure spool
p	Pressure
T	Temperature
t	Blade tip clearance
v	Velocity of the gas

Subscripts

0	Total condition
01	Total condition at entry
02	Total condition at exit
17	Station of the secondary flow of the engine, after the fan
2	Station of entry of the engine
25	Station after the booster and before the HPC
3	Station after the HPC and before the combustion chamber
4	Station after the combustion chamber and before the HPT
45	Station after the HPT and before the LPT
54	Station after the LPT
HPC	High pressure compressor
HPT	High pressure turbine
LPT	Low pressure turbine
s	Static condition
st	Standard condition

List of Acronyms

3D	Three Dimensional
ACC	Active Clearance Control
CAD	Computer-Aided Design
CDP	Compressor Discharge Pressure
CFD	Computational Fluid Dynamics
CNC	Computer Numerical Control
CTR	Correlation Test Report
EASA	European Aviation Safety Agency
EGT	Exhaust Gas Temperature
FAA	Federal Aviation Administration
FADEC	Full Authority Digital Engine Control
HD	Hot Day conditions
HPC	High Pressure Compressor
HPT	High Pressure Turbine
HSG	High Speed Grinding
IATA	International Air Transport Association
LPC	Low Pressure Compressor
LPT	Low Pressure Turbine
MBTA	Model Based Test Analysis
MRO	Maintenance, Repair and Overhaul

NATO North Atlantic Treaty Organization

OAT Outside Air Temperature

TAP ME TAP Maintenance & Engineering

TAP Transportes Aéreos Portugueses

TIG Tungsten Inert Gas

TSFC Thrust Specific Fuel Consumption

Chapter 1

Introduction

1.1 Overview

The turbofan engine is a type of gas turbine engines widely used for aircraft propulsion, developed in the fifties. This engine has three important advantages compared to other gas turbine engines, more specifically, to its predecessor, the jet engine. The turbofan engine develops much higher take-off thrust, it is much more fuel efficient, for subsonic flow, and it reduces considerably the noise produced. In the past decades, air transport became part of everyday life and therefore the demand in number and efficiency of airplanes increased quite significantly. This led to a massive increase on the requirement for turbofan engines, being the most commonly used on commercial flights today [1].

Due to the risk involved in flying and to its intense operating conditions, maintenance is a very important part of the life of an aircraft. Commonly an airplane is subjected to several maintenance procedures during its life. The aircraft maintenance costs are quite considerable, representing 10% to 15% of an airline's operating expenses. Engines are one of the three main areas of maintenance of a commercial aircraft, the other two being airframe and components. The one with higher costs will often be the engine maintenance [2]. According to a study from the International Air Transport Association (IATA) in 2015, engine maintenance costs represent 40% of the direct maintenance cost. The total maintenance, repair and overhaul (MRO) market was calculated to be worth 62.1 billion dollars in 2015 [3].

Transportes Aéreos Portugueses (TAP) is the main Portuguese airline, founded in 1945. It has a maintenance department, TAP Maintenance and Engineering (TAP ME), focused on performing maintenance to the main areas of an aircraft, currently having 70 years of experience in this field [4]. This thesis was developed in collaboration with TAP ME's facility in Lisbon, where the focus is the maintenance of turbofan engines.

1.2 Motivation

Minimizing the maintenance costs of aircraft engines has become a key issue for airline companies. In order to implement a proper maintenance, it is necessary to understand how each component of the engine is performing. Then it is possible to relate this performance to the maintenance procedures performed and, consequently, enhance them, which leads to a reduction of time and costs.

To study the performance of an engine, maintenance centers use test beds to measure their thermodynamic data, simulating flight conditions. This is possible by placing sensors on different stations of the engine, commonly known as the instrumentation of an engine. A proper instrumentation is essential for a useful performance study, since more knowledge on each component of the engine becomes available. To understand the conditions of each component separately, thermodynamic measurements between the components are required.

During the maintenance of an aircraft engine many components of the engines are worked on, however, there is a lot of focus on the high pressure compressor (HPC), one of the most important components of a turbofan engine. It is responsible for the substantial raise of the pressure of the supplied air to the combustion chamber. The HPC is considered one of the three components with the most influence on the thrust specific fuel consumption (TSFC), an important variable which represents the fuel efficiency of turbofan engines. A study presented by the North Atlantic Treaty Organization (NATO), states that a 1% increase in the efficiency of this component will decrease the TSFC by 0.7% [5]. This decrease is quite considerable, and therefore improving the HPC performance will have a noticeable effect on the engine's performance and operational cost. This topic is discussed in more detail on section 2.3.

This study was focused on one of the most intervened engines in TAP ME, the CFM56-3. This engine is one of the most used worldwide, serving the Boeing 737 - 300/400/500 aircrafts [6]. In TAP ME's test bed, this engine does not have an adequate instrumentation for the HPC, which is a substantial limitation for a performance study of this component. Thus, it is essential to produce an adequate sensor for this station of the CFM56-3. This study describes the development of a sensor that could give more detailed information on the HPC performance. With this information the maintenance procedures performed on the HPC by TAP ME can be improved, which will ultimately lead to cost and time savings for TAP ME.

1.3 Objective

The main objective of this thesis is the study of the performance of a particular turbofan engine, the CFM56-3. To achieve this, it is necessary to calculate the efficiency of one of the main components of the engine, the HPC. Thus, it is important to know the values of temperatures and pressures, before and after the HPC. Unfortunately, the sensor that TAP ME owns to obtain data from station 25, the station before the HPC, is easily broken and is currently not working. Therefore, it is necessary to introduce a new sensor. The first objective of this thesis was to conclude the development and the subsequent production of a sensor capable of measuring the temperature and pressure at station 25. The new sensors' design was inspired on the original one, although being completely developed in TAP ME.

Subsequently, this sensor was tested to check whether it was working properly.

This sensor will allow many different studies. For this thesis, two of those studies were selected. The first study was focused on using the sensor to start a series of performance studies that will help TAP ME diagnose how the maintenance procedures implemented affect the performance of the HPC. To achieve this, two aspects are important. First, to be capable of doing the HPC performance calculations, Gasturb™ a specialized software to study the performance of gas turbines, was used. To use this software it is essential to have a model of the engine in study. TAP ME has a model engine for the CFM56-3, and it was designed for the design point of the CFM56-3B2 rate of the engine. However, the engines available to analyse in this thesis were tested on the CFM56-3C rate, which operates on a different operating point than the CFM56-3B2 rate. As it is further explained in Chapter 5, to use Gasturb™ properly it is essential to extrapolate the CFM56-3B2 model to the conditions of the CFM56-3C rate, which became one of the objectives of this thesis.

The following objective is to understand properly the influence of the variables that TAP ME controls on its maintenance procedures on the HPC performance. Due to the data available from TAP ME, the experimental part of the study was only focused on one of these variables, the blade tip clearance. The tip clearance is defined as the gap between a blade and the casing around it. It is essential to avoid rubbing and damage to the blades, but greater tip clearances will lead to decreased efficiencies. A literature review of studies related to experimental studies of the blade tip clearance is required to understand how experimental work with this variable should be carried on.

The second study was focused on understanding the relevance of the sensor produced in the calculation of the HPC efficiency. The goal is to quantify how different the results would be with and without the use of the sensor. In the future, this study will help decide if similar sensors are worth developing for other engines. For example, TAP ME's test bed only has a sensor capable of measuring temperature on station 25 for the CFM56-5B engine, and this study could help understand if it is worth it to add a pressure measurement to this sensor.

To know the temperature and pressure values without the sensor an approach advised by the developer of Gasturb™ Joachim Kurzke, was followed. The approach consists of using the value of a model engine and it is explained in chapter 5. Additionally, CFM, the manufacturing company of the CFM56-3 engine, recommends a correlation for the temperature value when it is unknown. With this suggestions, there are in total four alternative scenarios to having a T_{25}/P_{25} sensor. T_{25} and P_{25} represent the temperature and pressure at station 25, respectively. The four alternatives are listed below:

- No sensor data available and the T_{25} and P_{25} values obtained from the Gasturb™ model engine.
- T_{25} sensor and the P_{25} value obtained from the Gasturb™ model engine.
- P_{25} sensor and the T_{25} value obtained from the Gasturb™ model engine.
- P_{25} sensor and the T_{25} value obtained from the CFM correlation.

The HPC efficiency and other performance parameters are calculated for the different scenarios and compared to the ones obtained with the T_{25}/P_{25} sensor data, to understand if they are a reliable

replacement.

In conclusion, this thesis has four main objectives which are:

- Develop and produce a robust T25/P25 sensor.
- Extrapolate the Gasturb™ engine model to CFM56-3C conditions and use the software to do the performance calculations.
- Study the influence of the blade tip clearance on the HPC performance of CFM56-3 engines.
- Compare the performance results obtained with the T25/P25 sensor with the alternatives to the sensor.

1.4 Thesis outline

This thesis consists of seven chapters, including the current one, the introduction. A description of TAP ME is provided in chapter 2, followed by a description of the department's test bed, of the engine studied, the CFM56-3, and of the variables of focus during a turbofan engine maintenance procedure. To finish the chapter the performances studies previously developed in TAP ME are outlined, presenting their influence on the present thesis.

In Chapter 3, the literature review, information related to similar work is provided. To start the chapter, it is mentioned work related to the development of sensors for gas turbines, and more specifically on the CFM56-3. Then similar experimental studies based on the blade tip clearance are described, focusing on how the variable was evaluated.

Chapter 4 describes the development and production of the temperature and pressure sensor on station 25 of the CFM56-3, before the HPC. After the sensor production, it was necessary to test it. The methods to do so and the results obtained are described at the end of the chapter.

Chapter 5 is where the next step is given after the sensor production and its measurements are used. In this chapter, the performance calculations of the HPCs of the engines tested are done with the assistance of the Gasturb™ software. The software is here described and the procedures necessary to obtain the results are outlined.

In chapter 6 the results are presented. There are two sets of results, the first set is related to the performance study of the blade tip clearance. It consists of attempting to relate this variable's data from the HPC with the efficiencies obtained on Gasturb™ . The second set is related to the sensor and its goal is to reveal how useful the T_{25}/P_{25} sensor developed is by comparing the results obtained with and without the sensor.

In the final chapter, the conclusions of the study are presented and suggestions for future work are given.

Chapter 2

TAP Maintenance and Engineering

TAP ME is the maintenance department of TAP Portugal. Its central facility is located in Lisbon and the department employs a total of 4000 technicians, trained and qualified to provide quality services of maintenance and engineering to airplanes, engines and components. TAP ME is recognized internationally and adequately certified by many aeronautical authorities, including the European Aviation Safety Agency (EASA) and the North American Federal Aviation Administration (FAA). The department was created in 1945 to ensure the maintenance of TAP's fleet, starting to provide this service to third parties in the seventies. Currently TAP ME is a leading global Maintenance, Repair and Overhaul (MRO) organization, providing operator services and solutions to Airbus, Boeing and Embraer fleets, that range from airframe, engines, and components, to engineering and material support. TAP ME's maintenance centers are spread by three locations, Lisbon, in Portugal, Rio de Janeiro and Porto Alegre, in Brazil. The Rio de Janeiro center is focused on many areas of an aircraft but not on engines, Porto Alegre is the center for turboprop engines and Lisbon the one for turbofan engines. At Lisbon's facility, where this thesis was developed, MRO services are approved for Airbus A300-600, A310, A330, A340, A320 family, and for engine models CFM56-3, -5A, -5B, -5C, -7B and CF6-80C2 [4].

2.1 Test bed

Test beds are facilities used by maintenance centers, which help to understand an engine condition and how it will operate during a flight. These facilities can be of two kinds, sea level and flight level. The sea level ones are intended to simulate the engine operation at sea level altitude, as the take-off regime. Flight level test beds have the objective of reproducing the conditions the engines are subjected to when operated at altitude. Additionally, a different type of distinction between test beds exists. This distinction is associated with the positioning of the engines during the test, which might be indoor or outdoor. More insight on test bed facilities is available on the work of Walsh and Fletcher [7].

To evaluate the performance of their engines, TAP ME submits them to a flight test on a sea level indoor test bed. An engine is commonly tested after its maintenance procedures are concluded. TAP ME's test bed is a large test facility with a cross section of 8.65 m height by 9.75 m width, represented

in schematic form in Figure 2.1. The inlet air passes through noise reduction splitters and bird screen, on the left of Figure 2.1, before the test bed working section. The exhaust gases of the engines pass through a conventional cylindrical augmenter, with a diffuser section going then up through a folded vertical exhaust stack [8].

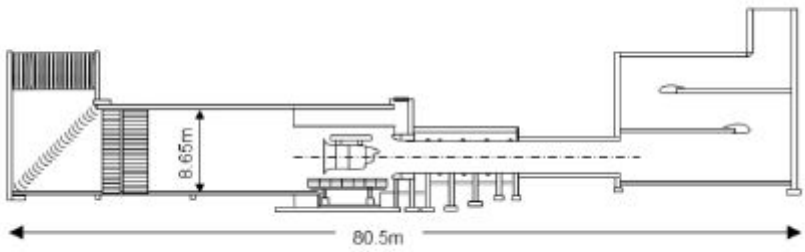

Figure 2.1: TAP ME's test bed [9]

TAP ME collects a limited amount of thermodynamic data during their engine tests. This problem arises since there are no sensors available for every important station of the engines, which occurs for two reasons. Firstly, not every station is relevant for the approval of the maintenance implemented on the engine. Secondly, due to the challenge of placing a sensor in some stations of the engine. For example, station 4, just after the combustion chamber, withstands such high temperatures that any sensor placed there would be damaged. The different stations are described on the following section after a description of the CFM56-3 engine.

The measurements obtained from these sensors, during the tests on the engines, have corrections applied to them. Two sets of corrections are applied, one associated with the conditions of the day, the standard day corrections, and the other related to the test bed itself, the facility modifiers [8]. These corrections allow comparisons between engines tested in different ambient conditions and in different facilities. For a further explanation on this, the ambient corrections are explained and used in section 5.1 and the facility modifiers are explained on the work of Martins [10].

In the following section, the CFM56-3 engine will be described, with an introductory description of turbofan engines.

2.2 Introduction to the CFM56-3 engine

This thesis is focused on the CFM56-3, a turbofan engine, therefore it is important to understand how this type of engine operates. In Figure 2.2, a scheme of a turbofan engine is provided for a better understanding of its components which are described next.

A turbofan is a modified version of a turbojet engine. Both share the same basic core of an inlet, compressor, burner, turbine, and nozzle, but the turbofan engine has its main principle on the movement of a great amount of air at a not very high speed, and this is possible through the fan, which does not exist on a turbojet engine. The fan is a large, many-bladed compressor stage located at the front of the engine. After this component the flow is divided in two ducts, the hot stream, which flows through the

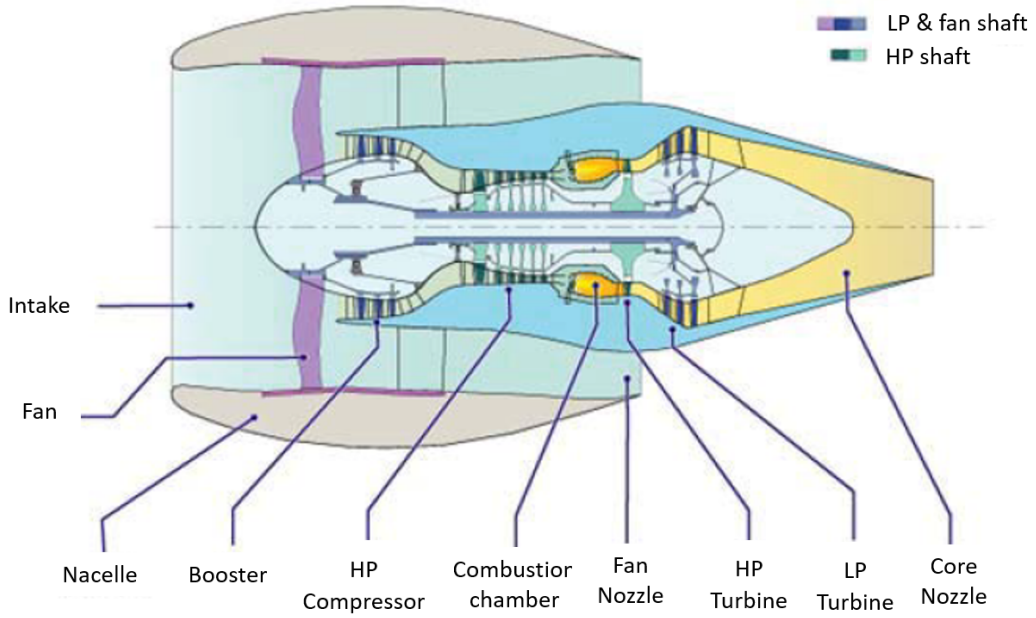

Figure 2.2: Representation of a turbofan engine

core of the engine, to the HPC, and the cold stream, which passes through the bypass duct, as seen in Figure 2.2. The ratio between the mass flow rate of the two streams is defined as the bypass ratio, one of the most relevant parameters of a turbofan engine. Downstream from the HPC, the hot flow enters the combustion chamber where fuel is burned to provide energy to the turbines. Commonly turbofan engines have two turbines, although more complex ones have three. One spool is used to power the high pressure compressor and another spool to turn the large fan and the booster.

The flow from the hot stream is important to extract energy from the combustion, but it is not responsible for producing most of the thrust. This is ensured by the cold flow, which represents up to 90% of the total amount of air entering the engine, and produces around 80% of the total thrust delivered by the engine. The main principle is to apply a smaller compression to a larger amount of air, when compared with a jet engine, which ultimately results in a higher fuel efficiency. This principle will lead to a reduced velocity of the exhaust stream. A lower velocity leads to a lower jet noise, one of the main advantages of the turbofan engines [1].

At this point, a description of the engine under study is easier to understand. The CFM56-3 is a turbofan engine developed by CFM International, in the seventies and certified in 1984. This engine was designed for the 737 - 300/400/500 aircrafts [6]. It belongs to the CFM56 series, the world's most popular engine, with an aircraft with its engines taking-off every four seconds [6]. The engine is characterized by a large bypass ratio, 5 to 1, and two shafts. This engine exists in different versions or rates considering its available thrust. Thrust is the force produced by the engine, responsible for the motion of the aircraft. All versions have the same main features and the different rates are obtained from derates of a version with engine thrust of 102.4 kN. The different versions are presented in Table 2.1. As it will be explained in chapter 5, this thesis will focus on the rate with the higher trust, the CFM56-3C.

The CFM56-3 has two big systems, the low pressure system and the high pressure system. The

Table 2.1: Different rates of the CFM56-3 [11]

Version	Thrust (lb)	Thrust (kN)
CFM56-3B1	20000	89.0
CFM56-3B2	22000	97.9
CFM56-3C	23500	104.5
CFM56-3B1 Derated	18500	82.3

first one has as main components, the fan, which is coupled to the booster or intermediate pressure compressor. Together they form the low pressure compressor (LPC). The fan is responsible for compressing the cold flow, and applies an initial compression to the hot flow which then passes through the booster, composed by three compression stages. These two compressors are driven by the rotation of the low pressure turbine (LPT), which has four stages. The high pressure system is composed by the high pressure compressor (HPC), which has nine compression stages and is responsible for compressing the air just before it enters the annular combustion chamber. This component is the focus of this thesis. This compressor is driven by the high pressure turbine (HPT), which has just one stage. Between the HPC and the HPT, there is an annular combustion chamber which, through the burning of fuel, provides energy to the flow in order to drive both turbines [11]. The engine has yet a third system, the accessory drive station, responsible for extracting energy from the high pressure spool to drive the engine accessories. It is also responsible for transmitting power from the starter to the high pressure rotor, during the engine start [11]. The CFM56-3 is also characterized by a cooling system designed for the turbine blades and casing of the HPT and for the combustion chamber. This system is further explained in section 2.3.

Throughout the present thesis, different aerodynamic stations of the CFM56-3 engine will be mentioned, therefore a description of the stations along this engine will be provided next. In Figure 2.3, a scheme of the engine is provided for a better understanding of the stations described. Additionally, in this figure are represented the sensors available on TAP ME's test bed for the CFM56-3 engine, before this study started [12].

The first station is station 2, at the entry of the engine. Station 17 is in the bypass duct after the air has passed through the fan. Station 21 is also after the fan but on the hot flow and before the booster. At TAP ME's test bed, no measurements are taken in this station. Station 25, the main focus of this thesis, is the station after the booster and before the HPC. As it has been mentioned, the sensor from this station is damaged motivating the development of a new sensor, the basis of this work. For this station, the manufacturer of the engine, CFM International, recommends a correlation to calculate the T_{25} value, when the temperature is not measured [11]:

$$T_{25} = T_2 + \Delta T_{25}\left(N_1\right) \tag{2.1}$$

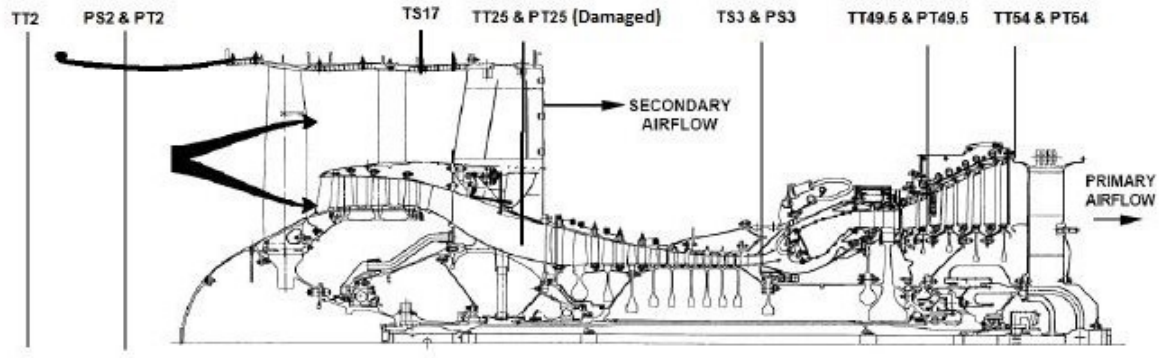

Figure 2.3: Aerodynamic stations measured in TAP ME's test bed for CFM56-3 adapted from [12]. TT represents the total temperature, TS represents the static temperature, PT represents the total pressure and PS represents the static pressure.

This correlation assumes a dependence of T_{25} on T_2, and on ΔT_{25} a factor dependent of the low pressure system spool rotation (N_1), and possible to be obtained from a table provided by CFM [9]. This correlation is part of the study presented in section 6.2.

Station 3 is located after the HPC, as observed in Figure 2.3. After this station the combustion chamber is reached, where the combustion occurs, providing energy to the flow and therefore heating it. Station 4 is just after the combustion chamber, where the temperature may reach 1650 K. Therefore, it is very difficult for TAP ME to place a sensor at this location due to the harsh conditions experienced there. However, this is not the only station of the turbines with no measurements. In station 45, after the HPT and before the LPT, TAP ME also does not have a sensor capable of collecting temperature and pressure values. This, however, has already been attempted by Henriques [13]. This process will be later explained in chapter 3. The absence of measurements in stations 4 and 45 prevents a performance study on the HPT. However, there are two sensors in the LPT. The first is in station 49.5, in the second stage of the LPT, and measures the Exhaust Gas Temperature (EGT). As it will be explained in the next section, this is one of the most important variables to evaluate the condition of a turbofan engine [9]. Station 54, after the LPT, has the last sensor of the engine. All of these sensors measure temperature and pressure except the ones at station 17 and 49.5, which just measure temperature [9].

In order to evaluate the CFM56-3 engine condition in a test bed, it is submitted to certain regimes, related to the low pressure spool rotational speed, N_1. The regimes tested and their respective N_1 are presented in Table 2.2.

A more detailed description of the CFM56-3 engines is presented in a report from CFM International [11].

2.3 Maintenance of turbofan engines

The basic principles of performing maintenance to a turbofan engine will be described in this section.

Table 2.2: Different regimes tested on a performance test for the CFM56-3C engine [9]

Regime	N1 (rpm)
Maximum Continuous #1	4804
Take-off	4942
Maximum Continuous #2	4804

Engine shop maintenance includes two primary elements, performance restoration and life limited parts replacement. Performance restoration is often necessary due to a deterioration of the engine core parts, damaged by heat, erosion and fatigue, sooner than predicted. The most affected area is on the turbines, where due to the engine operation, the high temperatures induce an accelerated wear and cracking of the blades, which decreases the performance. The common approach is to dismantle the core module and inspect, balance, repair or replace the blades, rotors and stators. The life limited part replacement is associated to a specifically defined operating life of the engine parts, at the end of which, these must be replaced. These parts are the rotating compressor and turbine hubs, shafts or disks within the engine [2].

As mentioned before, after the maintenance procedures are finished, the engine condition needs to be checked and this is done through a test bed run. To check the engine condition, there are three important parameters monitored by TAP ME on their performance tests: thrust, vibration level and EGT margin. The most important is the minimum thrust. This variable is tested by setting the engine to its different regimes and measuring the thrust produced. A minimum thrust has to be delivered to approve the engine, which for the CFM56-3C is 104.5 kN [11]. Some engine maintenance providers use the engine pressure ratio to measure this parameter [14]. The second parameter is the vibration level of the engine, if this is too high it is dangerous to use this engine during a flight, therefore procedures can be done on the test bed to reduce vibrations. This is possible through the positioning, in specific stations of the engine, of screws to achieve force equilibrium, therefore reducing the vibrations. The third parameter is the EGT margin, a parameter related to the performance of the engine, which is the one mostly focused on this thesis. This variable consists of the difference between critical EGT and the EGT value measured. The critical EGT is the value of temperature at which the turbine blades would be damaged due to the heat, therefore it is a limit that cannot be surpassed. The EGT margin is a complex parameter, since it depends not only on the performance of the engine but also on the ambient conditions. The Critical EGT for the CFM56-3C, is 1181.15 K for Hot Day (HD) conditions, a form of representation of the variable which is explained ahead. The EGT margin has to be positive, and its desired value is stipulated with the TAP ME's customer.

The EGT margin is a very important variable due to its direct relation with the TSFC, which translates the necessary fuel by the engine to develop a certain amount of thrust. A lower EGT margin represents a higher TSFC, as may be easily understood in the scheme of Figure 2.4. As stated by CFM "When EGT margin decrease, Fuel Burn increase + 10°EGT = + 0.7% TSFC" [11].

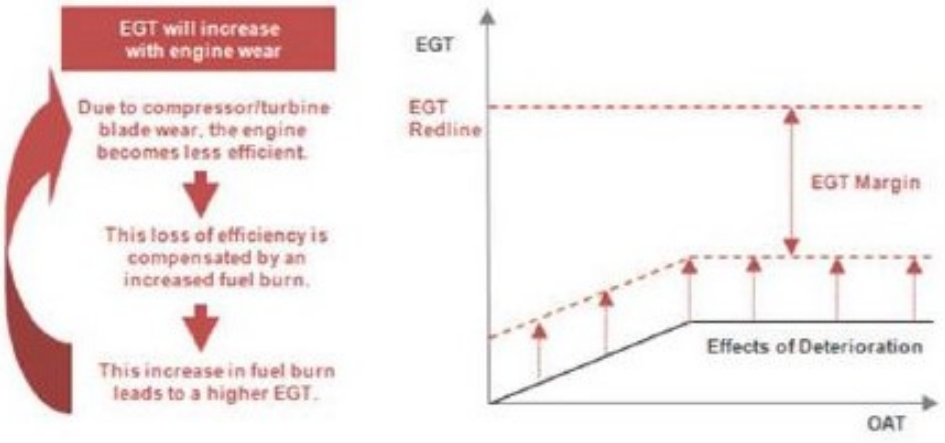

Figure 2.4: Importance of EGT margin as a performance parameter [2]

As it may be noticed in Figure 2.3, the EGT is measured on the second stage of the LPT. However, other temperatures could be measured in other stations of the turbines, nevertheless, this station is considered the best to measure this variable, and it is important to know why. There are three main temperatures after the combustion chamber: T_4, T_{45} and EGT. T_4 is the burner exit temperature, therefore its value is affected by the amount of cooling air employed by the HPC, necessary to cool the LPT blades. Thus any measurement performed in this station of the engine does not include all the hot flow of the engine, and its value could lead to wrong interpretations of the engine condition. T_{45} is measured at the LPT inlet, which is still affected by the same problem [15]. At the EGT station, the flow is already independent of the bypass cooling air flows, since at that point all of these have already rejoined the main stream of air [16]. Thus, EGT becomes the best option for performance studies.

The calculation of the EGT margin may be done for Standard or HD conditions, although this last one is the option commonly chosen [16]. For HD conditions, an Outside Air Temperature (OAT) of 303 K or 30 ℃ is assumed. This condition is applied because the EGT margin is considerably affected by the OAT as it may concluded from Figure 2.4. With the increase of the OAT the EGT margin decreases, since a higher OAT leads to a higher EGT because the inlet air is at higher temperatures. The Critical EGT is a constant limit so it remains the same, therefore the difference between these two temperatures, the EGT margin, decreases. It can also be observed that, after a certain OAT the EGT stops increasing and remains constant. This is due to the Full Authority Digital Engine Control (FADEC), a control system of the engine that modulates the variable bleed valves, variable stator vanes, bore cooling valves and HPT and LPT active clearance control valves to prevent the increase of the EGT, which could lead to damage of components of the engine [6].

A restored EGT margins following an engine first shop visit, is commonly around 70% lower than the new engine margin [14]. Additionally, during the engine normal operation, the EGT margin is deteriorated as well [2].

The HPC holds a substantial influence on the TSFC, and therefore on the EGT margin, of an engine, as it may be concluded from Figure 2.5.

In this figure, the results of a study executed by NATO [5] are presented. The objective was to

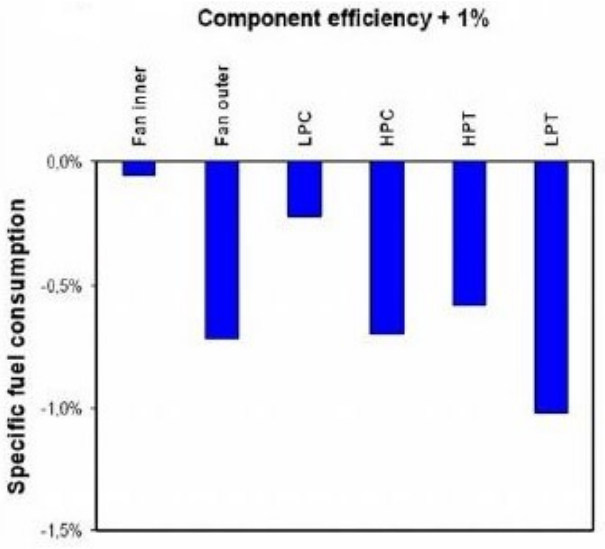

Figure 2.5: Variation of TSFC with 1% efficiency variation on the different turbofan components adapted from [14]

separately increase the efficiency of each of the main components of a turbofan engine, and conclude which of these components has the largest influence on the TSFC. As it may be observed in Figure 2.5, the component responsible for the higher TSFC variation is the LPT, followed by the fan and the HPC. A 1% efficiency increase on the HPC, resulted in close to 0.7% decrease on the TSFC. Therefore, a study of approaches to increase the HPC efficiency will result in a significant enhancement of the performance of a turbofan engine. TAP ME can achieve this by studying the influence of the procedures carried out on the HPC. Therefore, it is necessary to understand which are the procedures and variables used in TAP ME's workshops to perform the HPC maintenance. Below, are introduced the four variables considered by TAP ME as the ones with greater influence on the HPC.

1. Blade Chord.

   The blade chord is one of the main aspects that characterizes an airfoil. It is defined as the maximum distance between the leading edge and the trailing edge of an airfoil [17]. As it will be further explained in chapter 3, this variable has an important impact on the efficiency of the HPC. Therefore, TAP ME, assigns a minimum chord length, below which the chord has to either be repaired or be replaced by a new blade. In parallel with the present thesis, another study was being conducted in TAP ME by Baptista [18]. His objective was to understand how the choice between the two options, repaired compressor blade and replacement by a new one, would affect the HPC efficiency [18]. This study was conducted for the CFM56-5B engine.

2. Blade tip clearance

   The HPC is characterized by a required gap between the surrounding casing and the compressor rotor blades. This rotor blade tip clearance is described in Figure 2.6. This gap is essential to avoid rubbing between the compressor blades and its casing, which would cause great wear and damage. Tip clearance represents one of the basic problems in turbomachinery, due to its negative

impact on the efficiency of a compressor [5]. To minimize this effect, the tip clearance should be kept as small as possible. However, due to the possibility of a variation higher than expected of the blade's size due to thermal variations and inertial forces, this is an important risk to consider. The thermal variations, occur due to the different engine operating conditions, occuring during a flight, and modify the density of the components. The inertial forces are related to rotational movement of the rotors which subjects the blades and the casing around them to centripetal forces. It is therefore advisable by manufacturers, to provide a liberal clearance in order to avoid rubbing during the most unfavorable conditions [19]. After a tip clearance repair this gap increases during the engine operation and the main reasons for this are explained by Martins [10].

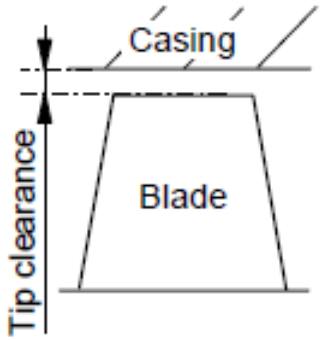

Figure 2.6: Blade tip clearance definition, adapted from [5]

To define the tip clearance of the HPC blades, in a maintenance procedure, two processes are necessary. Firstly, the compressor outside casing diameter is measured and the medium value is determined. Subtracting this value by the tip clearance intended, the blade height required is defined. Secondly, to set the blade height, a high speed grinding (HSG) machine is used. It grinds the blade tips of the rotor while it is being spun at high speed, which may reach the 7000 rpm. This equipment is provided with measuring systems, which ensure a considerably high degree of accuracy, with diameter tolerances that can be held to 0.025 mm [20].

Two examples of the HPC casing diameter measurements are presented in Figure 2.7 a) and b).

Figure 2.7 a) represents a casing with a regular diameter, since all the points measured are close to the medium diameter line. This line is the one on the middle of the green zone of the figures. Figure 2.7 b) has several points considerably distant from the medium diameter. Considering that for these two engines, the tip clearance defined on TAP ME's workshop would be the same, the distance between the medium diameter of the casing and the tip of the blades would also be the same. However, due to irregularity of the casing of Figure 2.7 b), the real tip clearance would be different, which could lead to different efficiencies obtained for the two HPCs. The engine of Figure 2.7 b) would likely be the one with a smaller efficiency, since it has a higher tip clearance. The ideal would be to repair the casing of this engine, which can be done through a process named skin cut repair. However, this process is expensive, which is why it is not currently used at TAP ME. If, through tip clearance studies such as the one of this thesis, it would be concluded that this

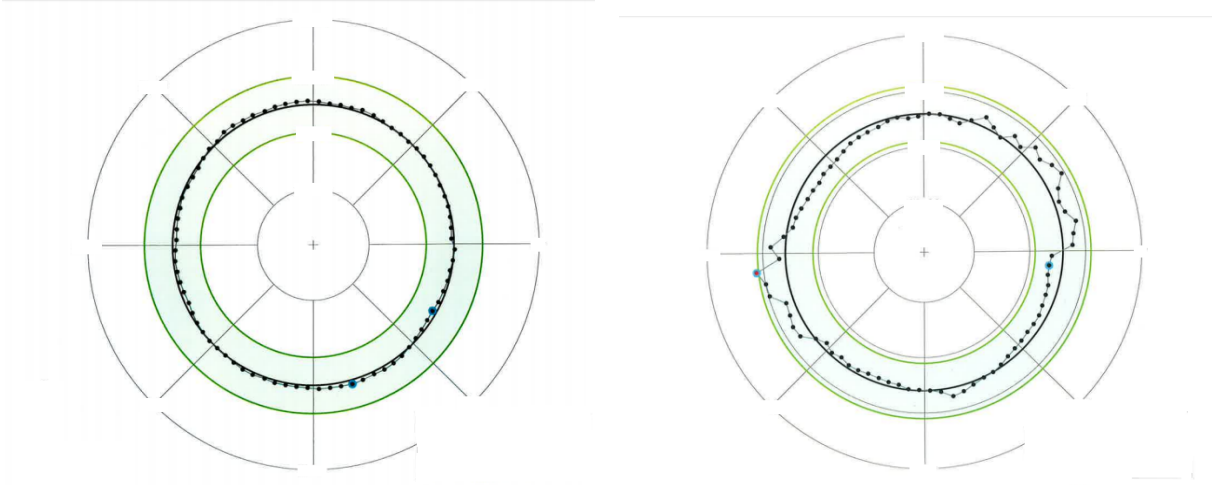

(a) Example of a HPC casing with a regular surface (scale deleted for confidentiality reasons) [21]

(b) Example of a HPC casing with an irregular surface (scale deleted for confidentiality reasons) [21]

Figure 2.7: Examples of HPC casing diameter measurements [21]

process would increase significantly the efficiency of the HPC, then the investment on the skin cut repair procedure could compensate despite of its high cost.

3. CDP seal

   CDP is an acronym for Compressor Discharge Pressure and it characterizes the area of discharge of the HPC. It can be said that the compound CDP seal is probably one of the two most important seals of the engine and has a big responsibility on its behaviour and performance of the engine. As it can be noticed in Figure 2.8 a), this seal is installed at the end of the HPC, just before the combustion chamber. This seal controls the pressure of the interior cavity of the casing of the combustion chamber, which is basically the path where part of the air from the HPC flows to provide cooling to the combustion chamber. This cooling air has a big influence on the behaviour of the combustion chamber and therefore, on the efficiency and stability of the combustion. Thus, a slight variation on the CDP seal will influence greatly the EGT on a CFM56-3 engine [9]. So this variable should be considered on a performance study of the HPC. For research studies related to this variable, references [22] and [23] are recommended.

   The seal is essentially composed of a circular ring with a five step stair to improve its efficiency. The height of the stairs is defined during the maintenance process, which affects the amount of air passing through it. This is how this variable is controlled.

4. Seal teeth clearance

   Seal teeth is a method of minimizing flow leakage axially between the rotor and stators of a compressor. As it may be observed in Figure 2.8 b), a ring seal is placed under the stator, with annular sealing teeth or steps, extending in a radial inward direction and adapted to cooperate with sealing surfaces of the rotating component. These seals are efficient and generally easy to install into engines, and reduce the spillage flow. The optimization of the seal is accomplished by machining individual teeth within a packing ring to different heights, which is the method applied in TAP ME

[24]. Support on studying the performance of a compressor, related to this seal, may be found in the work of Zhang et al. [25] and Wellborn et al. [26].

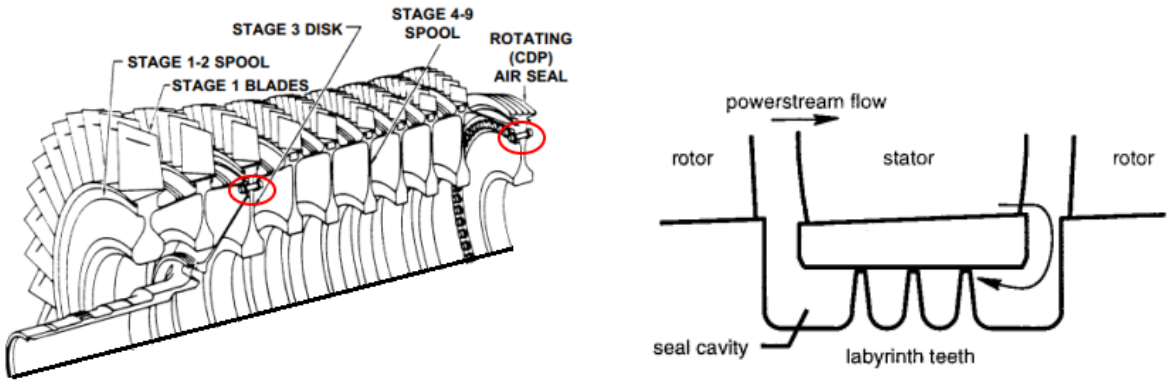

(a) CDP seal on a HPC representation, adapted from [9]

(b) Seal teeth clearance [26]

Figure 2.8: Different variables of the HPC

The initial objective of this thesis was to accomplish a performance study focused on all these four variables. However, due to a limitation on the amount of data for these variables except for the blade tip clearance, it was decided to focus just on this one. This limitation is further explained in chapter 5. Of these four variables, the blade tip clearance is, together with the blade chord, one of the two most important variables of the HPC. This will be understood ahead, in the literature review.

Studying the blade tip clearance on an axial multi-stage compressor can be complex. Some thought on how to correlate it with the HPC performance parameters is done on chapter 3, through a literature review where other experimental studies are listed.

2.4 Previous research work done in TAP ME

In recent years, TAP ME has collaborated with master thesis students, to study the performance of their engines. The most recent students started working with a software, Gasturb™ that calculates the thermodynamic cycle of gas turbine engines, thus supporting performance studies. Júlio Ridaura [16] was the first student to work on this. He concluded that due to the limited amount of information that the test bed results provide, to study the performance of the engines handled by TAP ME, it would be necessary to create a model of the CFM56-3 engine in the Gasturb™ software. This concept of the model is further explained in section 5.3. Ridaura started working on this model, which was improved and finished by Martins [10]. However, Martins [10] concluded that for the model to be useful on studying the HPC, it was necessary to possess test bed measurements from station 25. This station of the engine was explained in section 1.3 and its location may be observed in Figure 2.3. To solve this problem, TAP ME needed to develop a sensor of temperature and pressure, and this was the assignment of Quintal [27]. His objective was to develop a new sensor, appropriate for the test bed existing in TAP ME. The present thesis will focus on continuing these last two assignments, namely to continue the development and production of the sensor and use it together with the Gasturb™ model developed by Martins, to

initiate the performance analysis of CFM56-3 engines tested in TAP ME. This thesis will focus mainly on the HPC and on the blade tip clearance variable.

Chapter 3

Literature Review

In this chapter, the relevant research to this thesis is presented. It is divided in two sections. The first one 3.1, is related to the first objective of this thesis, the production of a temperature and pressure sensor for TAP ME's test bed. The objective was to find research related to sensors similar to this one, already produced, understand the problems faced by the authors and attempt to prevent them.

Section 3.2, supports the performance study related to the blade tip clearance of the HPC to be accomplished. Work related to the variable tip clearance and its influence on the HPC will be listed. This section is divided in two sub-sections, each with a different perspective of the study of the tip clearance. Sub-section 3.1.1 is an introduction to this variable, how it affects the performance and also a presentation of how engine manufacturers deal with this problem. Sub-section 3.1.2 is based on the description of experimental studies done on the HPC related to this variable. This part is particularly important since the experimental results presented in this thesis were analysed based on the research discussed in this chapter.

3.1 Gas turbine sensors developed

After a wide literature review, no work was found related to the development or production of a sensor for station 25, for any kind of engines. On the development of the sensors, there is a vast literature related to studies of tip clearance, where the sensors are positioned on the tip of the blade. In these studies, the objective is to understand how the tip clearance is altered during the engine operation. These studies aim to improve compressor design and do not focus on maintenance procedures. The work of Flotow et al. [28] is an example of one of these studies, which is widely referenced.

For maintenance, some studies related to monitoring of the sensors results were found, using statistical correlations. The objective is to understand if the sensors used on the test beds are working properly and which need replacement or repair. An example of one of these studies is the work of Dewallef and Borguet [29].

For sensors of different stations of the engine, the only work found was the one done on TAP ME by Henriques [12]. This author studied the production of sensors for two different stations of the CFM56-3.

The first was for station 17, on the cold flow, after the fan, and the second was for station 45 after the HPT. For the first station, the sensor owned by TAP ME was lacking the temperature measurement. The solution found was to add an opening to a lid close to that station, through which a temperature sensor could be installed. For the object of this study, station 25 as described in chapter 4, the process adopted was similar, except that the openings used were already present in the engine. For station 45, the sensor installed was not so successful. Due to the risk of damage, it is difficult to place a sensor to measure the total pressure and temperature values. The solution adopted was to produce a sensor capable of measuring static values, and together with the velocity magnitude, it would be possible to obtain the value of the total component desired. However, due to turbulent behaviour of the flow after the HPT, a considerable gradient of temperature and pressure develops at that station. This gradient makes the measurement quite difficult, leading to large errors on the results, compared to the ones expected [13]. Fortunately, this problem is not so serious in station 25, where the flow has a reduced velocity, when compared to station 45, which indicates the flow is not as turbulent as in the turbines stages. The difference between total and static components of a flow is explained in chapter 4, with reference to the distinctive methods of the measurements of these variables.

3.2 Blade tip clearance

3.2.1 Introduction

Blade tip clearance is a problem common to all axial compressors. This variable has an importance on the HPC efficiency, impacting the overall performance of the engine, which as stated in chapter 2, can be monitored by the EGT margin. As stated by Aircraft Commerce [14], in an article related to the CFM56-3 and to tip clearance, "In some cases reducing the gap between the blade tip and casing wall by one mil [0.025 mm] can add about 0.1 degree of EGT margin. One example is the clearance of the HPC blades. The standard clearance is 80 mil [2.03 mm], but the minimum is 54 mil [1.37 mm], so reducing the clearance by 26 mil [0.66 mm] adds about three degrees of EGT margin." [14].

In turbines, the influence of the tip clearance is even greater [2]. A study conducted by NATO [5] states that a 0.25 mm reduction in turbine tip clearance leads to an increase on the engine EGT Margin of up to 10 ℃ and an increase in turbine efficiency of up to 1%. The result would be a reduction in TSFC close to 1% with a proportional reduction in emissions. This reduction could save a total of 160 million dollars per year in fuel costs for the current civil aircraft fleet.

To mitigate this problem, manufacturers developed cooling systems for the blades and casing, to control their tip clearance through the engine's operation. These methods help preventing the decrease of the HPC and HPT efficiency. These systems are much more often developed for the turbine blades, although there are also engines applying it on their compressors [5]. The CFM56-3 engine is an example with only a cooling system for the HPT blades.

The most common cooling method used is active clearance control (ACC). For this method the amount of cooling air is scheduled over an operating parameter, such as corrected speed or pressure

ratio [5]. This system has a positive influence on fuel consumption, safety, reliability and maintenance cost of the engine.

Concluding, tip clearance is a problem for compressors, responsible for a substantial loss of efficiency. It is important to understand how these losses are studied, which is the objective of the following sub-section, where tip clearance experimental studies are listed.

3.2.2 Experimental studies

According to researchers in the area, the blade tip clearance and the blade chord are considered two of the main variables impacting the efficiency of an axial compressor [30]. The objective of this work is to study the impact of the tip clearance on the HPC. Therefore, below are described experimental studies related to the impact of the tip clearance on the performance of axial compressors. This review was helpful to chose the approach used in this work.

Experimental studies on tip clearance flow have been extensively carried out for more than sixty years. Two recent papers were found from Danish et al. [31] and Dong et al. [32], from 2016 and 2014, respectively, which present a review of the experimental tip clearance studies performed over the years. These studies focus on different variables and approaches to study the tip clearance, which are listed below.

One relevant assumption encountered was the use of only the three first stages of an axial compressor, since these are considered to have a significantly higher importance on the performance of a compressor than the remaining stages [33]. In a study performed by Domercq and Escuret [34], where the influence of the tip clearance on a multistage compressor is analysed, the focus of the authors is just on the first three stages. In this work, the tip clearance is studied together with the pressure ratio and the compressor efficiency. $\frac{p_{02}}{p_{01}}$ represents the pressure ratio of the compressor, defined as the ratio between the total pressure of the flow entering the compressor and the one at its exit. Similarly to the efficiency, the pressure ratio of a compressor is lower for higher tip clearances, since a wider gap leads to extra air passing without being compressed, thus the air on the end of this component is not as compressed. In order to handle the tip clearance variable specifically, these authors used the dimensionless tip clearance, *d*, defined as the ratio between the absolute tip clearance, *t* and the blade height, H_b:

$$d = \frac{t}{H_b} \tag{3.1}$$

The use of this variable is suggested by several researchers as Dong et al. [32], Saravanamutto et al. [33], Kurzke [35] and Wisler [36]. This last author, summarized a large set of experimental data, provided by General Electrics, and concluded that for an increase in tip clearance corresponding to 1% of blade height the result would be a 2% loss of efficiency [36]. The blade height definition provided by Wilson [37] is given by the difference between the radius at the tip of the blade and the radius at the hub, see Figure 3.1.

However, the dimensionless tip clearance was not the only variable found to influence the tip clearance losses. Actually, there is an alternative approach further applied, which is the ratio between the tip

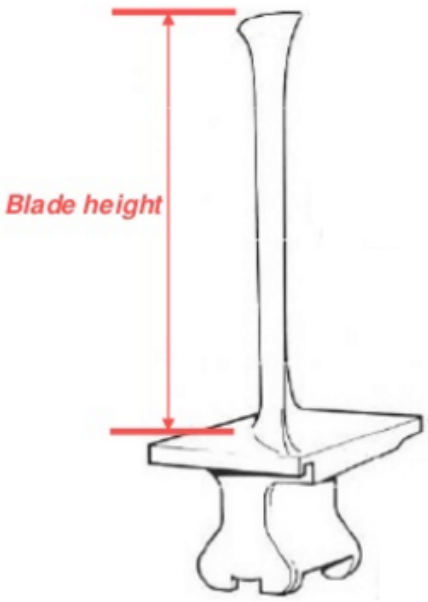

Figure 3.1: Definition of blade height [37]

clearance, *t*, and the chord, *c*, the tip clearance-chord ratio, τ:

$$\tau = \frac{t}{c} \tag{3.2}$$

This approach is adopted by Lakshminarayana and Horlock [38]. In their study, the authors used the ratio between tip clearance and chord, therefore, studying, together, the two main variables responsible for losses on an axial compressor [38]. This approach has already been used for some years. Smith [39], a researcher, who in 1984 focused on correlating the tip clearance-chord ratio with the pressure ratio rise, concluded that a 1% chord length increase in tip clearance would lead to a 4.6% loss in peak pressure rise. Ramakrishna and Govardhan [40] adopted as performance parameters, the pressure ratio and the corrected mass flow, a concept related to the amount of air passing through the compressor, detailed on section 5.1. Sakulkaew et al. [41] concluded that for clearances gaps of 0.8% to 3.4% of the span of the blade, the efficiency is considerably deteriorated with increase of the tip clearance. This effect is less sensitive to tip clearance for gaps greater than these range. These authors also used the efficiency as a parameter of performance of the compressor.

An alternative parameter, considered relevant by references [41, 42] to study the performance of a compressor, is the polytropic efficiency. This variable represents the efficiency of a stage of a multistage compressor, assuming that all stages have the same efficiency. To obtain this variable it is assumed that the isentropic efficiency is the same for all stages and it is derived from a complex formula helpful to calculate the polytropic efficiency, $\eta^{\star}$, through the overall efficiency of the compressor, η_c, the pressure ratio and the heat capacity ratio, γ [42, 43]:

$$\eta^{*} = \frac{\gamma-1}{\gamma} \frac{log\left(\frac{p_{02}}{p_{01}}\right)}{log\left(\frac{\frac{p_{02}}{p_{01}}^{\left(\frac{\gamma-1}{\gamma}\right)}-1}{\eta_c}+1\right)} \tag{3.3}$$

Gasturb™ uses, as well, this formula to calculate this parameter [35].

Quite a few of the studies just mentioned, combine the experimental component of the research with Computational Fluid Dynamics (CFD) analysis. This is due to the complexity of studying a compressor with a large number of stages.

In summary, there are two main variables used to study the tip clearance, the dimensionless tip clearance: and the tip clearance-chord ratio. The latter is the most widely adopted due to the addition of the chord variable, which is related to the profile losses, one of main causes of deterioration of the compressor performance [30]. As parameters of performance of compressors, four variables were found to be the most commonly used: compressor isentropic efficiency, pressure ratio, polytropic efficiency and corrected mass flow. The research mentioned above allows to conclude that the tip clearance has a substantial impact on the performance of an axial flow compressor.

Chapter 4

Sensor development and production

In this chapter the procedures implemented to design and produce the sensor for station 25 of the CFM56-3 engine is described. The development of this sensor had already been started before this thesis by TAP ME, so the objective of this thesis was to conclude this development and produce the sensor. In section 4.1, the background of the development already done on the sensor is described. In section 4.2, the procedures to produce the sensor and finish its development are described. In section 4.3, the tests performed to validate the quality of the sensor are explained.

An important fact to clarify is that this sensor is not a mandatory sensor on TAP ME's test bed for them to approve the performance of an engine after the maintenance procedures. The sensor enables the calculation of the efficiency of the HPC, therefore providing data that will support performance studies for this component. Ultimately, the objective is to increase the efficiency of the HPC.

4.1 Background

In order to measure the temperature and pressure at station 25, TAP ME had a sensor sold by CFM, which is illustrated in Figure 4.1. In past years, this sensor has not been used due to its inoperability during the majority of the test bed runs. The main reason was the pressure tube, responsible for connecting the sensor to the test bed. This tube is quite rigid, which makes difficult to assemble and disassemble the sensor [16]. This sensor is only supposed to be used during the test bed runs, it is not used during the engine normal operation, therefore it must be easy to assemble and disassemble from its position on the engine. This becomes an even larger problem because its placement on the engine requires many bendings of the pressure tube, since the space where it is positioned is tight.

Reference [10] states that only 9.1 % of the engines tested by TAP ME collected information at station 25. In 2017 this value should be even lower, since it has not been used since 2015. The last of these sensors acquired was already the third one bought by TAP ME from CFM and they all got broken. Therefore, a new T_{25}/P_{25} sensor is necessary. Firstly, to work on the design and production of this new sensor, it is necessary to understand the conditions that it will be subjected to. Station 25 is characterized by values of total temperature commonly between 370 and 395 K, and of total pressure in

Figure 4.1: Previous sensor used in TAP ME's test bed [12]

the range of 220 kPa to 240 kPa [9].

In 2015, Martins [10] concluded in his thesis that a proper performance study of the HPC could not be done without the T_{25}/P_{25} data, stating "this station is essential to isolate the booster from the HPC in order to study their relationships with the engine performance". Therefore, TAP ME decided to produce the sensor itself, instead of depending on one from CFM which was not practical to use. This implied designing a new sensor, which was done by the intern Dinarte Quintal [27]. His objective was to create a sensor easy to install by the technicians of the test bed, capable of measuring temperature and pressure. Quintal [27] had a limitation: due to confidentiality issues, TAP does not possess the technical drawings of the engine, which makes it difficult to know the exact dimensions of its components [27]. Measuring manually, Quintal was able to determine approximately the dimensions needed. His intention was to use the same location of the previous sensor, but use a different way of connecting the sensor to the test bed. Figure 4.2 presents the location where the sensor is installed on the engine, which helps to understand the main cause why the pressure tube needs to be bent, therefore causing its malfunctioning. This figure also contains the design of the sensor produced by Quintal [27].

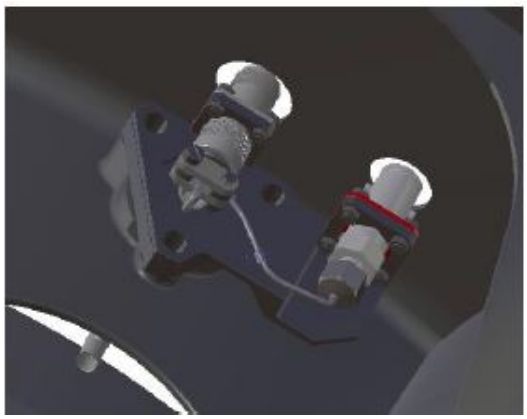

Figure 4.2: Positioning of the sensor on the CFM56-3 engine - Top view [27]

Figure 4.3 has the side and top views of the new sensor in computer-aided design (CAD). The design

has 4 main components, which are numbered in this figure, and are described next:

1. Probe, a component which has a thermocouple and a pressure tube inside it and exposes them to contact with the flow. The pressure tube is attached to a pneumatic plug, the pressure connector, component three, which then sends a pneumatic signal to the test bed where then the pressure is read. A thermocouple is a sensor capable of measuring temperature, through two welded wires of different metals on its tip. The two metals react differently to temperature changes and therefore create an electric voltage which can be measured and converted to a temperature measurement. A thermocouple was used due to its simplicity, robustness and affordability.
2. Pressure connector which channels the air from the pressure tube to a socket from the test bed.
3. Temperature plug that receives the thermocouple electrical wires and makes a connection, through pins and sockets, to a socket on the test bed.
4. Central support of the sensor that connects all the other components.

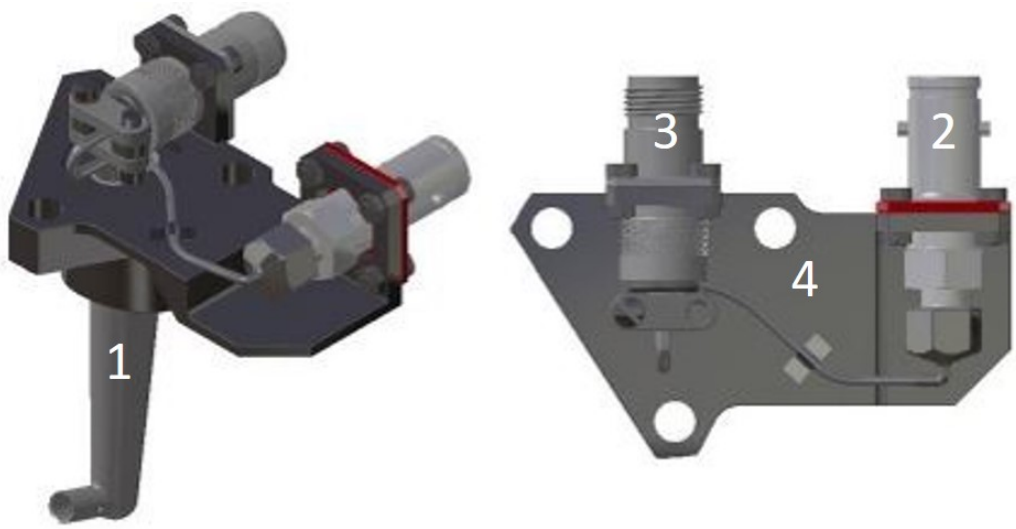

Figure 4.3: New sensor designed in CAD with its components numbered [27]

Component one already existed at TAP, since it was part of the previous CFM sensor, presented in Figure 4.1. The thermocouple and pressure tube inside had to be replaced, because they were damaged, as explained in sub-section 4.2.2. The other three components did not exist in TAP ME. The pressure connector and the temperature plug had to be ordered to specialised manufacturers. Component four is the central support. It serves the purpose of supporting the other parts and it was produced in TAP ME. The other components have predetermined dimensions, because they are standard components produced by external manufacturers. However, component four was entirely produced and developed in TAP ME, so it did not have limitations on dimensions, being the only part that could be adjusted to fit the engine dimensions.

This solution is an improvement over the old one since it does not rely on long tubes directly attached to the sensor. The tubes, which will be hereafter named test bed connections, are inserted separately

after the positioning of the sensor, so there is no need to apply torsion and bending on them. The attachment occurs on components two and three, on the pressure and temperature connections, respectively. The technical drawings of the central support and of the entire sensor are presented in Appendix, in Figures A.1 and A.2, respectively.

The previous CFM sensor measured total pressure and temperature, and the objective is that the new one measures them as well. However, there are more kinds of pressure and temperature of flow, and it is important to understand why this sensor measures the total component. When studying the pressure and temperature of a flow, it is necessary to take into account the three types of components that characterize it: the total component, also referred to as stagnation component, and the static and dynamic components. The total component, as it is represented in equation (4.1) for the pressure variable, p, is the sum of the static and dynamic components [33].

$$p_{total} = p_{static} + p_{dynamic} \tag{4.1}$$

Along this thesis, the total component of temperature and pressure is represented as T and p, respectively. The static component is, as defined by White [17], "the component at any point in the frictionless flow where the velocity is zero" and it does not account for the component related to the movement of the flow. This movement is associated to the dynamic component, which represents the kinetic energy of the flowing flow, and depends on the flow velocity. Along this thesis, the static component of temperature and pressure are represented by T_s and P_s, respectively.

If total and static components are different, they must have different measurement techniques. Static conditions can only be determined accurately by measuring it in such a manner that the velocity component has no influence on the measurement at all. This is carried out by measuring it through a small hole at the wall of the duct, or alternavely, using a pitot static tube, where holes are positioned at right angles to the flow on the surface of the tube. The total component has to be measured inside the flow, parallel and opposite to the fluid direction, to bring the flow to rest, using a pitot tube. This was the type of measurement used in the previous sensor and was the one used in the new sensor as well. This measurement may be used for temperature and pressure, therefore both variables can be measured on the same pitot tube [44]. The difference between the two types of measurement is illustrated in Figure 4.4.

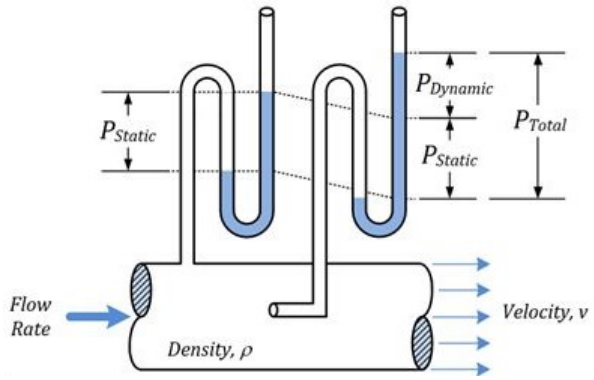

Figure 4.4: Difference between total and static pressure [44]

The objective of this thesis was to manufacture the sensor designed in CAD into a real sensor and test it on the engine. In section 4.2 it is described how this was performed.

4.2 Production of the sensor

4.2.1 3D printing

As mentioned in the previous section, the exact measurements of the engine are not known, and since the space where the sensor is placed is tight, it means the dimensions of the sensor are a very critical factor. The largest issue was if the two plugs would be aligned with the two corresponding openings where they fit on the engine. To build the sensor it would be necessary to invest financial capital and an important amount of time, so it would not make sense to do it without being completely certain it would fit into the engine. To have that assurance, the chosen solution was to use a 3D printer to test the CAD, as it was determined to be the most effective approach. 3D printers are becoming commonly used nowadays to test designs like this one, among other advantages. An example of one of the 3D models of the sensor produced is illustrated in Figure 4.5.

Figure 4.5: Final 3D printed model

In total, three 3D models had to be produced, since the first two did not fit properly on the engine. Figure A.3, in the Appendix, illustrates one of the models tested that did not fit into the engine. The two failed tests were due to the temperature plug, component three, not having enough space, on its respective opening of the engine, to attach to the test bed connection. Some change had to be made to the central support to correct this problem.

This was achieved by reducing slightly the thickness of the central support and by tilting the support of the temperature plug, therefore moving it down. Through a combination of the two modifications, at the third attempt of the 3D assembly, a viable result was obtained as presented in Figure 4.6.

As it can be observed in this figure, component two of the engine is placed in a position on the engine

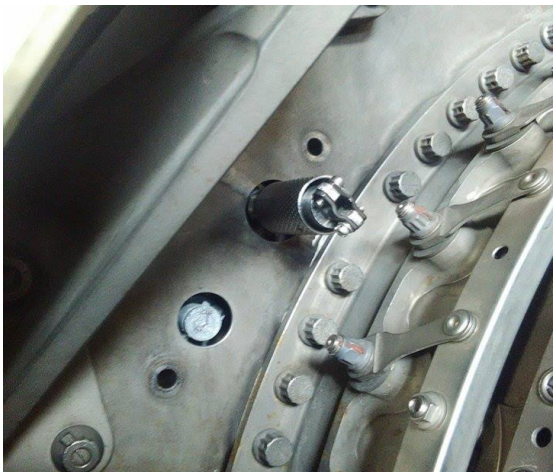

Figure 4.6: Successful test of 3D model with temperature plug attached

opening that allows it to be attached to a temperature plug. This indicated that the design T_{25}/P_{25} sensor was ready to be advanced to the next step, the production of the individual parts.

4.2.2 Acquisition of the parts

As mentioned previously, component one, the probe, was used from the previous sensor, so it did not need to be acquired. Components two and three, the pressure connector and temperature plug, were ordered to their respective suppliers. The technical data from these two components is presented in Figures A.5 and A.6, respectively, in Appendix. Component four the central support was produced in TAP ME, it was manufactured in one of TAP's workshops, with a computer numerical control (CNC) machine with 3+3 degrees of freedom. Figure A.7, on the Appendix, presents the component being produced. The material used for its production was stainless steel as this was the material of the pressure connector ordered. This components' manufacturer recommends an exposure below a temperature limit of 450 K, which is quite higher than the maximum temperature for station 25 of the CFM56-3. The process just took one hour and presented a good quality, as it can be observed in Figure 4.7. With this part concluded and the arrival of the other parts ordered, the sensor could be assembled.

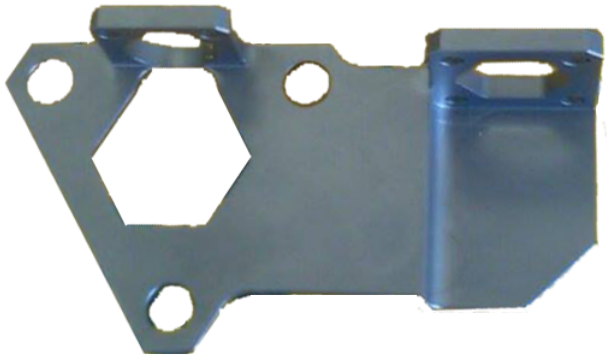

Figure 4.7: Central support of the sensor, produced in TAP ME

4.2.3 Assembly of the sensor

The mounting of the sensor parts included several steps. Firstly, the thermocouple wires and the pressure tube were positioned inside the probe, component 1, and were surrounded by silicone, so the air would not go up this component. The thermocouple used was type K, composed by chromel, a metal formed by 90% nickel and 10% chromium which is non-magnetic, and alumel, a metal composed by 95% nickel, 2% manganese, 2% aluminium and 1% silicon, which is slightly magnetic. This type of thermocouple is considered to read accurately values of temperature between 5 K and 1645 K [45], therefore its range includes the temperatures expected at station 25. Table 4.1 describes the linear relation between voltage and temperature at each 100℃ suggested by Benedict [46], for a type K thermocouple. The unit used was ℃ instead of K since it was the unit used by this author. This relation simplifies calculations, however, the real type K thermocouple curve is not linear and is represented in Figure 4.8, along with other thermocouples and their respective materials.

Table 4.1: Nominal Seebeck coefficients (thermoelectric power) for a type K thermocouple [46]

Temperature (C)	Seebeck Coefficient (μ/C)	Temperature (C)	Seebeck Coefficient (μ/C)
-200	15.3	500	42.6
-100	30.5	600	42.5
0	39.5	700	41.9
100	41.4	800	41.0
200	40.0	900	40.0
300	41.4	1000	38.9
400	42.2		

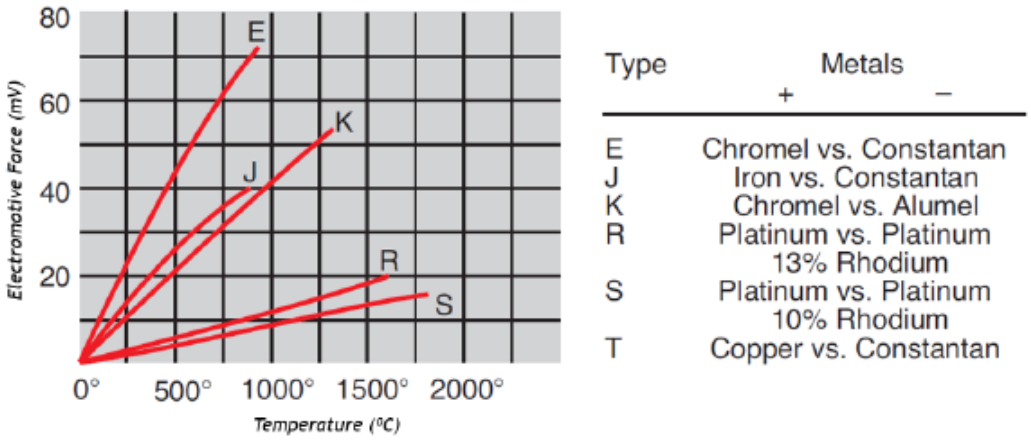

Figure 4.8: Temperature curves of different thermocouples [27]

The pressure tube needs to pass through the different components of the sensor, as it is possible to observe in Figure A.9, in Appendix. Therefore, bending needed to be applied to this tube, which was performed using a thread of nylon inside it. This simple process was essential to prevent the strangulation of the tube, which would lead to the blockage of the air passage.

Component two, which was ordered from outside of TAP ME, could not be directly installed on the sensor. The pressure connector did not have a conic head, which is essential to seal the passage of the air. Additionally, the thread of its head did not match the receiving end of the test bed connection. This was easily fixed on TAP's workshops, through the manufacturing of a conic head, specifically for this component. Afterwards, it was connected to the pressure connector with room-temperature-vulcanization silicone. The result of this procedure is presented in Figure A.8, in Appendix.

The last step was to connect the different components. The connection between the central support and the probe was accomplished through welding. The process selected was Tungsten Inert Gas (TIG). This is a commonly used welding process in TAP ME procedures and it is very appropriate to perform small weld beads as the one intended, and has a small heat input, therefore not overly affecting the material [47]. The remaining connections were done with screws. The sensor production was then concluded. The final version is presented in Figure 4.9 on its front view. The back and side view, are available in Appendix in Figures A.9 and A.10.

Figure 4.9: Concluded sensor - front view

It was then necessary to have connections to the test bed. The former connections from the CFM sensor were reused to provide adequate connections to components two and three. These connections are presented in Figure A.11 and A.12 in the Appendix. The electrical connection of the thermocouple to the temperature connection is done using two pins and two sockets.

4.3 Testing

This section provides a description on how the T_{25}/P_{25} sensor was tested to check its quality and reliability.

4.3.1 Calibration test

To verify the accuracy of the temperature measured by the sensor through the thermocouple, a calibration test was done in a TAP facility specialised in this sort of tests. If the test revealed a different value from the real one, troubleshooting of the sensor could be done before advancing to a test with an engine in the test bed. The test consisted of putting the tip of the sensor in a tank with silicone oil at a controlled temperature of 393 K. Then, with a container of ice to set a cold reference point to 273 K (0℃) and the sensor, both connected to an electronic temperature controller, the value measured by the sensor can be obtained [46]. This procedure is displayed in Figure 4.10. For a better understanding of the procedure for this test, the work of Benedict [46] is recommended. The sensor proved to be accurate, by measuring exactly 393 K. No similar test was available to calibrate the pressure of the sensor, since it is just responsible for the passage of a pneumatic signal from the sensor from the sensor to the test bed. The measurement is done on a transducer on TAP ME's test bed, where the calibration is done periodically, every six months. This calibration is done through a software which automatically performs three types of calibration re-zero, span, and multi-point adjustments. For more information on this, the work of Esterline[48] is recommended.

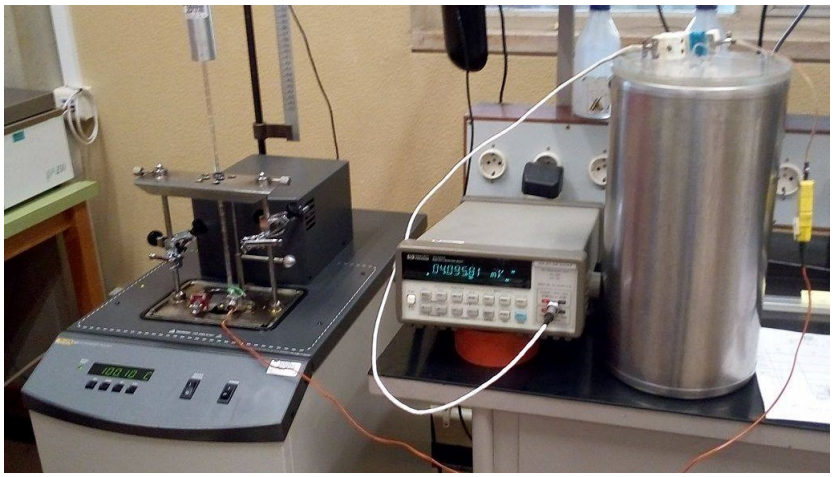

Figure 4.10: Sensor temperature calibration test

4.3.2 Test on the engine

The first question to validate was if the new sensor could be properly installed on the engine. This was tested on an engine in TAP ME's workshop. An issue was found caused by the tip of the temperature plug that was protruding too much. This was an issue that had already been dealt with, during the 3D

model tests. It was caused by the 3D model and the final sensor having small dimensional differences. It was solved by cutting approximately 5 mm from the tip of the temperature plug. This cut reached the thread but it did not prevent the connection of the temperature plug on the sensor to its test bed connection, the one that may be observed in Figure A.12. The sensor could now be properly installed so it could be further tested during an engine run on the test bed.

In the first test, the temperature reading was 328.04 K, a value substantially outside the expected range of 370 K to 390 K, as mentioned in section 4.1. The measurement was certainly incorrect since the difference was quite high. However, the pressure read was 33.0 psi, or 231.6 kPa, a value in the expected range. Therefore, it was concluded that only the temperature measurement was incorrect.

To perform troubleshooting on the sensor to understand the reasons for the above incorrect temperature measurement, it was necessary to understand how a thermocouple circuit works. This is represented in Figure 4.11. As explained in the beginning of the chapter, the thermocouple is composed by two metals of different materials welded on one end. Each metal produces a different electrical potential that varies according to changes in temperature, as represented in section A of Figure 4.11. This rate of change is different for each of the metals in the thermocouple, so a thermocouple produces a voltage that increases with temperature, which is read in section E of Figure 4.11. This is described as the Sebeck effect [49].

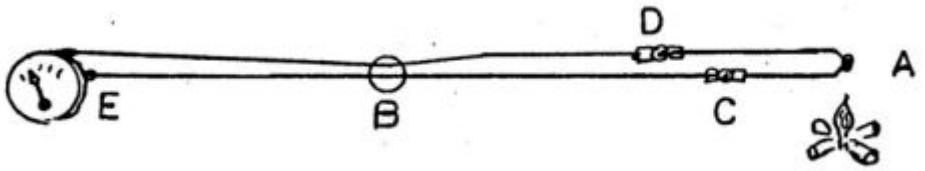

Figure 4.11: Thermocouple circuit [49]

The problem was occurring in section C and D of Figure 4.11, which on the T_{25}/P_{25} sensor consists on the coupling between the temperature plug and the temperature test bed connection. In this coupling, the continuity of the materials has to be kept to ensure a proper reading of the measurements. The connection is done by sockets and pins, therefore the pins have to connect to the sockets of the same material to assure the metal continuity, essential for the passage of the voltage obtained on the thermocouple measurement. However, the materials of the two sockets were swapped, the alumel socket was connected to the chromel pin and the chromel socket to the alumel pin. This led to the generation of a voltage by itself that affected the readings in the test bed. This value translated the temperature at the position where the swapped materials were connected. The solution to solve this problem was to put the two sockets on their correct position, each one with the pin of its respective material. As stated by Benedict [46], problems similar to this one appear quite often when working with thermocouples, and so extra attention has to be given to the connections .

The second calibration test was done with the sensor and the test bed connections, the source of the problem, and is presented in Figure 4.12. The result was 372.8 K for 373 K of reference on the silicone

oil tank. This meant the sensor and its connections were apt to measure temperature, and the problem was fixed.

In total, the new T_{25}/P_{25} sensor was used two times on CFM56-3 engines on TAP ME's test bed. The measurements carried out by the sensor are presented in Table 4.2. The temperature and pressure values presented in this table are the corrected values, explained in section 2.2, which take into account the ambient conditions of temperature and pressure, so a more appropriate comparison can be done between the tests. In Table 4.2, engine 1 is the engine tested with an unsuccessful measurement, where the thermocouple problem was discovered and the value read was 328.04 K. Engine 2 was the second attempt using the sensor, which presented positive results, with a value of 374.14 K, inside the range of temperatures expected 370 K to 390 K. It is possible to observe that the temperature values are quite different, this was due to the incorrect reading of the sensor during the test of engine 1. For the pressure measurement, both results were inside the expected range.

Unfortunately, it was not possible to test the sensor in more engines, but the test of engine 2, provides confidence in the quality of the sensor.

Finally, it is important to be aware that the thermocouple measurement will not be exact. This type of thermocouple, type K, has 2.2 K of error margin, plus the error associated to the test bed conversion of the value. However, it is impossible not to suffer an error associated to a measurement, although a lower one would be possible with a different thermocouple. Nevertheless, it had a much higher cost which did not compensate for the intentions of TAP ME [45]. For the pressure measurement, the transducer available on TAP ME's test bed, Model 9016, is characterized by an error margin of 2.1 kPa [48].

Figure 4.12: Second sensor temperature calibration test

Table 4.2: Values measured with the new T_{25}/P_{25} sensor

Measurement	Engine 1	Engine 2
Corrected temperature (K)	328.04	374.14
Corrected Pressure (kPa)	231.62	231.99

Chapter 5

Performance Calculations

In this chapter it is explained how the calculations with the Gasturb™ software were accomplished. This software was essential for the development of this thesis because it allows the calculation of unknown variables, that were not possible to measure, and it has the ability of comparing different engines.

These calculations were possible after the manufacturing of the T_{25}/P_{25} sensor which was essential to collect the temperature and pressure values from the station just before the entry of the HPC. With these performance calculations it is intended to study the influence of the blade tip clearance on the HPC. Other variables, outside the scope of this thesis, might also be studied with these calculations. By studying their influence, the maintenance procedures can be optimized and therefore cost and time savings can be achieved. These calculations will also enable the second objective intended for this thesis, where the relevance of a sensor in station 25 is investigated.

However, the amount of data available was less than expected in the beginning of this thesis. One of the components used to produce the new sensor took more than three months to arrive, which led to the conclusion of the sensor just three months before the deadline of this work. This made the quantity of engines tested with the sensor very limited. Therefore, to have more data for this study, data from engines measured with the previous sensor owned by TAP ME was used. Unfortunately, due to the frequent damage of this sensor, data was only available on six CFM56-3 engines. This sensor was used for the last time in 2013, and the six engines were tested between 2011 and 2013. In 2017, the only values still on TAP ME's database were the blade tip clearance ones, which motivated the choice of this variable as the focus of the performance study of this thesis. Combining the old and new sensor measurements, there were in total seven engines available to study.

All the engines with available data were from the CFM56-3C rate. This rate is the highest for the CFM56-3 engine and it requires a higher velocity of the low pressure spool, compared to the others, as it may be observed in Table 2.2. The model developed in TAP ME by Martins [10], was done for CFM56-3B2, a lower rate. The model in Gasturb™ created for the engine for this rate, had to be adapted to higher velocities. The objective of this chapter is to describe how this adaptation of the Gasturb™ model, from one engine rate to another, could be accomplished and evaluate if the adaptation was adequate. As it will be shown, the results were not adequate and therefore a new model, suitable for the CFM56-3C

rate, was required. How it was developed, and its results, will be explained in this chapter as well.

This chapter is focused on presenting how the thermodynamic calculations were carried out, what difficulties were found, and which assumptions were necessary. These calculations depend on data from the test bed, so it is important to understand how this data is collected and what transformations are done to it. In section 5.1 this is presented, as well as an introduction to the Gasturb™ software, focusing on the main feature used, the Model Based Test Analysis (MBTA). This is the tool which enables the comparison between engines. Section 5.2 is centered on the Gasturb™ thermodynamic model engine, explaining its necessity. Here, the adaptation from Martins's model [10] to the necessary model is described, revealing the reason for its unsatisfactory results. Section 5.3 is focused on the development of the new engine model.

5.1 Test bed data and Gasturb™

The performance studies in TAP have to start from the data collected in test bed runs of the CFM56-3 engines. However, as mentioned in chapter 2, in the test bed run, the engines are studied in different regimes, so it was necessary to choose which one should be used. Since the most critical EGT margin is during the takeoff regime [2], this regime is the most relevant for the study of the engine performance. Therefore, the take-off regime was the one chosen for the performance studies.

From the test bed data, there are some variables which are essential for the performance calculations described in this chapter. Firstly, N_1 corresponds to the rotation of the pressure spool connecting the fan, booster and LPT all rotating at this speed, which is measured in rpm. N_2 represents the rotation of the high pressure spool which includes the HPC and the HPT that rotate at this speed, also is measured in rpm. w_2 represents the engine air mass flow rate and its units are kg/s. Thrust, as explained in chapter 2, is the force produced by the engine, responsible for the motion of the aircraft. Fuel flow represents the fuel mass flow rate used in the combustion chamber in kg/s. The ratio between this last variable and the thrust represents the TSFC, a very important variable, as explained in chapter 2. Along the engine there are temperature and pressures measured, and for this chapter the most relevant ones are from stations 2, 17, 25, 3 and 54. The numbering of these stations was explained in chapter 2 and it is possible to identify them in Figure 2.3. For these two sets of variables, corrections to the test bed measurements are necessary. Besides the facility corrections, mentioned in chapter 2 and explained on the work of Martins [10], additional corrections need to be done. These corrections are related to the ambient conditions and, therefore, are based on the values of T_2 and P_2, at the entry station of the engine. These corrections convert the measurements to standard day conditions, enabling comparisons between the results of engines with different atmospheric conditions. Using the dimensionless equations:

$$\theta = \frac{T_{01}}{T_{01_{st}}} \tag{5.1}$$

$$\delta = \frac{p_{01}}{p_{01_{st}}} \tag{5.2}$$

The temperature and pressure values are corrected for these standard conditions [43]. T_{01} and p_{01} represent the ambient temperature and pressure values measured during the test bed run, while $T_{01_{st}}$ and $p_{01_{st}}$ stand for the standard day references, which are 288.15 K and 101.325 kPa, respectively [43]. The correction factor θ and δ are then applied to every temperature and pressure values measured on the test bed. For further information, please refer to the works of Saravanamutto et al. [33] and Hill [50].

There is one extra correction necessary to the test bed data, related to station 3 of the engine, the one after the HPC. The measurement of temperature and pressure in this station of the engine are for static conditions and not total conditions. However, as explained in section 4.1, total conditions is the sum between static and dynamic conditions. This means that through these two, it is possible to calculate the total temperature and pressure. This can be done using:

$$T_0 = T + \frac{v^2}{2c_p} \tag{5.3}$$

$$\frac{p_0}{p} = \left(\frac{T_0}{T}\right)^{\frac{\gamma}{\gamma-1}} \tag{5.4}$$

In these equations γ is the heat capacity ratio, v the velocity of the gas and c_p the specific heat capacity at constant pressure. T_0 and p_0 are the total temperature and pressure, respectively and T and p are the static temperature and pressure, respectively [33]. The velocity values are used from Figure B.4 [51], in Appendix, a figure which is described in sub-section 5.3.2.

To understand how the calculations in this chapter were accomplished, it is important to be familiar with how the Gasturb™ software operates. Gasturb™ is a 0D software developed by Joachim Kurzke [35], a specialist in gas turbines, who has worked since the seventies in the field of gas turbine simulation and development, both at academic and industrial environments. A 0D CFD software does not account for geometry effects of the flow in study. Only the thermodynamic data along the flow is taken into consideration while performing the calculations [52]. Gasturb™ is currently on the thirteenth version. However, the version used in the present work was the eleventh, the one available at TAP ME. The software operates in two main modes, design and off-design.

In design mode, the design point of the engine is defined. Kurzke [15] recommends the higher power point of the engine as the best fit for the design point, which is the take-off regime. Off-design mode allows to simulate the operation of the engine in conditions different from the design point [35]. In his paper entitled "How to create a performance model of a gas turbine from a limited amount of information", Kurzke [15] describes a solution for the situation at TAP ME test bed, where the amount of thermodynamic data collected is limited. To deal with this problem, the author suggests the development of a model engine, a concept which is further explained in the following section.

The use of Gasturb™ is already well documented in the work developed at TAP ME by Martins [10]. Therefore, the Gasturb™ tools used in the present work are explained just briefly, with some figures

presented in Appendix. The focus is not on the software itself but more on the challenges found and assumptions made. However, there are two important features from the software, particularly useful for this thesis, that are the MBTA and the Limiters option. Due to their relevance, they are further explained than the others.

The MBTA tool has the objective of matching the model to a set of test data, comparing them. The comparisons are presented in the form of scaling factors. For example, the efficiency factor is a comparison between the efficiency of the component of the engine tested and the component of the model engine. If it is one the efficiency is the same, if it is higher than one the efficiency is higher and if it is lower than one the efficiency is lower. Additionally, for each component, there is another important factor, the flow factor. This variable represents the difference between the test engine corrected flow and the model corrected mass flow rate, for a certain component. Corrected mass flow rate is a variable helpful to study the mass flow rate of an engine component, also known as flow capacity and represented by [33]:

$$\dot{m}_{corrected} = \frac{\dot{m}\sqrt{T_{01}}}{p_{01}} \tag{5.5}$$

As stated by Kurzke [35] in the Gasturb™ manual, this variable is very important when studying the behaviour of a compressor. It is closely associated with its efficiency and pressure ratio and with the positioning of the HPC on its operating line. However, typically the efficiency and the flow factor will present a very similar behaviour, as mentioned by Kurzke [35] ”one percent loss in efficiency, will be accompanied by approximately 1 % loss in flow capacity”. The author also states that, in compressors, the tip clearance has a considerable impact on both these variables, therefore they will both be studied although a similar behaviour is expected [35].

An example of a MBTA test, from the software manual, is presented in Figure 5.1 and it will be used as a reference for a successful MBTA test along this thesis.

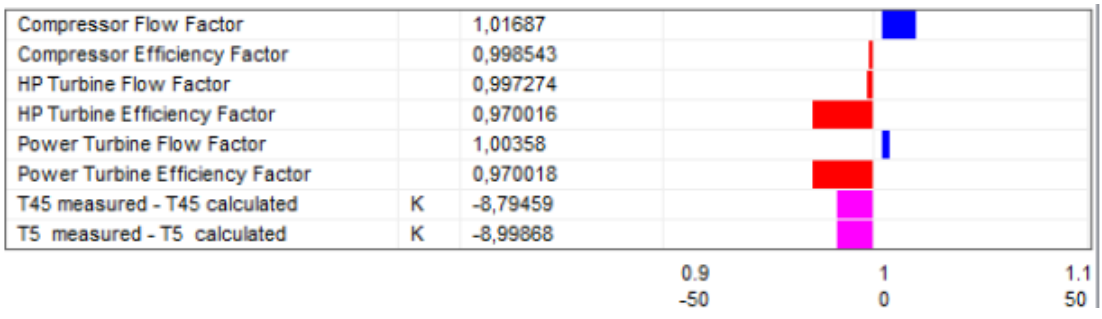

Figure 5.1: Example of MBTA test [35]

The Limiters option is a Gasturb™ convenient tool that interpolates or extrapolates variables for off-design conditions. The Limiters may be applied to more than one variable simultaneously. An example is presented, in Figure B.1 in the Appendix. More knowledge of these two features may be obtained in the work of the Gasturb™ developer Joachim Kurzke [35]. This tool is used in the following section.

The next section is focused on the concept of engine model in Gasturb™ and its application to the context of the present thesis.

5.2 Engine model

5.2.1 Purpose and problem

The idea of having an engine model is suggested by Kurzke [15] for any user working with Gasturb™.The Gasturb™ model is useful to check the effects of the degradations on the overall performance of the engine without needing to solve manually the entire thermodynamic cycle. Then tested engines are compared with this model engine, so that it can be detected which components of the engine are performing better or worse, and by how much. Therefore, the author suggests the model engine used should be stable and with reliable data, since it will be the basis of comparison to all the remaining data sets. Also, when there is a missing measurement from the test engine, the model engine is adapted to the test conditions and used.

Essentially, the choice of the engine to serve as model is quite critical. For this thesis, the engine selected as model was the one from the CFM Correlation Test Report (CTR) [8]. This report is based on a test performed to a CFM56-3 engine, with the intent of defining its facility modifiers on TAP ME's test bed, to correct the test bed run data. As stated by Martins [10], "the correlation engine can be used as a benchmark due to the amount of information available about its performance and because CFM assured it as a stable engine with minimum levels of degradation". This solution has already been adopted before by TAP ME and it is considered the best option among the available data.

As mentioned in section 2.3, the CFM56-3 engine has many different rates at which it can operate. Between these rates, there is no geometric difference between the engines, only on the operating conditions. Each of them works at a different N_1 velocity, which is a highly important variable of the engine [11]. This results in different levels of thrust between them, the CFM56-3B2 operates with a thrust of 97.9 kN and CFM56-3C with 104.5 kN. In most recent years, engines working at a rate of CFM56-3C have been the ones most frequent to pass through TAP ME workshops. Therefore, the data available for this thesis is from engines tested at the CFM56-3C rate. However, the engine model in Gasturb™ developed in TAP ME was focused for the CFM56-3B2 rate. Therefore, the engine model will have a N_1 of 4835 rpm and the engines studied have a N_1 of 4942 rpm for its take-off regime velocity. It does not make sense to compare tested engines to a model engine working at a different rate. Nevertheless, as mentioned in the previous section, Gasturb™ has a solution for this sort of problems, the Limiters tool. Using this tool, an extrapolation can be done to fit the rotational speed of the CFM56-3C. In the next sub-section, the quality of this solution is analysed.

5.2.2 Model testing

The amount of engines available for this thesis was limited to seven. The values corrected for station 25 and 3, essential to study the HPC, are presented in Table 5.1. As it may be observed for engine 7, the

value of P_{25} is considerably low. It should be between 220 and 230 kPa, and it is 180.92 kPa, therefore, the measurement probably was flawed and cannot be trusted [11]. It was replaced by the model value, 224.33 kPa, as suggested by Kurzke [35] in these situations.

Table 5.1: Thermodynamic data related to the HPC

Engine	1	2	3	4	5	6	7
T_{25} corrected (K)	371.01	370.57	369.97	370.19	374.14	369.50	370.84
P_{25} corrected (kPa)	229.53	225.85	231.49	229.86	231.99	220.24	180.92
T_3 corrected (K)	778.25	782.75	778.70	784.16	782.82	781.65	782.89
P_3 corrected (kPa)	2423.39	2502.62	2466.64	2474.55	2432.56	2470.66	2492.72

Using the Limiters option, Martin's model was extrapolated to simulate the conditions of the engine with N_1 at 4942 rpm. Then, with the data from the seven engines in study, the MBTA option was used to compare these engines with the model. The results were not adequate and arose some uncertainty on the quality of the solution being used. Figure 5.2 and B.5, in the Appendix, present the two most critical results obtained on the MBTA, for engines 6 and 3, respectively. Engine six presented the most critical result, with considerably higher efficiency and flow factor, when compared with the MBTA example from Figure 5.1. The most adverse outcome was the HPC flow factor with a value of 1.10, indicating a flow 10% higher than the model engine.

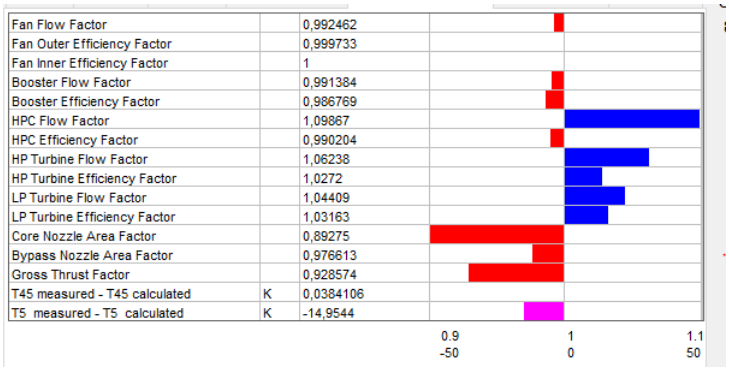

Figure 5.2: Result for engine 6 with the CFM56-3B2 model extrapolated

Due to these results and to the uncertainty and lack of control of having the extrapolation done by a software, it was decided that the best approach to this problem was to make a new model engine, specifically for the CFM56-3C engine. In this new model, there was an attempted to have more control, by doing some calculations manually and compare them with the ones obtained in the model. These will be explained in the next section. Another reason for not approving the solution tested here was that the efficiencies of the compressors, fan, booster and HPC, had values considerably high. As stated by

Boyce [53], axial flow compressors designed for airplanes have efficiencies between 80% and 85%. The values of the model were 90% for the fan, 88% for the booster and 87% for the HPC, values that are substantially higher. In sub-section 5.3.2, the method applied to avoid this problem on the new engine is explained.

5.3 New Gasturb™ model

In the present section, the procedures done to obtain the new Gasturb™ engine model specifically for the CFM56-3C rate, which enables performance calculations with the software, are described. This section is composed by four sub-sections, the first three related to the calculations necessary for the model and the last one with the presentation of the Gasturb™ model obtained. Sub-section 5.3.1 is related to an extra challenge on the conception of this model, when comparing with the one already done in TAP ME. In the CTR, the model engine used by Martins [10], the maximum N_1 rotation tested was 4835 rpm. This is the rotation at which the CFM56-3B2 engine rate operates. However, the CFM56-3C engine rate works at 4942 rpm. Unfortunately, there is no other stable test engine available in TAP ME besides the CTR. Therefore, it was necessary to extrapolate the data from N_1 at 4835 rpm to N_1 at 4942 rpm. This section explains how this was accomplished.

In Gasturb™ there are two helpful tools on the definition of the design point. The most important one is the Iterations option, which allows to iterate certain unknown values through target ones. For example for the HPC efficiency a good target is the temperature in station 3. After defining the iterations and running Gasturb™ the simulation may converge or not. In the first attempts, the software is unlikely to converge [35]. The other tool is the convergence monitor which helps in understanding how adequately the iterations are converging by presenting the square root of the error. The factor for convergence is that none of the iterations can have this value higher than 10^{-9}. Figure B.2, in Appendix presents this feature.

Sub-sections 5.3.2 and 5.3.3 are based on the iterations necessary to build the Gasturb™ model. This model is based on Martins' model [10] but the approach used was different. Martins [10] used eight iterations in his model calculation, which is quite a substantial value. The approach adopted here was to reduce this number, ultimately having more control on the converged result. Accordingly, in sub-section 5.3.2, the efficiencies of each component are calculated manually to have a benchmark on the efficiencies calculated by Gasturb™İn sub-section 5.3.3, the iterations chosen are explained along with the assumptions necessary to find the design point of the new Gasturb™ model.

5.3.1 Dimensional analysis and extrapolations

To understand how the engine would operate at a condition different from the one tested, the common solution for turbomachines is to use dimensional analysis. Dimensional analysis is a method that reduces the number and complexity of experimental variables. It is credited to E. Buckingham who outlined the method in 1914, hence its name: Buckingham Pi theorem. The objective of this approach

consists in grouping variables, thus simplifing experimental work and saving time and money due to the reduction of the number of variables necessary to measure. However, this method has other advantages. It helps in computational simulations, allowing to understand which variables these studies should focus on. The third benefit, and the one that this sub-section is focused on, are the scaling laws. These laws can convert data measured from a small and cheap model to design information for a large and expensive prototype. For a valid scaling law, it can be declared that a similarity exists between the model and the prototype [17].

For gas turbines there are four relevant dimensionless equations, which help studying them. These are presented in the following equations, adapted to this problem from [33]:

$$\left(\frac{N}{\sqrt{T_{01}}}\right)_{4835} = \left(\frac{N}{\sqrt{T_{01}}}\right)_{4942} \tag{5.6}$$

$$\left(\frac{p_{02}}{p_{01}}\right)_{4835} = \left(\frac{p_{02}}{p_{01}}\right)_{4942} \tag{5.7}$$

$$\left(\frac{\dot{m}\sqrt{T_{01}}}{p_{01}}\right)_{4835} = \left(\frac{\dot{m}\sqrt{T_{01}}}{p_{01}}\right)_{4942} \tag{5.8}$$

$$\left(\frac{\Delta T_0}{T_{01}}\right)_{4835} = \left(\frac{\Delta T_0}{T_{01}}\right)_{4942} \tag{5.9}$$

These equations are widely used in the design of gas turbine engines. The objective was to apply these equations as scaling laws and through them use the data collected with the N_1 = 4835 rpm test to know their values at N_1 = 4942 rpm conditions.

However, it was quickly understood that this solution was not feasible. To start, it was necessary to choose the equations that included N_1 since this was the variable that had to be changed, so the CFM56-3C conditions can be understood. This variable is present in equation (5.6). Consequently, the value of T_{01} would be different, in other words, for a compressor that received air directly from the environment, the ambient temperature and pressure values would be altered by this component's rotation. Since these values are ambient conditions, they have to be independent of the compressor, thus this is not a proper solution. Since N_1 was the only variable known at CFM56-3C conditions and, as just explained, this one cannot be used, there is no possibility of using scaling laws for this problem.

The only option left was to resort to an extrapolation of the CTR values using a data sheet. The CTR has values of the CFM56-3 engine tested for many velocities, from 2900 rpm to 4835 rpm and measuring relevant variables as temperatures and pressures. Through an extrapolation these values can be estimated at 4942 rpm. The extrapolation results with the data sheet were satisfying, with correlation coefficients, for a quadratic formula, of 0.99. In Figure 5.3 an example of one of these extrapolations is presented, in this case it is for the thrust. The data used for this extrapolation is presented in Table B.1, in Appendix, and in Figure 5.3 are represented by the black points. With these points a trendline which

relates the thrust and N_1 was obtained, and its equation is below the trendline. Using this equation it was possible to estimate the value of the thrust at 4942 rpm, and the point obtained was the yellow one in the plot, with 105.28 kN. Extrapolations like this one were conducted for the other variables defined as the most relevant for the conception of the model engine, which were listed on section 5.1. The outcome of these extrapolations is presented in Table 5.2. In this table the values at N_1 = 4835 rpm and at N_1 = 4942 rpm are presented.

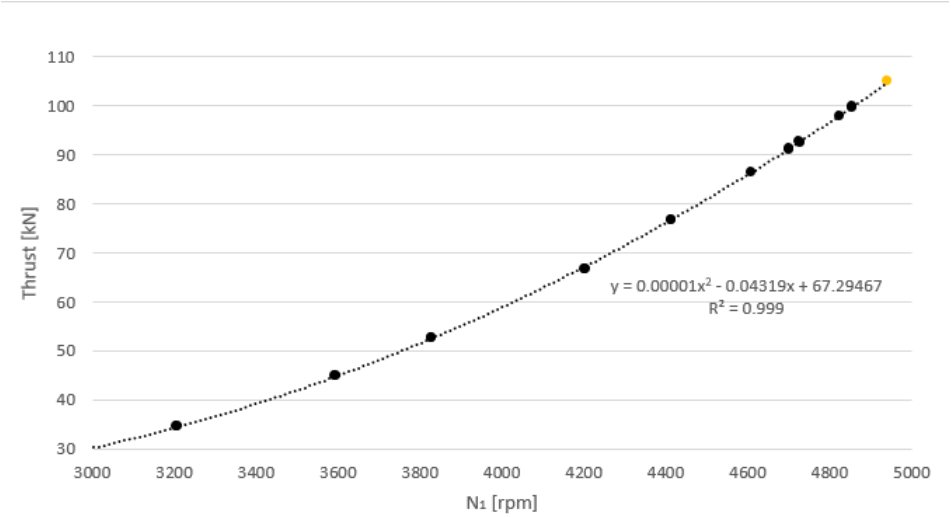

Figure 5.3: Extrapolation example

5.3.2 Calculation of efficiencies

As mentioned at the beggining of this section, with the previous model, the efficiencies for the engine's compressors were considerably higher than the ones of a common axial compressor. This sub-section has the objective of preventing this from occuring with the new model. The approach used was to not just trust on the values presented by the software but also attempt to have some critical evaluation of the results. The solution found was to calculate manually the isentropic efficiencies, through common thermodynamic equations [33]:

$$\eta_{Fan} = \frac{T_{17_S} - T_2}{T_{17} - T_2} \tag{5.10}$$

$$\eta_{HPC} = \frac{T_{3_S} - T_{25}}{T_3 - T_{25}} \tag{5.11}$$

$$\eta_{HPT} = \frac{T_{45_S} - T_4}{T_{45} - T_4} \tag{5.12}$$

$$\eta_{LPT} = \frac{T_{54_S} - T_{45}}{T_{54} - T_{45}} \tag{5.13}$$

Table 5.2: Extrapolation Results

Variable	Value for 4835 rpm	Value for 4942 rpm
N_2	14276.84 rpm	14418.06 rpm
$\dot{m}_2$	314.71 kg/s	322.82 kg/s
T_{17}	339.65 K	341.79 K
P_{17}	167.93 kPa	171.75 kPa
T_{25}	370.70 K	373.77 K
P_{25}	219.94 kPa	224.33 kPa
T_3	786.19 K	809.32 K
P_3	2371.00 kPa	2613.49 kPa
T_{54}	872.89 K	887.65 K
P_{54}	148.63 kPa	152.43 kPa
Fuel flow	1.09 kg/s	1.15 kg/s
Thrust	99.65 kN	105.28 kN

Each of these formulas is aimed at a different component of the engine. For the turbines calculations, equations (5.12) and (5.13), there is a substantial data limitation, the only measured data available are the temperature and pressure of station 54. This is a greater limitation due to the substantial influence of the turbines on the global performance of the engine. The EGT margin is highly influenced by the turbines efficiencies, since it is where this variable is measured [14]. Although the focus of this thesis is the HPC, if, in future studies, it is intended to simulate on Gasturb™ the influence of the HPC on the overall engine, reliable data of the turbines is necessary. By contacting CFM International, the manufacturer of CFM56-3, TAP ME obtained a figure representing the variation of the thermodynamic variables, pressure, temperature and flow velocity, along the engine. This figure describes the values of these variables at every station of the engine and it is available in Appendix, Figure B.4 [51]. Thus, the approach chosen was to calculate the efficiency of the turbines using the values from this figure but still use T_{54} and P_{54} from Table 5.2, in the model. It is assumed that the efficiencies of the engine that Figure B.4 represents are the same of the CTR. Due to lack of data, it was the only possible solution found.

In Table 5.3, the outcome of the calculations with equations (5.10) to (5.13) is presented.

The calculated values are close to the typical efficiencies of axial compressors and turbines sug-

Table 5.3: Calculated efficiencies

Component	Efficiency
$\eta_{Outerfan}$	0.869
η_{HPC}	0.822
η_{HPT}	0.873
η_{LPT}	0.912

gested by Boice [53]. The compressors, fan and HPC are close 0.85 of efficiency and the LPT and the HPT are close 0.9.

5.3.3 Gasturb™ iterations and the assumptions made

As recommended by Kurzke [15], to obtain the new model design point, it is necessary to do iterations. The objective in this thesis was to have a reduced number of iterations, and with the approach chosen to study the turbines, mentioned on the previous sub-section, this is possible. Martins [10] used eight iterations, and four of them were for the turbines, which in this case are not necessary since the efficiencies can be directly defined. Then by adjusting variables as pressure ratios, thrust, fuel flow and the remaining efficiencies manually, it is just necessary to iterate the compressors temperatures and the air flow entering the engine. In conclusion, four iterations were necessary, resulting in a reduction of four in the required number of iterations.

Two major assumptions were necessary to develop this engine model. The first, was the one stated for the turbines, where the efficiencies of a different CFM56-3C were assumed to be the same as of the CTR, selected for model engine. The second assumption was that the outer fan and the inner fan have the same efficiency, since they are the same components, although Gasturb™ separates them, as it may be seen in Figure 5.4. Outer fan represents the efficiency of compression of the air directed to the cold flow and inner fan for the compression of the hot flow.

While doing these iterations and adjustments at the design point of the model, it was realized that it would not be possible to obtain a convergence of Gasturb™ with all the values exactly equal to the ones of Tables 5.2 and 5.3. Therefore, it was defined as an objective for this model, to have less than 1% error on these variables.

5.3.4 Model obtained

After several attempts, an adequate design point was obtained, with an error smaller than 1% for all variables. The thermodynamic values that characterize this point are presented in Figure 5.4. It is important to mention that the Gasturb™ nomenclature for the engine stations is slightly different from the one used on this thesis. Gasturb™ defines station 17 as 13 and station 54 as 5.

Station	W kg/s	T K	P kPa	WRstd kg/s
amb		288,15	101,325	
2	322,005	288,15	101,325	322,820
13	269,217	341,79	171,746	173,421
21	52,788	317,69	136,789	41,161
22	52,788	317,69	136,789	41,161
24	52,788	373,77	224,334	27,223
25	52,788	373,77	224,334	27,223
3	52,788	812,84	2613,486	3,446
31	45,345	812,84	2613,486	
4	46,510	1651,00	2482,811	4,554
41	50,205	1594,48	2482,811	4,831
43	50,205	1202,71	597,842	
44	53,372	1180,97	597,842	
45	53,372	1180,97	597,842	18,357
49	53,372	879,50	152,430	
5	53,372	879,50	152,430	62,133
8	53,952	878,81	150,906	63,418
18	269,217	341,79	170,089	175,110
Bleed	0,000	812,84	2613,479	

Efficiency	isentr	polytr	RNI	P/P
Outer LPC	0,8700	0,8793	1,000	1,695
Inner LPC	0,8700	0,8754	1,000	1,350
IP Compressor	0,8550	0,8647	1,202	1,640
HP Compressor	0,8170	0,8655	1,624	11,650
Burner	0,9995			0,950
HP Turbine	0,8835	0,8651	3,322	4,153
LP Turbine	0,9079	0,8926	1,129	3,922

FN	=	106,31	kN
TSFC	=	10,9534	g/(kN*s)
WF	=	1,1645	kg/s
s NOX	=	0,9831	
Core Eff	=	0,4286	
Prop Eff	=	0,0000	
BPR	=	5,1000	
P2/P1	=	1,0000	
P3/P2	=	25,79	
P5/P2	=	1,5044	
P16/P6	=	1,12712	
P16/P2	=	1,67865	
P6/P5	=	0,99000	
A8	=	0,29330	m²
A18	=	0,74236	m²
XM8	=	0,79089	
XM18	=	0,89341	
WBld/W2	=	0,00000	
CD8	=	0,95011	
CD18	=	0,98814	
PWX	=	0,0	kW
V18/V8,id=		0,70310	
WBLD/W22	=	0,00000	
Wreci/W25=		0,00000	
Loading	=	100,00	%
e444 th	=	0,85734	
WBLD/W25	=	0,00000	

Figure 5.4: Thermodynamic data of the model obtained

Table 5.4 compares these values with the ones from Tables 5.2 and 5.3, the ones defined as initial targets. Due to convergence problems, it was not possible to create a design point with the exact data from these two tables. Table 5.4 presents the error of each variable of the converged model. In this table it is possible to observe that some variables have no difference between the extrapolated value and the converged one, the error is zero. These variables were the ones defined as targets of the convergence, which were mainly temperatures, pressures and the mass flow at the entry station. These were the only targets with which a convergence on Gasturb was reached. With the thrust, fuel flow and the efficiencies of the different components it was not possible to converge the engine model. For the thrust, one of the main parameters of an engine, the objective was to have the most reduced error possible, however the value obtained, 0.97%, was the lowest one possible. The model obtained was the only one with all the variables from Table 5.4 with errors below 1%.

After the design point is defined, it is necessary to establish the off-design part of the model. Extended information related to the off-design construction of the model engine can be found in Gasturb™ś manual [35] and on Martins' work [10]. Due to similarity of this part of the thesis with the work of Martins [10], it will not be described. However, an example of an off-design plot, for the thrust, is presented in Appendix in Figure B.3.

With the model completed, the thermodynamic calculations and the subsequent comparisons between engines can be accomplished. To achieve this, as mentioned before, MBTA option of Gasturb™ was used. The MBTA results for engines 3 and 6, which had poor results with the previous model, showed improved results with the new model. The most critical one was engine 6 and it is possible to observe its new improved results in Figure 5.5.

Table 5.4: Error of the CFM56-3C Gasturb™ model obtained

Variable	Extrapolated value	Converged value	Error of the model (%)
T_{17}	341.79 K	341.79 K	0
P_{17}	171.74 kPa	171.75 kPa	0
T_{25}	373.77 K	373.77 K	0
P_{25}	224.33 kPa	224.33 kPa	0
T_3	809.32 K	812.84 K	0.51
P_3	2613.49 kPa	2613.49 kPa	0
T_{54}	879.50 K	887.65 K	0.91
$\dot{m}_2$	322.82 kg/s	322.82 kg/s	0
Fuel flow	1.15 kg/s	1.16 kg/s	0.86
Thrust	105.28 kN	106.31 kN	0.97
η_{Fan}	0.869	0.870	0.11
η_{HPC}	0.822	0.817	0.61
η_{HPT}	0.873	0.884	0.92
η_{LPT}	0.912	0.908	0.44

Engine 3 has its results in Appendix in Figure B.6. Comparing these figures with their previous MBTA results, Figures 5.2 and B.5, it is possible to observe that the deviations from the model are much smaller, indicating that this model is more adequate for CFM56-3C engines. The results still have some divergence from the model, which indicates the model can still be improved. The turbine factors of Figures 5.5 and B.6 are high, which means the model could probably be improved, but without turbine measurements this is hard to achieve. This could be possible by having more sensors on the turbines, specially at station 45, between the two turbines.

For the HPC, which is the focus of this study, the results from Figures 5.5 and B.6 are much better than the ones of 5.2 and B.5. It can be concluded that, for this specific study, this model is more appropriate than the previous solution using the CFM56-3B2 model.

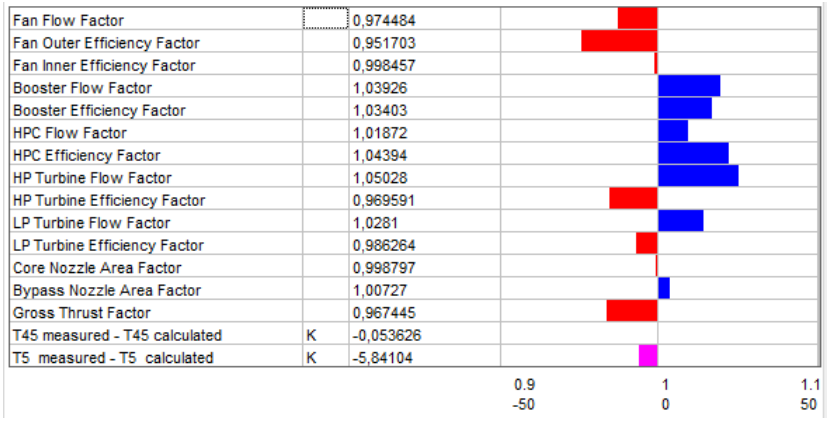

Figure 5.5: Result for engine 6 with the CFM56-3C model extrapolated

Chapter 6

Results and Discussion

Two sets of results are presented in this chapter. The first set, presented in section 6.1, is focused on the tip clearance of the HPC blades considering how it affects the behaviour of this component. The second set of results is related to the T_{25}/P_{25} sensor produced, and is presented in section 6.2. The objective is to understand the relevance of the measurements accomplished with the sensor, in the HPC efficiency calculations. To achieve this, five scenarios with different measurement possibilities are compared. In section 6.3, these results are interpreted and discussed.

6.1 Tip clearance influence on the high pressure compressor

In Table 6.1, the thermodynamic results obtained from the Gasturb™ calculations, described in chapter 5, are presented. Seven CFM56-3 engines are taken into consideration here. For each engine, four variables regarding the HPC component are presented: HPC efficiency, polytropic efficiency, pressure ratio and flow factor. In this section, these variables are correlated to the HPC values of the measured tip clearance defined.

Table 6.1: Thermodynamic data from the engines tested, used for the performance study

Engine	1	2	3	4	5	6	7
HPC efficiency (%)	83.09	84.28	82.95	82.44	83.24	84.63	84.45
HPC polytropic efficiency (%)	88.40	88.40	87.36	86.99	87.56	88.68	88.53
Flow factor	1.003	1.025	0.990	0.982	1.001	1.019	1.023
HPC pressure ratio	10.56	11.45	10.66	10.77	10.49	11.22	11.11

Table 6.2 presents the tip clearances of the seven engines studied established by TAP ME, for the first three stages of the HPC. As stated in chapter 3, the first three stages of the HPC are considered the most relevant and some experimental studies just consider these in their work. Therefore, only the

results for these stages are presented and focused on. The difference between the tip clearances of each engine seems small, however, when considering that, as mentioned in chapter 3, a difference of 0.025 mm in the HPC tip clearance adds about a 0.1 K on the EGT margin, the conclusion is different. Therefore, considerable differences are expected between the HPC performance parameters of the different engines.

Table 6.2: Geometrical data from the engines tested, used for the performance study

Engine	1	2	3	4	5	6	7
1^{st} stage Tip clearance (mm)	1.36	1.39	1.36	1.42	1.45	1.43	1.39
2^{nd} stage Tip clearance (mm)	1.20	1.22	1.19	1.18	1.25	1.26	1.23
3^{rd} stage Tip clearance (mm)	0.78	0.60	0.68	0.66	0.70	0.64	0.76

In Figure 6.1, the effect of the tip clearance of the first stage on the HPC efficiency is presented. However, for the blade tip clearance, the values known are for each stage and the HPC overall efficiency represents the entire compressor, not each stage. Thus, the results obtained would not be conclusive. Therefore, the approach chosen was to use the polytropic efficiency which is related to the efficiency of each compressor stage.

The following charts were done with the seven engines in the study and resorting to a second degree polynomial function to correlate their values. Higher polynomial degrees were not used since they would lead to complex correlations, which was not the objective.

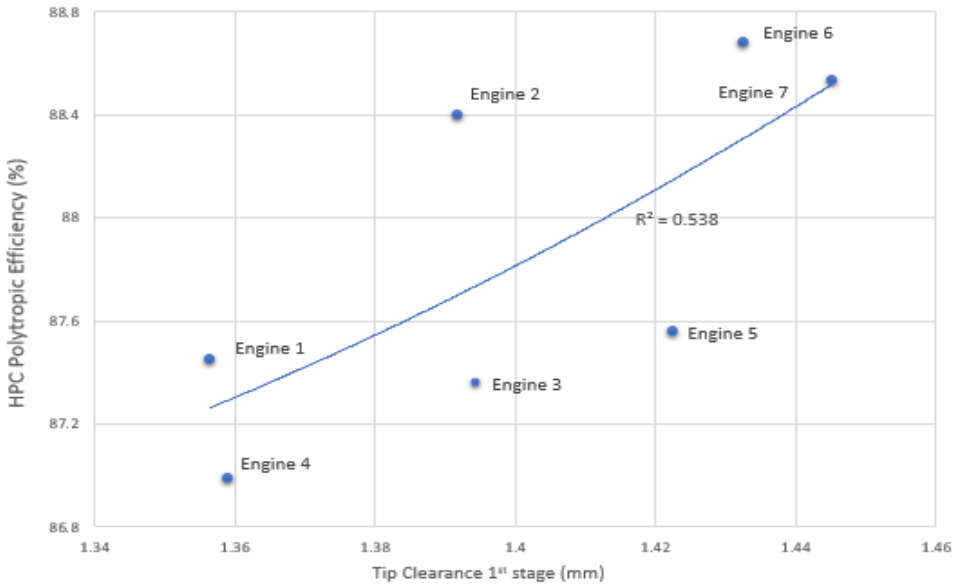

Figure 6.1: Effect of the first stage tip clearance on the polytropic efficiency

The curve obtained in this figure presents an opposite trend to the expected one. The efficiency is increasing with the tip clearance, which is an odd result, since with a greater tip clearance, the losses

are higher leading to a lower HPC efficiency. The correlation coefficient R^2, obtained was 0.54, which indicates that this correlation is inadequate. In Figure C.1, in Appendix the same analysis is done, for the second stage of the HPC.

This curve is similar to the one from Figure 6.1, with the polytropic efficiency increasing with the tip clearance, which is a trend opposite to the expected one. The correlation coefficient is slightly higher than the one before, with a value of 0.62, which is still a low value. However, the result is different in Figure 6.2, where the analysis of the third stage is done.

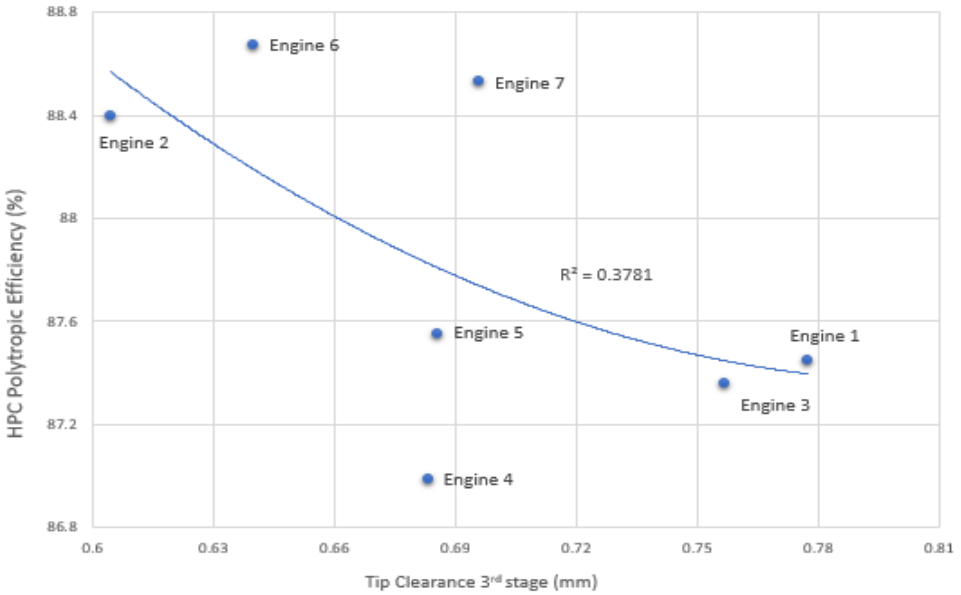

Figure 6.2: Effect of the third stage tip clearance on the polytropic efficiency

This curve presents the expected trend as the polytropic efficiency is decreasing with the increase of the tip clearance. However, the correlation coefficient is 0.38, the smallest so far. These erroneous results may be occurring because the stages are being studied separately, when they should be studied together since all three have a substantial impact on the overall compressor. This led to wonder if the approach of studying the stages separately was the appropriate one.

A different approach was attempted based on the use of a variable suggested by several authors, the dimensionless tip clearance. This variable consists on dividing the blade tip clearance value by the height of the respective blade, as represented by equation (3.1). However, the height of the blade is not measured on TAP ME's maintenance procedures, therefore, its value is not available for the engines studied. The solution used was to adopt a standard blade height measured from a CFM56-3 engine available on TAP ME's workshops. The values obtained were 8.92 cm, 6.72 cm, 5.43 cm, for the first, second and third stages, respectively. With these values it is possible to study the dimensionless tip clearance. However, if this is applied to the results from Figures 6.1, 6.2 and C.1, the outcome would be similar since all the values would be divided by the same constant. The approach chosen was to take advantage of the nondimensiolization of tip clearance to combine the three first stages of the HPC.

In summary, due to the erroneous results of Figures 6.1, 6.2 and C.1, an alternative approach was necessary which led to the use of the dimensionless tip clearance. It was used to combine the three

first stages and evaluate the overall compressor, not just the three separate stages. Therefore, the HPC parameter used for this curve was the HPC overall efficiency, instead of the polytropic efficiency. The result obtained is presented in Figure C.2.

The curve obtained presented again a different trend than the one expected, with the HPC efficiency decreasing at first and then increasing for higher dimensionless tip clearances. The correlation coefficient was much smaller with a value of 0.01. Therefore, the dimensionless tip clearance is not an adequate solution, since the correlation coefficients suggest it is worse than the one attempted in Figures 6.1, 6.2 and C.1. The two approaches used did provide adequate results. Unfortunately, due to lack of measurements of chord of the compressor blades, a third approach is not possible to study. The objective was to use the tip clearance-chord ratio, calculated using equation (3.2).

After the erroneous results obtained with the HPC efficiencies, it was decided to focus on another parameter used in several tip clearance studies, the HPC pressure ratio. The same four curves were done. In Figure 6.3, the effect of the tip clearance of the first stage on the HPC pressure ratio is presented.

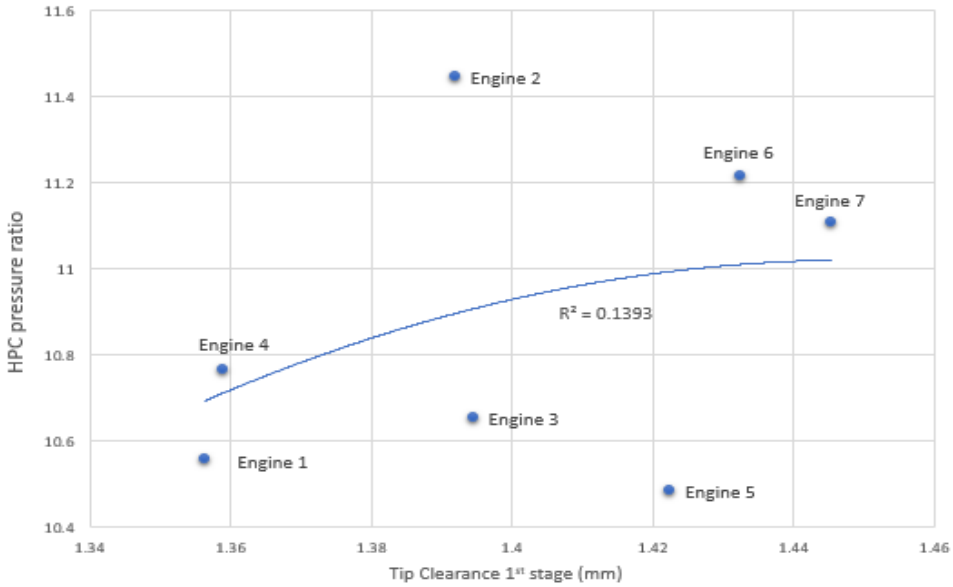

Figure 6.3: Effect of the first stage tip clearance on the HPC pressure ratio

This outcome is similar to the one of Figure 6.1, with the efficiency increasing with the tip clearance value. The correlation coefficient obtained was 0.14 which is considerably smaller than the one from the curve of Figure 6.1. In Figure C.3 the same analysis is done for the second stage of the HPC.

The curve represents, again, the pressure ratio increasing with the tip clearance and has a correlation coefficient of 0.44. Once more, the trend of results is the opposite of the expected one. Figure 6.4 is focused on the third stage.

This curve has a similar behaviour as Figure 6.2, since the pressure ratio decreases with the tip clearance, as expected. The correlation coefficient is the highest of the entire scope of curves, with a value of 0.70. This different trend for the third stage results is likely to be related to other unaccounted parameters of the HPC that changed besides of the HPC, for example the blade chord.

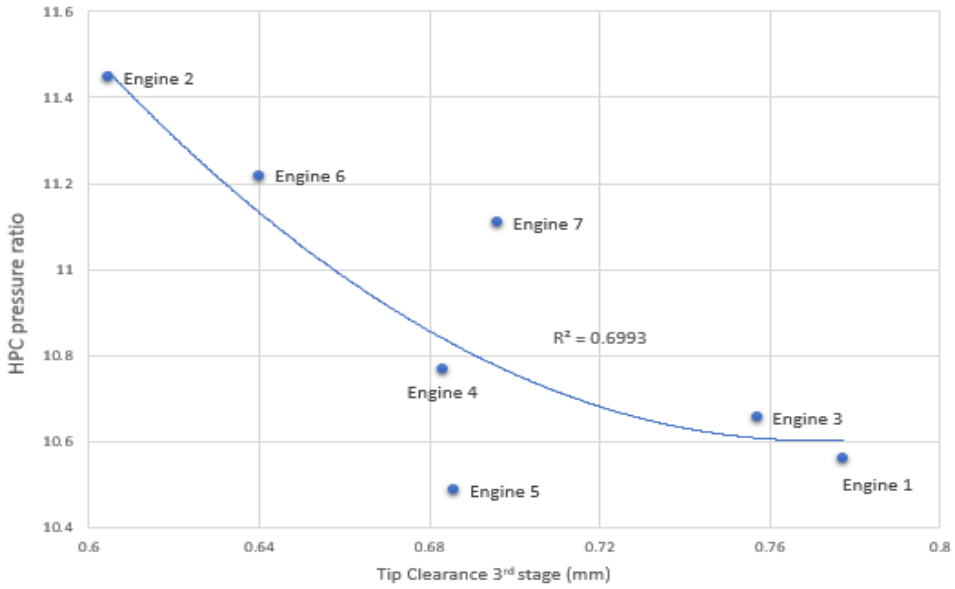

Figure 6.4: Effect of the third stage tip clearance on the HPC pressure ratio

Lastly, the approach done in Figure C.1, using the dimensionless tip clearance was adopted for the pressure ratio in Figure C.2.

The outcome obtained has a correlation coefficient of 0.3, not as small as the one of Figure C.1, but still smaller than the others. This result confirms that the dimensionless tip clearance approach used here is not reliable.

The curves done above are presented as well for the HPC flow factor in Figures C.5, C.6, C.7 and C.8, on the Appendix. The results are very similar to the efficiency curves of Figures 6.1, 6.2, C.1 and C.2. It can be concluded that the tip clearance has a very similar impact on the HPC efficiency and on the HPC flow factor, due to the very similar correlation coefficients obtained. Therefore, this leads to the conclusion that this variable is not essential for the study of the effect of tip clearance on the HPC.

The results obtained from this section, seems to suggest that the third stage was having a greater impact on the HPC performance than the others. However, the correlation coefficients of all the curves plotted were too small to make such affirmation with certainty. The only possible conclusion is that the two approaches used are not the most appropriate to study the tip clearance, for the conditions encountered on this thesis. In the studies referred in chapter 3, when the tip dimensionless clearance was handled, the blade chord was constant. The chord is considered to have a considerable impact on the total losses of the compressor. Therefore, this variable should be constant to enable an independent study of the tip clearance. In the tests from TAP ME, the value of this variable was not measured, although it can be assumed that it is not constant. As stated in chapter 3, researchers that dealt with this situation have turned to a different solution, using the tip clearance-chord ratio. Unfortunately, in this thesis, the blade chord values are not available, although, considering the results from section 6.1, it can be understood that it would be the best option to study the tip clearance. By having a ratio combining tip clearance and blade chord, the two main variables responsible for axial compressors losses would be studied together.

6.2 T_{25}/P_{25} sensor relevance

In order to complete a performance study of the HPC without a T_{25}/P_{25} sensor developed, Kurzke [15] recommends the use of the values from the model engine. In chapter 5, this solution was adopted in the MBTA tests for the stations without instrumentation on TAP ME's test bed. Therefore, it is possible to calculate the performance parameters obtained if the sensor was not developed. Currently, TAP ME has available for the CFM56-5B engine, a T_{25} sensor. This motivated another addition to this study, to understand if just measuring pressure or temperature would result in much different results in Gasturb™If that would be the case, it could motivate TAP ME to add a pressure measurement to their current sensor. Additionally, there is another intention for the current study. As mentioned in chapter 2 and presented in equation (2.1), CFM recommends a correlation based on the N_1 and T_2 values to calculate the T_{25} value, when a measurement is not possible. The validity of this solution is tested to understand if it is a reasonable alternative to the use of a sensor. Therefore, the thermodynamic values of five different scenarios are compared. These scenarios are presented below.

- Calculations done using values from the T_{25}/P_{25} sensor.
- Calculations done without any sensor data, with the T_{25} and P_{25} values obtained from the model engine.
- Calculations done with the value from a T_{25} sensor and with P_{25} obtained from the model engine.
- Calculations done with the value from a P_{25} sensor and with T_{25} obtained from the model engine.
- Calculations done with the value from a P_{25} sensor and with T_{25} obtained from the CFM correlation.

One of the engines used had a very low $P25$ value, 180.92 kPa, when values between 220 and 230 kPa are expected. This is presented in Table 5.1 and it led to the conclusion that it was an incorrect reading from the sensor. Thus, the $P25$ model value was adopted for the calculations of this engine. Therefore, the data from this engine is not used on this section, because this engine results are dependent on the model engine data and a comparison between it and the model data would not be independent. Therefore, the results presented are just for six engines. Figure 6.5 presents a chart of the HPC efficiency values of the five scenarios allowing a comparison between them.

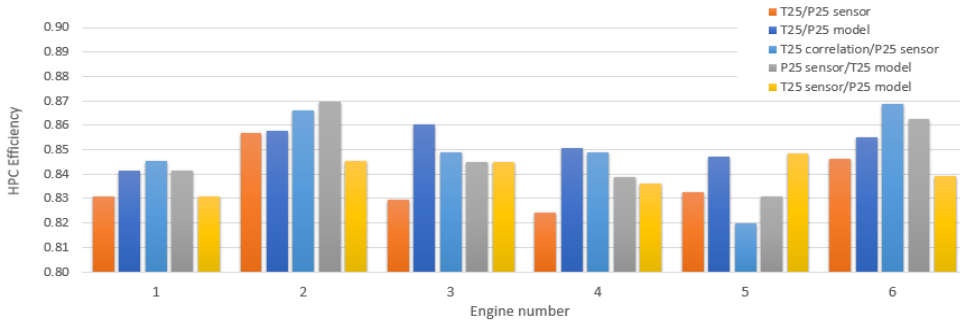

Figure 6.5: Comparison of the HPC efficiency obtained in Gasturb™ for five different scenarios of the T_{25}/P_{25} sensor

This plot allows for a visual comparison, but it is hard to have a concrete perception of the differences between the scenarios. To help with this, the results are displayed in Table 6.3. This table presents the difference of the HPC efficiency, in percentage, between the real value, considered to be the value obtained using the sensor, and the other four scenarios. The absolute averages of these differences are also presented.

Table 6.3: Difference between the HPC efficiency obtained with the T_{25}/P_{25} sensor and the one obtained with the other four scenarios (%)

Engine	1	2	3	4	5	6	Absolute average
T_{25}/P_{25} Model	-1.27	-0.09	-3.74	-3.20	-1.76	-1.06	2.01
P_{25} sensor and T_{25} model	0.00	1.35	-1.86	-1.45	-1.94	0.84	1.24
T_{25} sensor and P_{25} model	-1.27	-1.46	-1.85	-1.73	0.18	-1.92	1.40
T_{25} CFM correlation and P_{25} sensor	1.70	1.07	2.27	2.89	-1.54	2.61	2.01

From this table it can be understood that the results with the engine model are the ones with larger differences with an average error of 2% in the efficiency value. Without the sensor, this scenario would be the only option to use, thus a performance study on the HPC would be compromised by a 2% error. If two engines had HPC efficiency of 83%, one of them could be calculated by Gasturb™ to have 81% and the other 85%, which is quite a significant difference. For the P_{25} sensor and T_{25} sensor scenarios the averages of the differences have values of 1.24% and 1.40%, respectively. These values are quite close, and are smaller than the first scenario. The fourth scenario, the one with the CFM correlation, presents an average difference of 2.01%, a high value close to the one of the first scenario. The same analysis is done for the pressure ratio in Figure 6.6 and in Table 6.4.

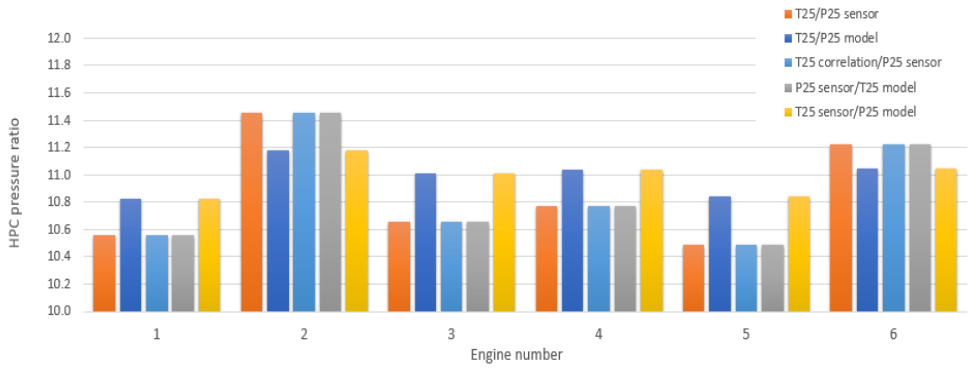

Figure 6.6: Comparison of the HPC pressure ratio obtained in Gasturb™ for five different scenarios of the T_{25}/P_{25} sensor

In Figure 6.6, the results are just dependent on the pressure values, therefore, the scenarios with the same pressure value used have obviously the same results. This is observed in Table 6.4 where the

Table 6.4: Difference between the HPC pressure ratio obtained with the T_{25}/P_{25} sensor and the one obtained with the other four scenarios (%)

Engine	1	2	3	4	5	6	Absolute average
T_{25}/P_{25} model	2.40	-2.42	3.18	2.45	3.23	-1.54	2.53
P_{25} sensor and T_{25} model	0.00	0.00	0.00	0.00	0.00	0.00	0.00
T_{25} sensor and P_{25} model	2.40	-2.42	3.18	2.45	3.23	-1.54	2.53
T_{25} CFM correlation and P_{25} sensor	0.00	0.00	0.00	0.00	0.00	0.00	0.00

first and third scenarios have an average difference of efficiency of 2.53%, a considerably high value. The other scenarios do not present any difference to the T_{25}/P_{25} sensor results. Figure 6.7 and Table 6.5 present the analysis for the polytropic efficiency.

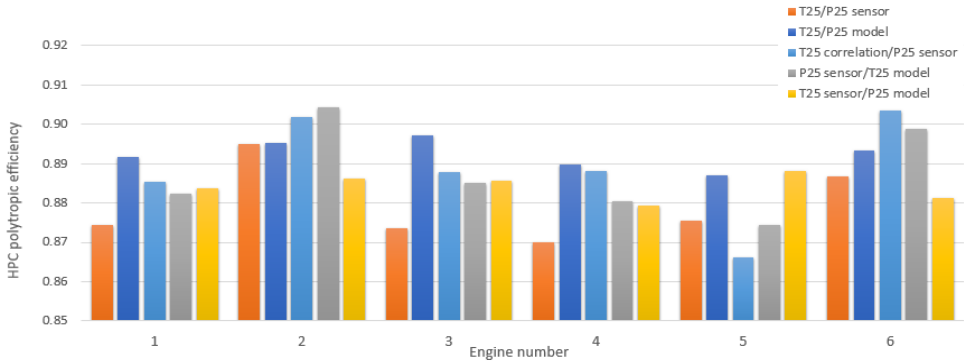

Figure 6.7: Comparison of the HPC polytropic efficiency obtained in Gasturb™ for five different scenarios of the T_{25}/P_{25} sensor

Table 6.5: Difference between the HPC polytropic efficiency obtained with the T_{25}/P_{25} sensor and the one obtained with the other four scenarios (%)

Engine	1	2	3	4	5	6	Absolute average
T_{25}/P_{25} model	1.93	0.02	2.62	2.24	1.27	0.72	1.62
P_{25} sensor and T_{25} model	0.90	1.02	1.29	1.20	-0.13	1.34	0.98
T_{25} sensor and P_{25} model	1.04	-1.00	1.34	1.06	1.41	-0.62	1.08
T_{25} CFM correlation and P_{25} sensor	1.22	0.75	1.61	2.05	-1.09	1.85	1.43

As in Figure 6.5, Figure 6.7 reveals differences between all the scenarios with no particular relation between them. In Table 6.5, it is possible to observe that for the polytropic efficiency the differences are smaller than the ones obtained for the other two variables. The results are identical to the ones of the HPC efficiency, with the T_{25}/P_{25} sensor as the one with the higher error, 1.62%, followed by the CFM correlation scenario with 1.43%. The second and third scenarios have an error close to 1% and are again quite similar. Figure 6.8 and Table 6.6 present the analysis for the flow factor.

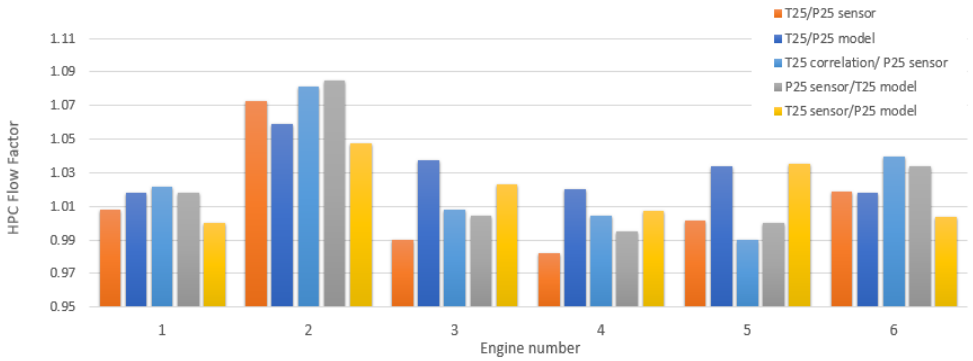

Figure 6.8: Comparison of the HPC flow factor obtained in Gasturb™ for five different scenarios of the T_{25}/P_{25} sensor

Table 6.6: Difference between the HPC flow factor obtained with the T_{25}/P_{25} sensor and the one obtained with the other four scenarios (%)

Engine	1	2	3	4	5	6	Absolute average
T_{25}/P_{25} model	-0.95	1.30	-4.72	-3.91	-3.26	0.04	2.83
P_{25} sensor and T_{25} model	0.00	2.38	-3.27	-2.56	-3.40	1.49	2.19
T_{25} sensor and P_{25} model	-1.79	-1.11	-1.40	-1.33	0.14	-1.46	1.20
T_{25} CFM correlation and P_{25} sensor	1.28	0.81	1.73	2.22	-1.16	2.00	1.53

Again this figure reveals differences between all the scenarios with no particular relation between them. In Table 6.6, the error obtained with the T_{25}/P_{25} model is the highest so far, with a value of 2.83% of difference on the flow factor. The CFM correlation scenario presents a value of 1.53%, not as high as 2.83%, but still considerably high. The second scenario has an error of 2.19%, also a considerably high value a result, which is 1% higher than for the third scenario. The difference between these two was not so high as the results presented in the other tables. The T_{25} sensor is the scenario with the best results.

It is possible to observe the four charts, from Figures 6.5 to 6.8 in Appendix C, in Figures C.9 to C.12, in a larger format, to allow their examination with improved detail.

This study had the objective of understanding how significant the T_{25}/P_{25} sensor is on the results of four important variables, calculated with Gasturb™Às understood in Figures 6.5 to 6.8, the results are considerably different between the five scenarios analysed, with no particular pattern between them. Thus, the charts are interesting to realise that there are, in fact, important differences between the outcome of the five scenarios, nevertheless it is difficult to reach conclusions analysing them. Hence, the need for Tables 6.3 to 6.6.

In these tables, the real scenario, the one where the calculations are performed with the T_{25}/P_{25} sensor, is compared with the others. On these comparisons it is possible to understand that the T_{25}/P_{25} model has the worst average of results, which is not surprising, since it is the scenario with less measured data.

The P_{25} sensor and T_{25} sensor, have smaller differences, typically between 1% and 1.5%, except for the pressure ratio. These errors are still considerably high, justifying the importance of having both variables measured. Additionally, it is not possible to distinguish which measurement, T_{25} or P_{25}, would allow accomplishing a smaller error.

The correlation scenario performed equally or worst than the P_{25} sensor, for three of the four performance parameters studied, raising some doubts on the correlation's quality.

Chapter 7

Conclusions and Future Work

7.1 Achievements

The first achievement of this thesis was the successful production of a sensor capable of measuring temperature and pressure for the CFM56-3 engine, at the station between the booster and the HPC. This sensor had its development concluded through 3D models produced with a 3D printer, essential to test the assembly and disassembly of the sensor on the engine. Afterwards, the sensor was produced, calibrated and tested with positive results.

The second achievement was the development of a Gasturb™ model engine, explicitly for the CFM56-3C rate, the one which most often passes through TAP ME's workshops. However, this step had a considerable constraint, since the only available data was the one of an engine performing at lower rotations. Therefore, in this thesis, a method to extrapolate an engine's data and develop a model with it was achieved.

After the model was concluded, it was possible to study the tip clearance effect on the performance of the HPC. In this study, the dimensionless tip clearance was used and the results obtained presented unreliable trends, most of them with an opposite behaviour than the expected one. Therefore, the main conclusion is that for this particular situation, another approach should be carried out, the use of the tip clearance-chord ratio. According to the literature researched, this variable allows the addressing of the two main blade features accountable for the losses of an axial compressor, the tip clearance and the blade chord.

The final achievement was reached through a study of the relevance of the T_{25}/P_{25} sensor. Scenarios of alternative measurements were tested, even testing the reliability of a correlation defined by CFM, to replace the T_{25} measurement. This correlation presented a considerable error and did not prove to be a good option. In the comparison between an isolated temperature measurement and an isolated pressure measurement, it was not possible to conclude which one gave the best results, although they both performed better than the CFM correlation. Considering the entire scope of results, it can be stated that the investment on the development and production of a temperature and pressure sensor for station 25 is a substantially superior option than its alternatives. Therefore, this study motivates the addition

of a pressure measurement in the T_{25} sensor of the CFM56-5B engine available in TAP ME's test bed. This would prevent considerable errors in the calculations of the HPC performance parameters. Errors which on this study were higher than 1%.

Both these studies were performed with a low amount of test engine data, nevertheless, the conclusions of this thesis are important. Therefore, it would be relevant to test a wider set of engines in order to reinforce the confidence in the results.

7.2 Future work

After this thesis, further research studies could be conducted, such as:

- Adopt test bed runs always using the T25/P25 sensor so more HPC performance studies can be possible.
- Continue the tip clearance study by adopting the tip clearance-chord ratio, which was found to be adopted by a substantial number of researchers working in this field. To achieve this, it is essential to perform detailed measurements of the HPC blade chord length during the maintenance procedures of a turbofan engine.
- Extend the amount of variables studied, focusing at least, on the four variables described in section 2.3, blade chord, tip clearance, seal teeth clearance and CDP seal. They are not independent from each other, therefore they should not be studied independently.
- To improve the engine's overall behaviour, the focus cannot rely only on the HPC. Gasturb™ tools can be applied to understand the HPC and the operation of the engine, studying the impact of this component's performance on TSFC or EGT margin. To achieve this, it is important to have an improved CFM56-3C model, which is still limited by the lack of turbine data. Therefore, the instrumentation of TAP ME's test bed should be improved, increasing the data collected from these components, more specifically in station 45 between the HPT and LPT.

Bibliography

[1] R. Storm, M. Skor, L. Koch, T. Benson, and C. Galica. *Pushing the Envelope: A NASA Guide to Engines*. National Aeronautics and Space Administration, Glenn Research Center, 2007.

[2] S. Ackert. Engine Maintenance Concepts for Financiers: Elements of Turbofan Shop Maintenance Costs. Technical report, Aircraft Monitor, 2011.

[3] G. Cros. Industry Trends Maintenance Cost. Technical report, International Air Transport Association, 2015.

[4] Aircraft Maintenance Facilities — TAP M&E [Online] Available at: https://www.tap-mro.com/Pages/About TAP ME/Maintenance-Centres.aspx. [Accessed on 2017-07-26].

[5] D. Culley. More Intelligent Gas Turbine Engines. Technical report, NATO, RTO, TR-AVT-128, 2009.

[6] CFM International. Flight Ops Support - Overview. Technical report, 2005.

[7] P. Walsh and P. Flechter. *Gas turbine performance*. Blackwell Science, Second edition, 2004.

[8] P. Compenat and F. Trimouille. Correlation Test Report of TAP Air Portugal. Technical report, CFM International, 1991.

[9] J. Leite. *CFM56-3 Basic Engine B737-300, Formação Profissional TAP, Revision 3*. TAP Portugal, Internal document, 1992.

[10] D. Martins. Off-Design Performance Prediction of the CFM56-3 Aircraft Engine. Master's thesis, Instituto Superior Técnico, 2015.

[11] CFM International. CFM56-3 General engine data - Training [Online] Available at: http://www.air.flyingway.com/books/engineering/CFM56-3/ctc-142_Line_Maintenance.pdf. [Accessed on 2017-06-18].

[12] A. Henriques. Análise da influência dos procedimentos de manutenção do reactor no seu desempenho em Banco de Ensaio. Technical report, TAP Maintenance & Engineering, Internal document, 2010.

[13] A. Henriques. Análise da influência dos procedimentos de manutenção do motor CFM56-3 no seu desempenho em Banco de Ensaio. Technical report, TAP Maintenance & Engineering, Internal document, 2011.

[14] Aircraft Commerce (redaction). CFM56-3 Maintenance Analysis & Budget. *Aircraft Commerce*, 45 (5):18–28, 2006.

[15] J. Kurzke. How to Create a Performance Model of a Gas Turbine From a Limited Amount of Information. *In proceedings of the Turbo Exposition, Power for Land, Sea, and Air, American Society of Mechanical Engineers*, GT2005-68536, 2005.

[16] A. Ridaura. Correlation analysis between HPC blade chord and compressor efficiency for the CFM56-3. Master's thesis, Instituto Superior Técnico, 2014.

[17] F. White. *Fluid Mechanics*. McGraw-Hill, Seventh edition, 2009.

[18] F. Baptista. A 0-D Off-Design Performance Prediction Model of the CFM56-5B Turbofan Engine. Master's thesis, Instituto Superior Técnico, Lisbon, Portugal, 2017.

[19] C. Wu and W. Wu. Analysis of Tip-Clearance Flow in Turbomachines. Technical report, Polytechnic Institute of Brooklyn, Department of Mechanical Engineering, DTIC AD0036783, 1954.

[20] Blade Tips Grinding Machine DANTIP — DANOBAT [Online] Available at: https://www.danobatgroup.com/en/mbtg-dantip. [Accessed on 2017-08-29].

[21] Private Communication - TAP Portugal.

[22] R. Hendricks, T. Griffin, and T. Kline. Relative Performance Comparison Between Baseline Labyrinth and Dual-Brush Compressor Discharge Seals in a T-700 Engine Test. *In proceedings of the 39th International Gas Turbine and Aeroengine Congress and Exposition, American Society of Mechanical Engineers, The Hague, Netherlands, June 13-16*, 1994.

[23] B. Steinetz, R. Hendricks, and J. Munson. Advanced Seal Technology Role in Meeting Next Generation Turbine Engine Goals. *In proceedings of the NATO RTO, Applied Vehicle Technology Symposium on Design Principles and Methods for Aircraft Gas Turbine Engines*, 11, 1998.

[24] M. Florin and B. Spa. Seal teeth. *United States Patent*, US 3846899 A, 2002.

[25] N. Zhang, H. Xuan, X. Guo, C. Guan, and W. Hong. Investigation of high-speed rubbing behavior of labyrinth-honeycomb seal for turbine engine application . *Journal of Zhejiang University-SCIENCE A*, 17(12):947–960, 2016.

[26] S. Wellborn, I. Tolchinsky, and T. Okiishi. Modeling Shrouded Stator Cavity Flows in Axial-Flow Compressors. *Journal of Turbomachinery, American Society of Mechanical Engineers*, 122(1): 55–61, 2000.

[27] D. Quintal. Desenvolvimento e Otimização de Sensores para Ensaio do Motor CFM56-3. Master's thesis, Universidade da Beira Interior, 2017.

[28] A. Flotow, M. Mercadal, and P. Tappert. Health Monitoring and Prognostics of Blades and Disks with Blade Tip Sensors. *In proceedings of Aerospace Conference*, 6(6):433–440, 2000.

[29] P. Dewallef and S. Borguet. A Methodology to Improve the Robustness of Gas Turbine Engine Performance Monitoring Against Sensor Faults. *Journal of Engineering for Gas Turbines and Power, American Society of Mechanical Engineers*, 135(5):1–7, 2013.

[30] J. Denton. Loss mechanisms in turbomachines. *Journal of Turbomachinery, American Society of Mechanical Engineers*, 115(4):621 – 656, 1993.

[31] S. Danish, S. Qureshi, M. Imran, S. Khan, M. Sarfraz, A. El-Leathy, H. Al-Ansary, and M. Wei. Effect of Tip Clearance and Rotor-Stator Axial Gap on the Efficiency of a Multistage Compressor. *Applied Thermal Engineering*, 99:988–995, 2016.

[32] Y. Dong, Z. Xinqian, and L. Qiushi. An 11-stage axial compressor performance simulation considering the change of tip clearance in different operating conditions. *Institution of Mechanical Engineers, Part A: Journal of Power and Energy*, 228(6):614–625, 2014.

[33] H. Saravanamutto, H. Cohen and G. Rogers. *Gas Turbine Theory*. Longman Scientific and Technical, Fifth edition, 2006.

[34] O. Domercq and J. Escuret. Tip clearance effect on high-pressure compressor stage matching. *Institution of Mechanical Engineers, Part A: Journal of Power and Energy*, 221(6):759–767, 2007.

[35] J. Kurzke. *GasTurb 12, Design and Off-Design Performance of Gas Turbines*. GasTurb GmbH, 2015.

[36] D. Wisler. Advanced compressor and fan systems. Technical report, General Electric Aircraft Engine Business Group, Cincinatti, OH, USA, 1988.

[37] D. Wilson. *The Design of High-Efficiency Turbomachinery and Gas Turbines*. MIT Press, Fifth edition, 1984.

[38] B. Lakshminarayana and J. Horlock. Review: Secondary Flows and Losses in Cascades and Axial - Flow Turbomachines. *International Journal of Mechanical Sciences*, 5(3):287–307, 1963.

[39] L. Smith. The effect of tip clearance on the peak pressure rise of axial-flow fans and compressors. *In proceedings of the Symposium on Stall, American Society of Mechanical Engineers*, (TR-AVT-128), 1958.

[40] P. Ramakrishna and M. Govardhan. Stall Characteristics and Tip Clearance Effects in Forward Swept Axial Compressor Rotors. *Journal of Thermal Science*, 18(1):40–47, 2009.

[41] S. Sakulkaew, C. Tan, E. Donahoo, C. Cornelius, and M. Montgomery. Compressor Efficiency Variation With Rotor Tip Gap From Vanishing to Large Clearance. *Journal of Turbomachinery, American Society of Mechanical Engineers*, 135(3):1–10, 2013.

[42] T. Frost, A. Anderson, and B. Agnew. A hybrid gas turbine cycle (Brayton/Ericsson): An alternative to conventional combined gas and steam turbine power plant. *Institution of Mechanical Engineers, Part A: Journal of Power and Energy*, 211(2):121–131, 2005.

[43] J. Borges. *Propulsão, Folhas de Apoio*. AEIST, 2001.

[44] Engineered software, inc [Online] Available at: https://eng-software.com/about-us/press/2016/4/understanding-the-distinction-between-total-static-and-dynamic-pressure/. [Accessed on 2017-07-20].

[45] Thermocouples, wires and connectors — OMEGA Engineering [Online] Available at: http://www.omega.com/toc_asp/frameset.html?book=Temperature&file=TC_GEN_SPECS_REF. [Accessed on 2017-07-15].

[46] R. Benedict. *Fundamentals of Temperature, Pressure, and Flow Measurements*. John Wiley & Sons, Third edition, 1984.

[47] J. Santos and L. Quintino. *Processos de Soldadura*. Edições Técnicas ISQ, 1993.

[48] Esterline. *NetScanner System (9016, 9021 and 9022) User's Manual*. Pressure Systems, Inc, 2007.

[49] C. Road. Practical thermocouple troubleshooting. Technical report, Tanis Aircraft Products, 2006.

[50] P. Hill and C. Peterson. *Mechanics and Thermodynamics of Propulsion*. Addison-Wesley Publishing Company, Second edition, 1992.

[51] Private Communication - CFM International.

[52] H. Kitajima, M. Oshima, T. Iwai, Y. Ohhara, Y. Yajima, and K. Mitsudo. Computational fluid dynamics study of intra - arterial chemotherapy for oral cancer. *BioMedical Engineering Online*, 16(1):1–26, 2017.

[53] M. Boyce. *Gas Turbine Enginnering Handbook*. Butterworth-Hienemann, Second edition, 2003.

Appendix A

Production of the sensor

A.1 Technical Drawings

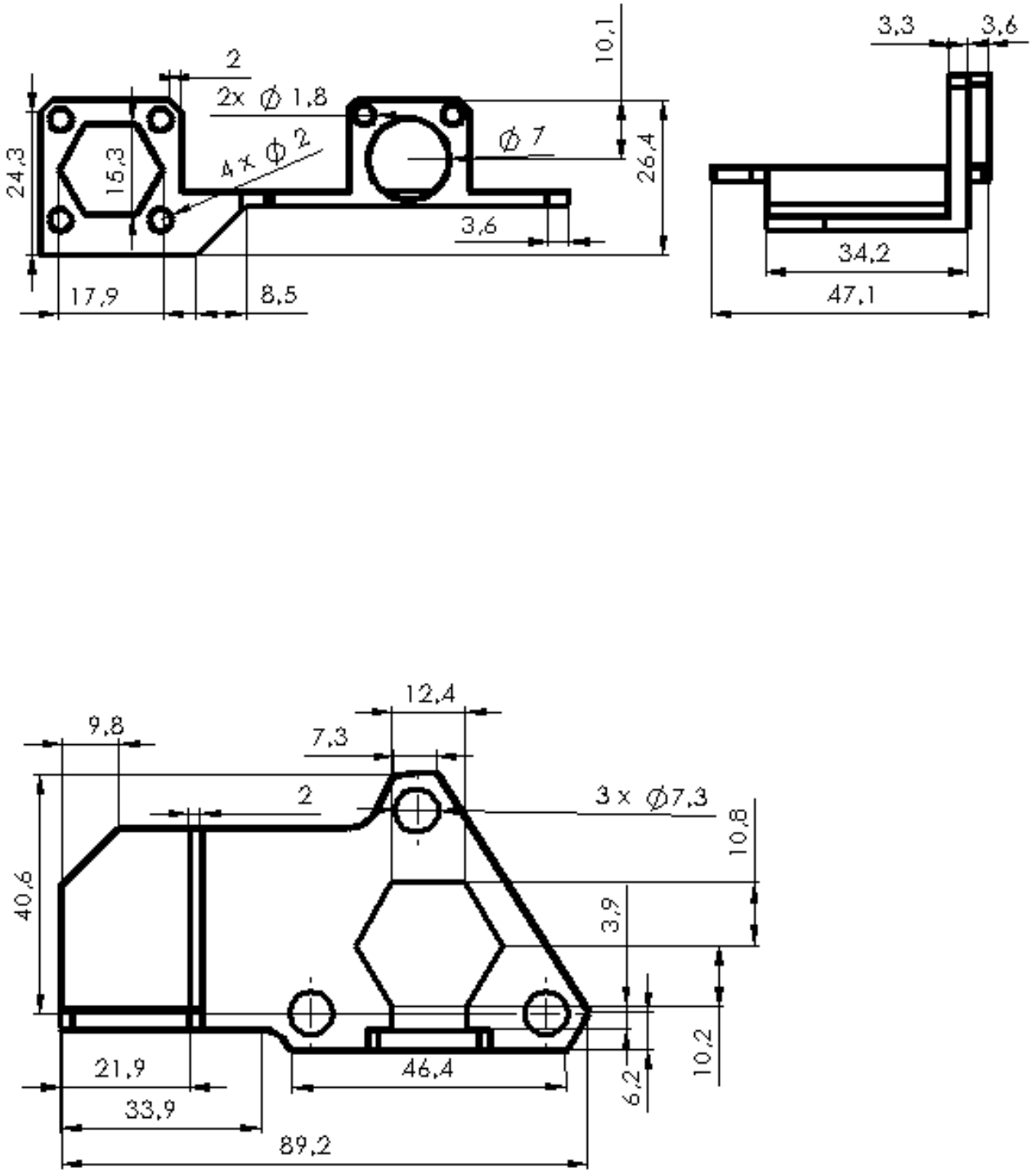

Figure A.1: Technical drawing of the central support of the T25/P25 sensor

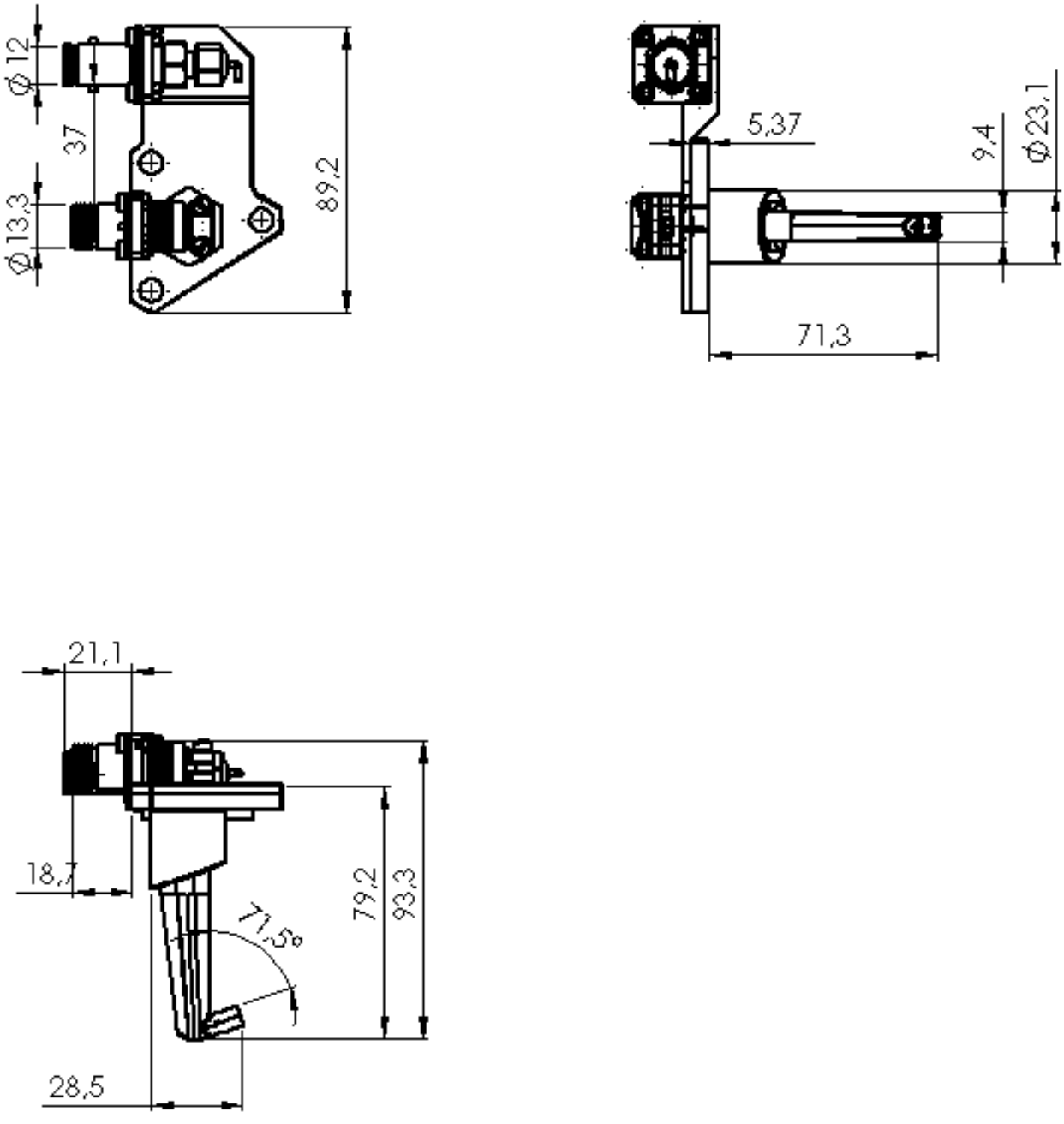

Figure A.2: Technical drawing of the T25/P25 sensor

A.2 3D model tests

Figure A.3: Unsuccessful test of the 3D model positioning on the engine

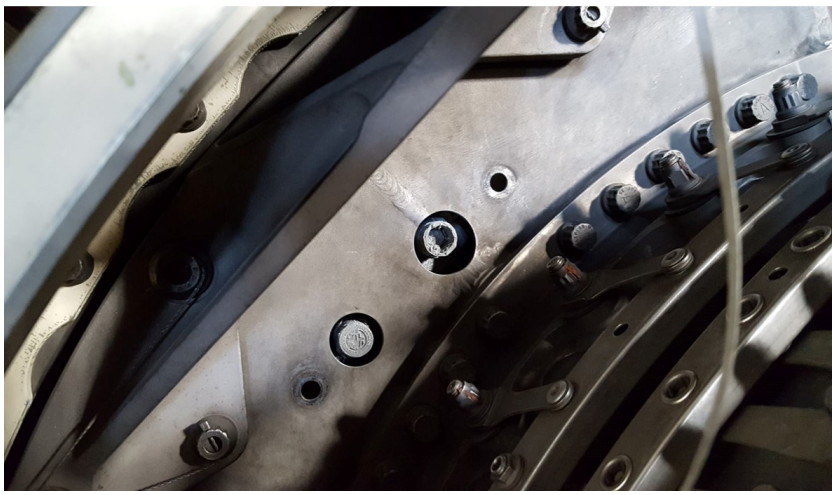

Figure A.4: Successful test of 3D model

A.3 Technical data of the ordered components

Staubli HCB 03 Pressure Connector

Technical Characteristics			
Material:	316L Stainless Steel		
Bore Diameter:	3 mm		
Máx Working Pressure:	350 bar		
Operating Temperature: (depending on the seal material)	Fluorocarbon (FPM): -10ºC to 200ºC Perfluoroelastomer (FFKM): 0ºC to 250ºC Fluorosilicon (FMQ): -40ºC to 175ºC		
Component	Dimensions [mm]		Model Drawing
Bulkhead Socket	Thread	NPT 1/8	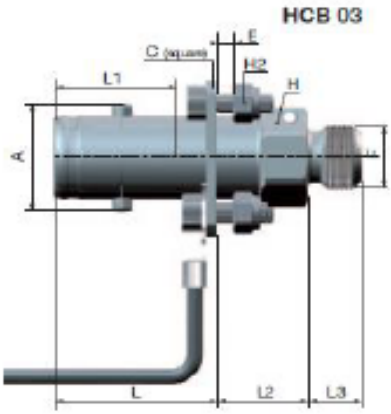
P/N: HCB 03.2250/J/KR/BM	A	16,5	
	C	24	
	L	24,5	
	L1	18	
	L2	13,5	
	L3	9,5	
	L_total	47,5	
	E_min/máx	1/3,5	
	H_flats	14	
	H2_flats	5,5	
Plug	Thread	NPT 1/8	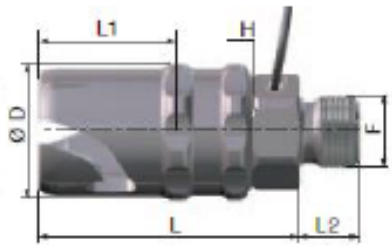
P/N: HCB 03.7250/J	Dia.	19	
	L	35,5	
	L1	18	
	L2	9,5	
	L_total	14	
	H_flats	45	

Figure A.5: Technical data of the pressure connector

Esterline SOURIAU 8533 Series Class K or Similar

Technical Features		
Class	K	
Material:	Shell: Stainless Steel / Plating: Passivated / Seal: Silicone elastomer	
High Vibration Resistant:	Random 5 Hz to 2000 Hz at $1G^2/Hz$ (2 x 8 hours)	
HighTemperature Resistant:	-65°C a 200°C	
Fireproof:	6 min under a 1100°C flame	
Component	**Dimensions [mm]**	**Model Drawing**
Square Flange Receptacle	Thread	½"-20 UNF
SOURIAU ID	Dia. A Máx	14,27
P/N: 8533 0 K S 08 03 P N	Dia. B Máx	12,7
or	C Máx	20,75
TAP M&E Item ID	D	15,09
Component	**Dimensions [mm]**	**Model Drawing**
P/N: EN2997 S0 08 03 M N	Dia. E	3,10/3,30
Plug	B Thread	½"-20 UNF
SOURIAU ID	Dia. A Máx	21,30
P/N: 8533 4 K S 08 03 S N		
or		
TAP M&E Item ID		
P/N: EN2997 K6 08 03 F N		

Figure A.6: Technical data of the temperature plug

A.4 Final sensor

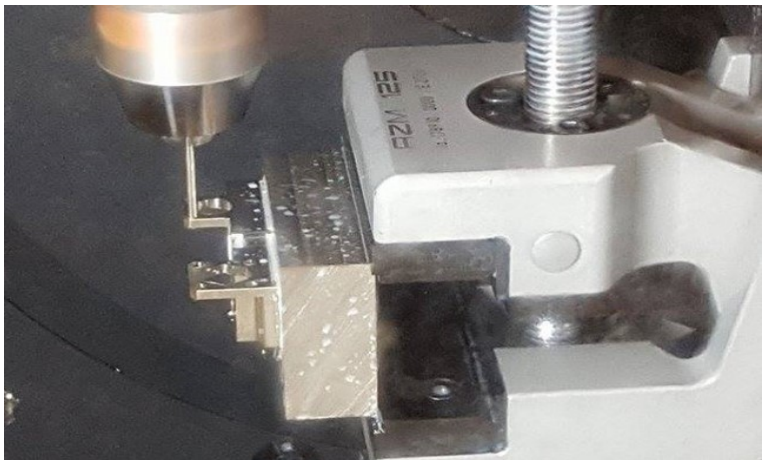

Figure A.7: Production of the central part of the sensor

Figure A.8: Conic head necessary to maintain the air seal during the pressure measurement

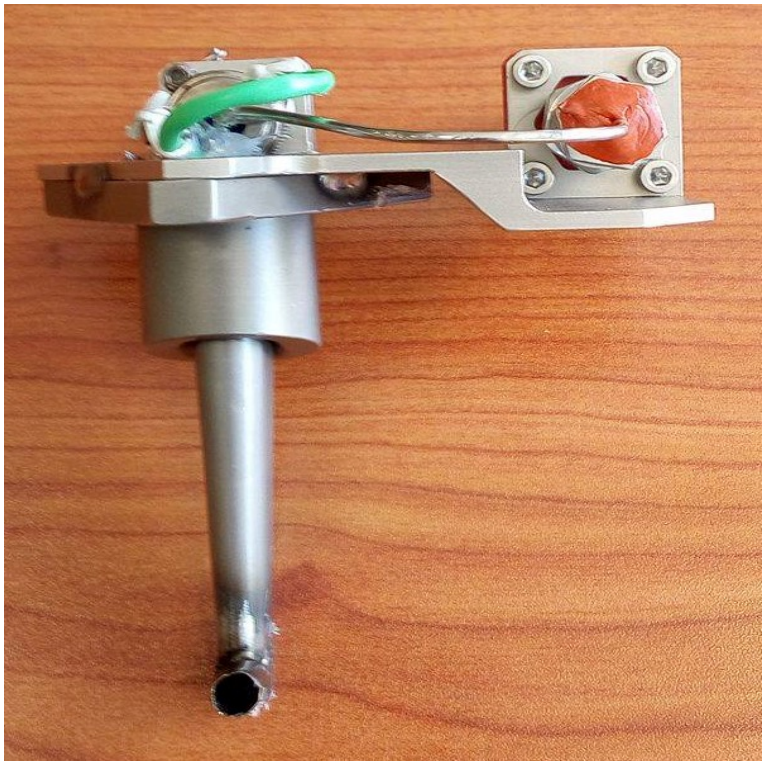

Figure A.9: Concluded sensor - back view

Figure A.10: Concluded sensor - side view

A.5 Test bed connections

Figure A.11: Pressure connection from the sensor to the test bed

Figure A.12: Temperature connection from the sensor to the test bed

Appendix B

Technical Datasheets

B.1 Gasturb™ features

Steady State | Modifiers | Transient | Limiters | Var. Geometry | Iteration

Inactive | Max | Max+Min | Min | Refresh

Max Limits | Min Limits

	Value	Setting	On/Off
Low Press Spool Speed NL [%]	101,0	101	On ✓
Corr Low Spool Speed NLR [%]	101,0	0	Off
High Press Spool Speed NH [%]	100,9	0	Off
Corr High Spool Speed NHR [%]	100,7	0	Off
Comp Exit Temperature T3 [K]	816	0	Off
Compr Exit Pressure P3 [kPa]	2676	0	Off
HPT Rotor Inlet Temp T41 [K]	1610	0	Off
LPT Inlet Temp T45 [K]	1193	0	Off
Turb Exit Temperature T5 [K]	894	0	Off
Fuel Flow [kg/s]	1,1909	0	Off
Net Thrust [kN]	106,5707	0	Off

Figure B.1: Limiters feature from Gasturb™

Loop No.2 | Sum of errors squared = 2,67227E-10

No.	Variable	Value	Relative Value	Error	Value
1	Isentr.IPC Efficiency	0,898655		Booster Exit Temp T2	2,87358E-06
2	Isentr.HPC Efficiency	0,809065		HPC Exit Temperatur	2,26055E-06
3	Isentr.LPT Efficiency	0,889165		LPT Exit Pressure P5	-9,52371E-06
4	Bypass Duct Pressure Ratio	0,977163		Bypass Nozzle Area	5,98213E-16
5	Design Core Nozzle Angle [°]	18,4165		Core Nozzle Area	1,27734E-05

Figure B.2: Convergence monitor

Table B.1: Values used for the extrapolation of the thrust

N_1 in rpm	Thrust in kN	N_1 in rpm	Thrust in kN
3008.75	29.99	4414.20	76.70
3003.96	29.96	4414.45	76.66
3206.97	34.59	4609.92	86.50
3204.51	34.55	4699.89	91.16
3593.56	45.05	4698.98	91.09
3592.42	45.02	4725.89	92.60
3828.21	52.67	4727.53	92.59
3828.21	52.66	4822.97	97.90
4204.49	66.65	4834.57	99.75
4200.64	66.68	4835.10	99.65

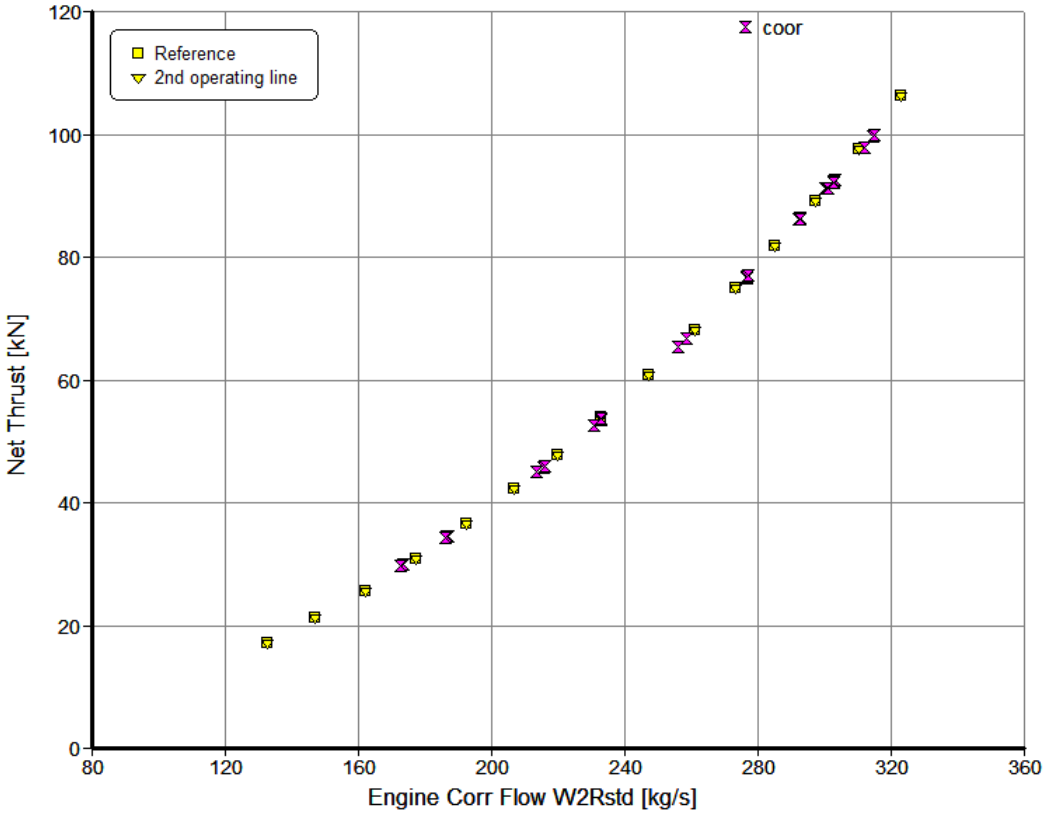

Figure B.3: Off-design curve for thrust on the new Gasturb™ model

B.2 Thermodynamic data along the CFM56-3

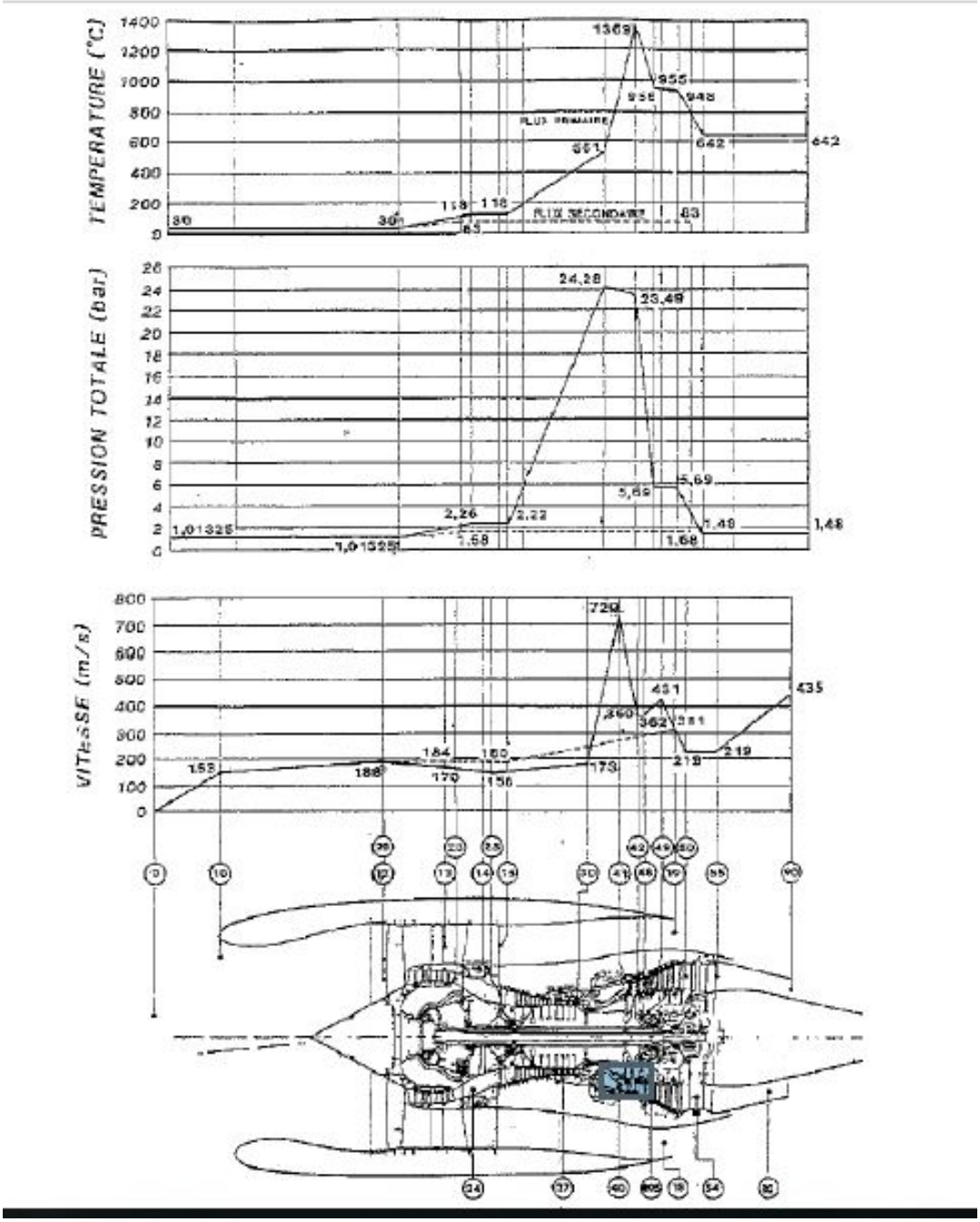

Figure B.4: Data from the CFM56-3 provided by its manufacturer [51]

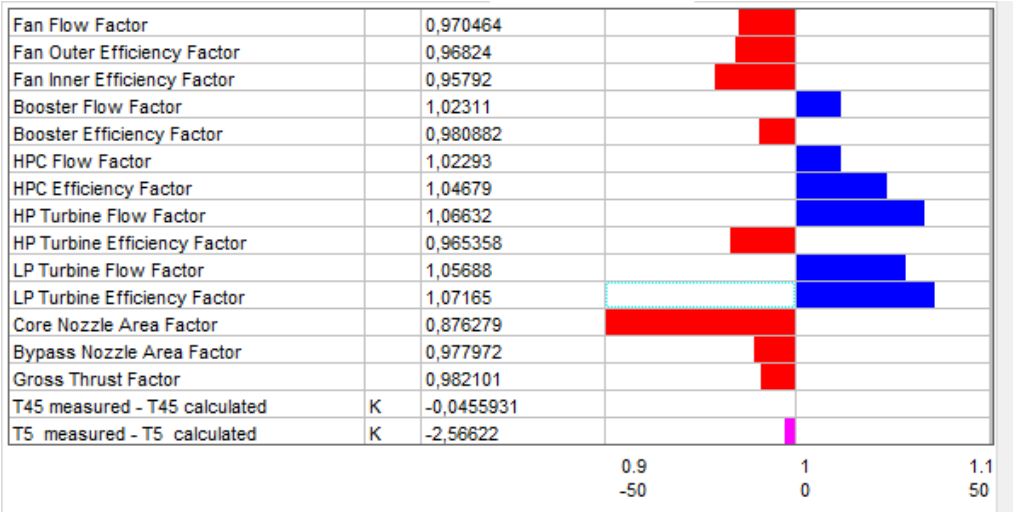

Figure B.5: Result for engine 3 with the CFM56-3B2 model extrapolated

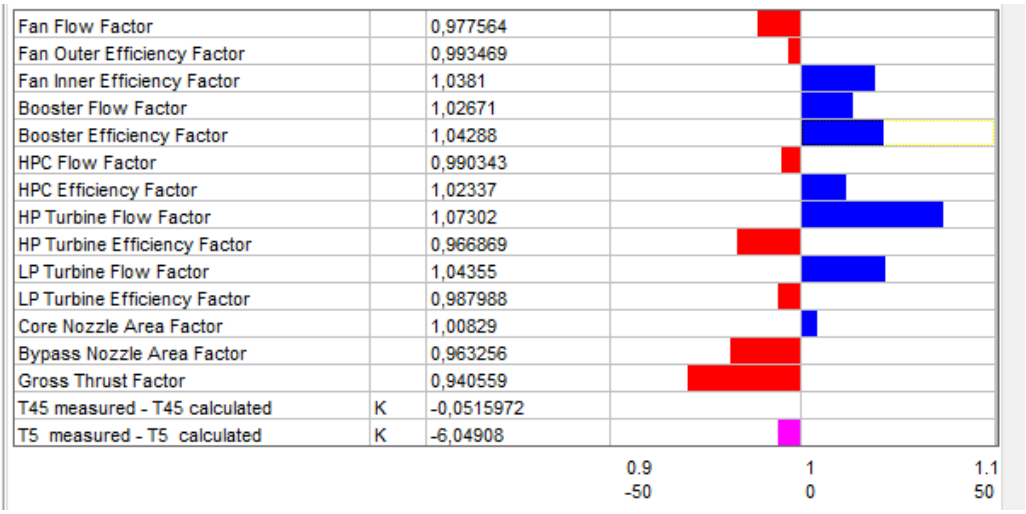

Figure B.6: Result for engine 3 with the CFM56-3C model

Appendix C

Results

C.1 Tip clearance study - HPC efficiency results

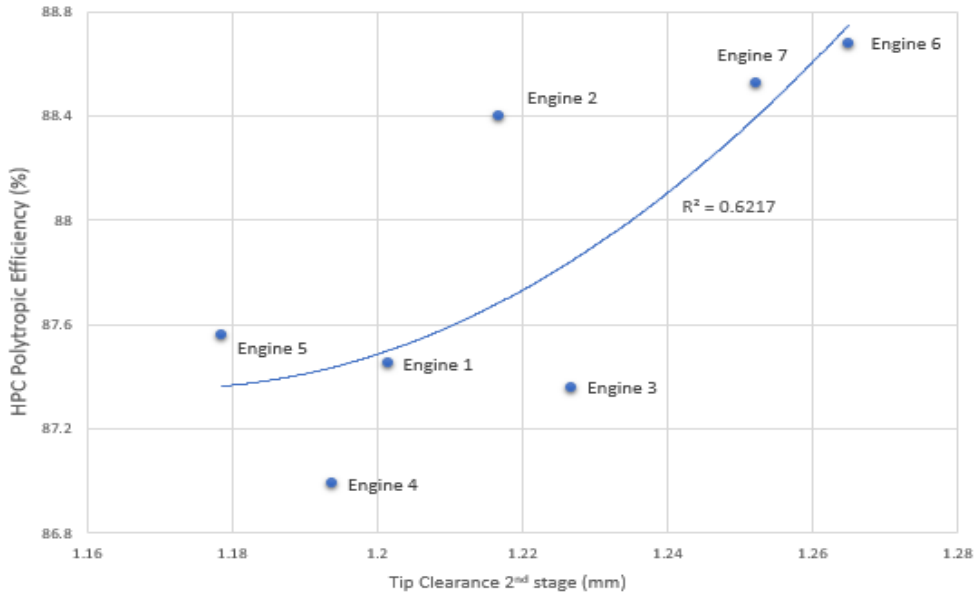

Figure C.1: Effect of the second stage tip clearance on the polytropic efficiency

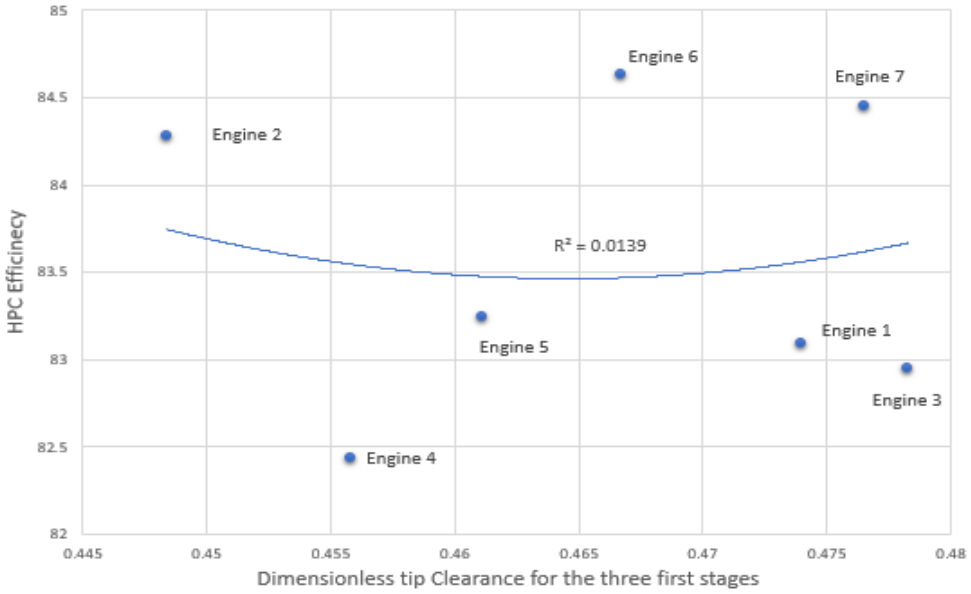

Figure C.2: Effect of the sum of the dimensionless tip clearance of the first three stages on the HPC efficiency

C.2 Tip clearance study - HPC pressure ratio results

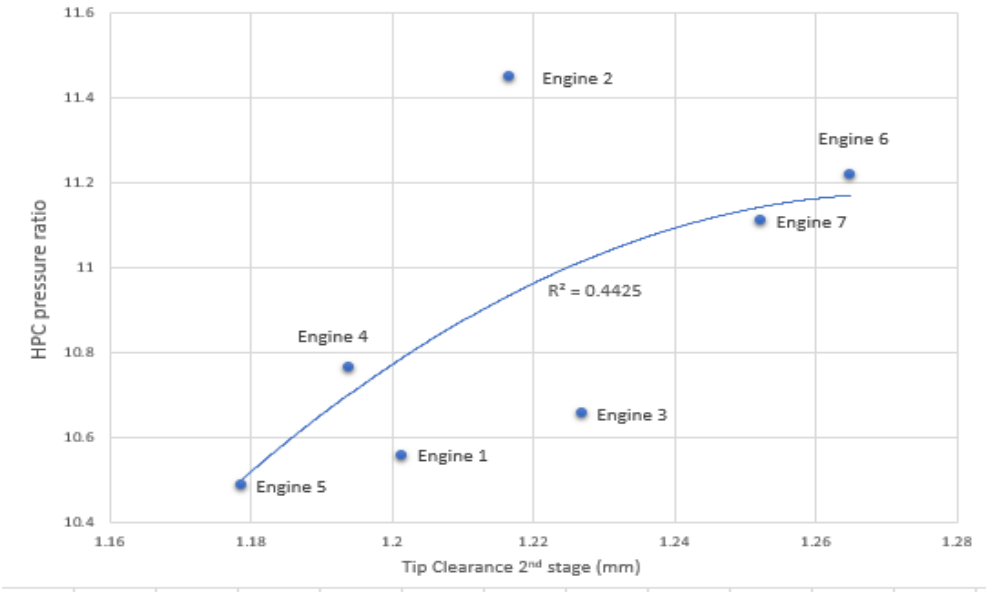

Figure C.3: Effect of the second stage tip clearance on the HPC pressure ratio

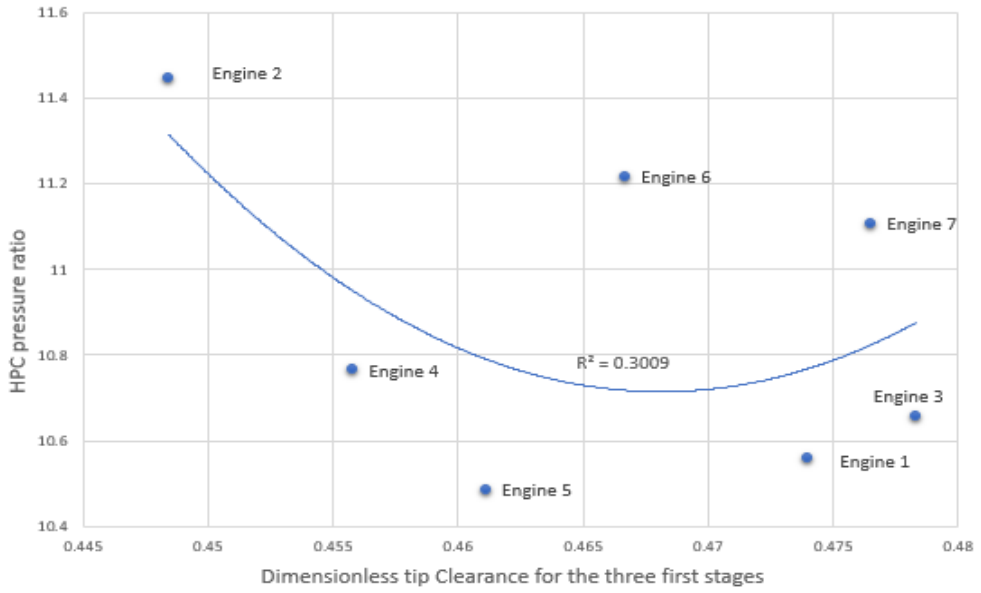

Figure C.4: Effect of the sum of the dimensionless tip clearance of the first three stages on the HPC pressure ratio

C.3 Tip clearance study - flow factor results

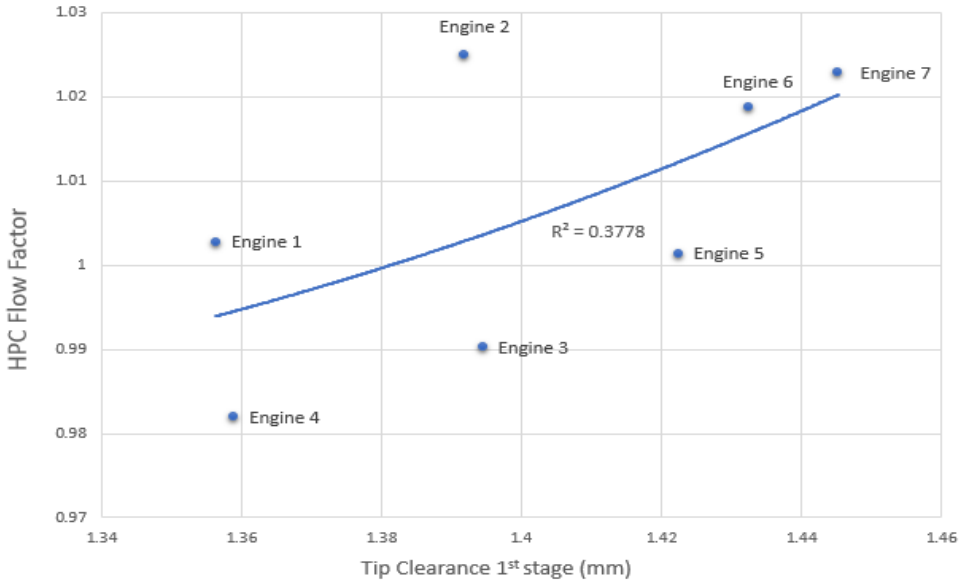

Figure C.5: Effect of the first stage tip clearance on HPC flow factor

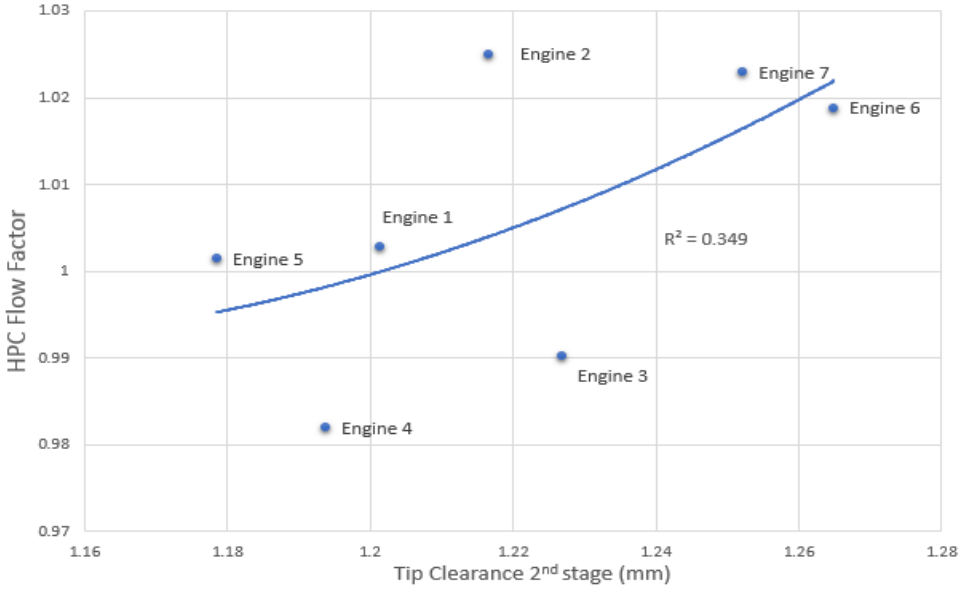

Figure C.6: Effect of the second stage tip clearance on HPC flow factor

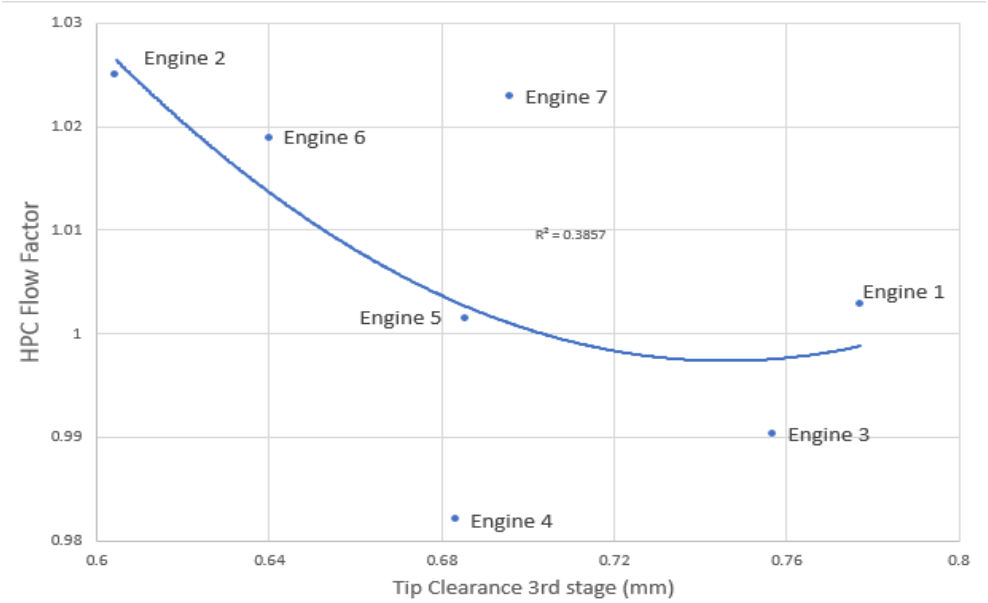

Figure C.7: Effect of the third stage tip clearance on HPC flow factor

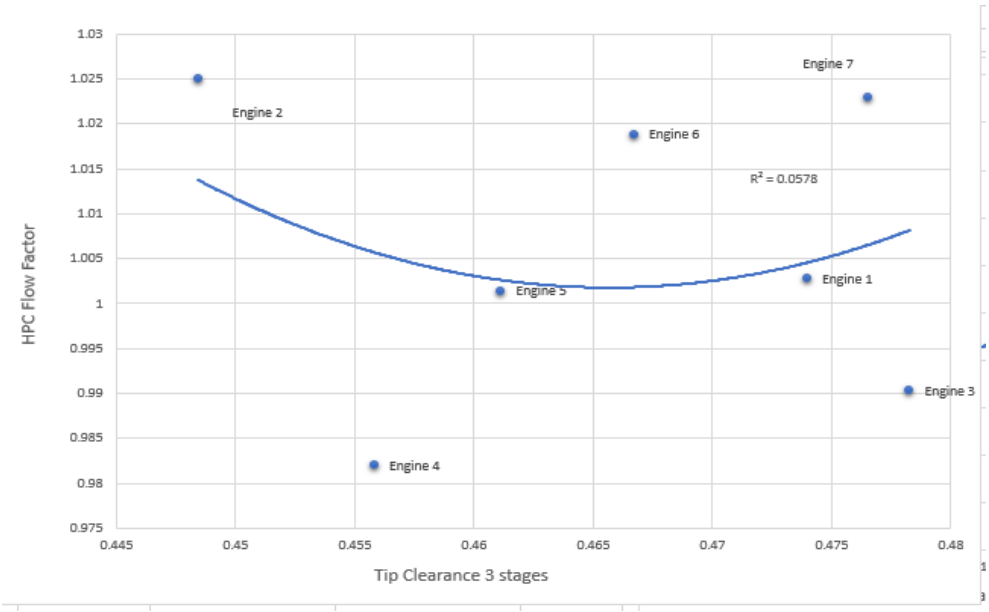

Figure C.8: Effect of the sum of the dimensionless tip clearance of the first three stages on the HPC flow factor

C.4 Sensor comparisons

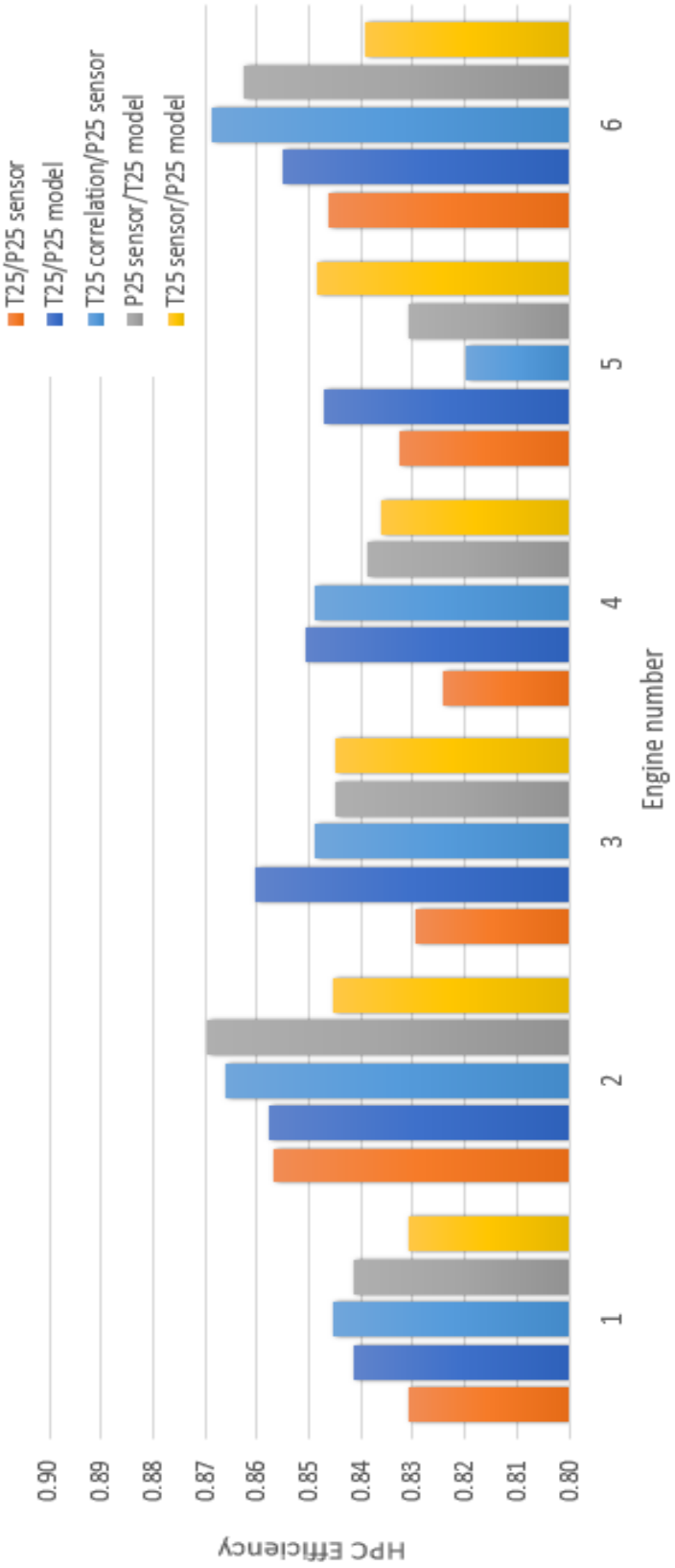

Figure C.9: Comparison of the HPC efficiency obtained in Gasturb™ for five different scenarios of the T_{25}/P_{25} sensor

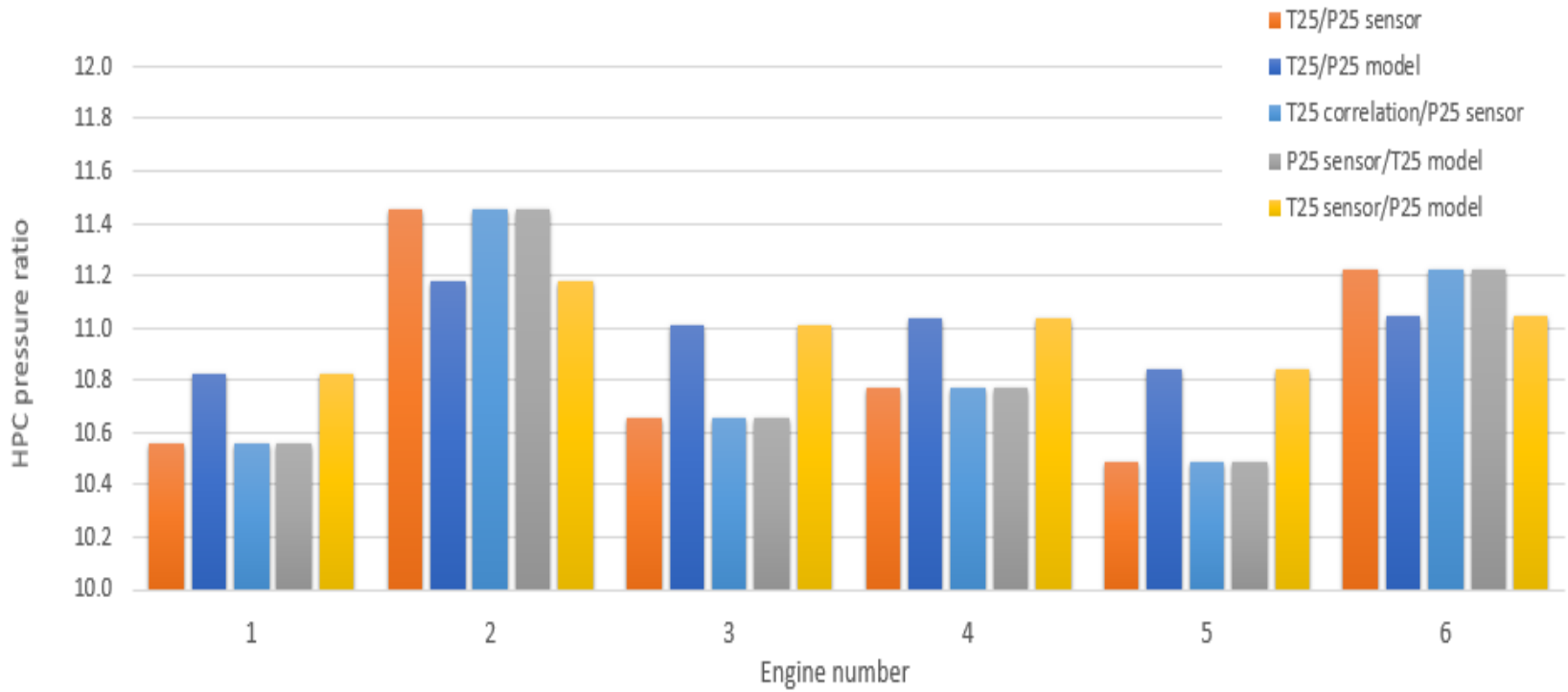

Figure C.10: Comparison of the HPC pressure ratio obtained in Gasturb™ for five different scenarios of the T_{25}/P_{25} sensor

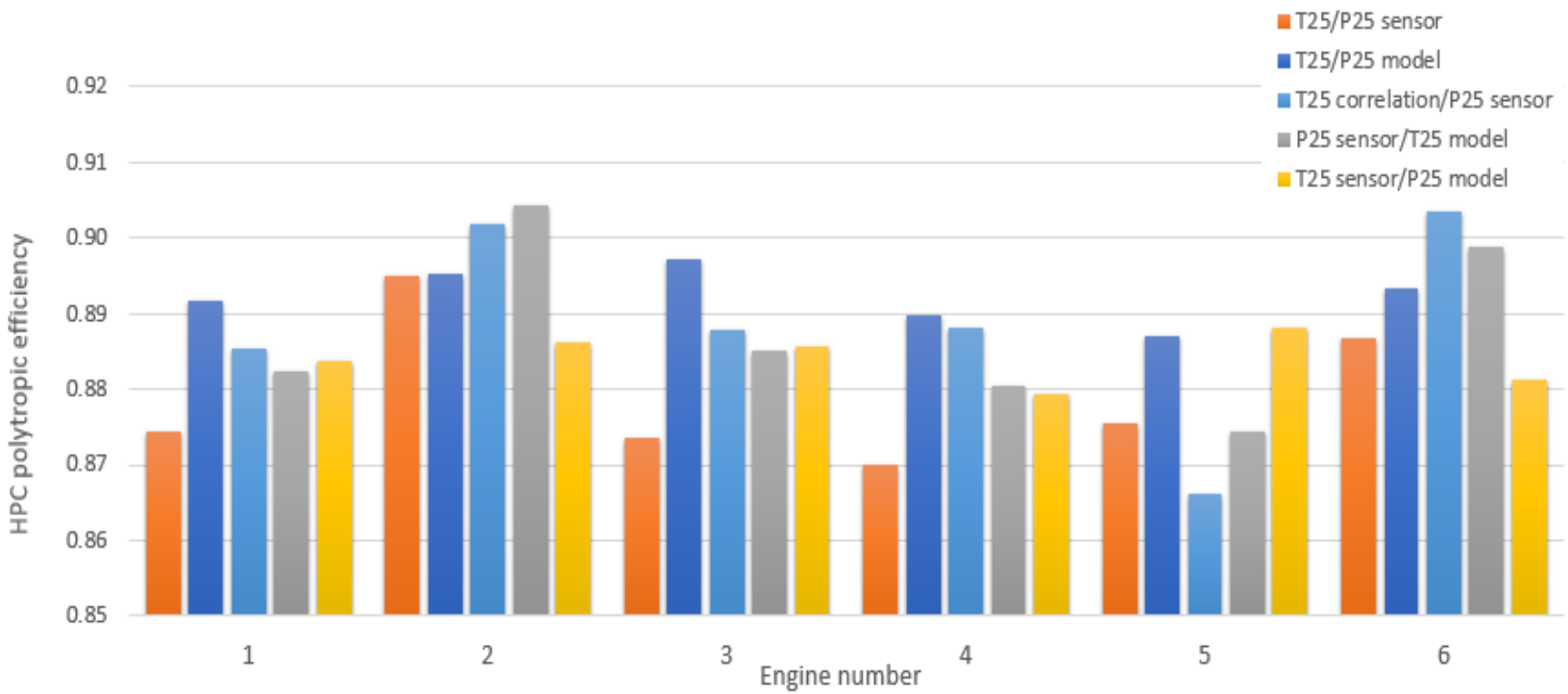

Figure C.11: Comparison of the HPC polytropic efficiency obtained in Gasturb™ for five different scenarios of the T_{25}/P_{25} sensor

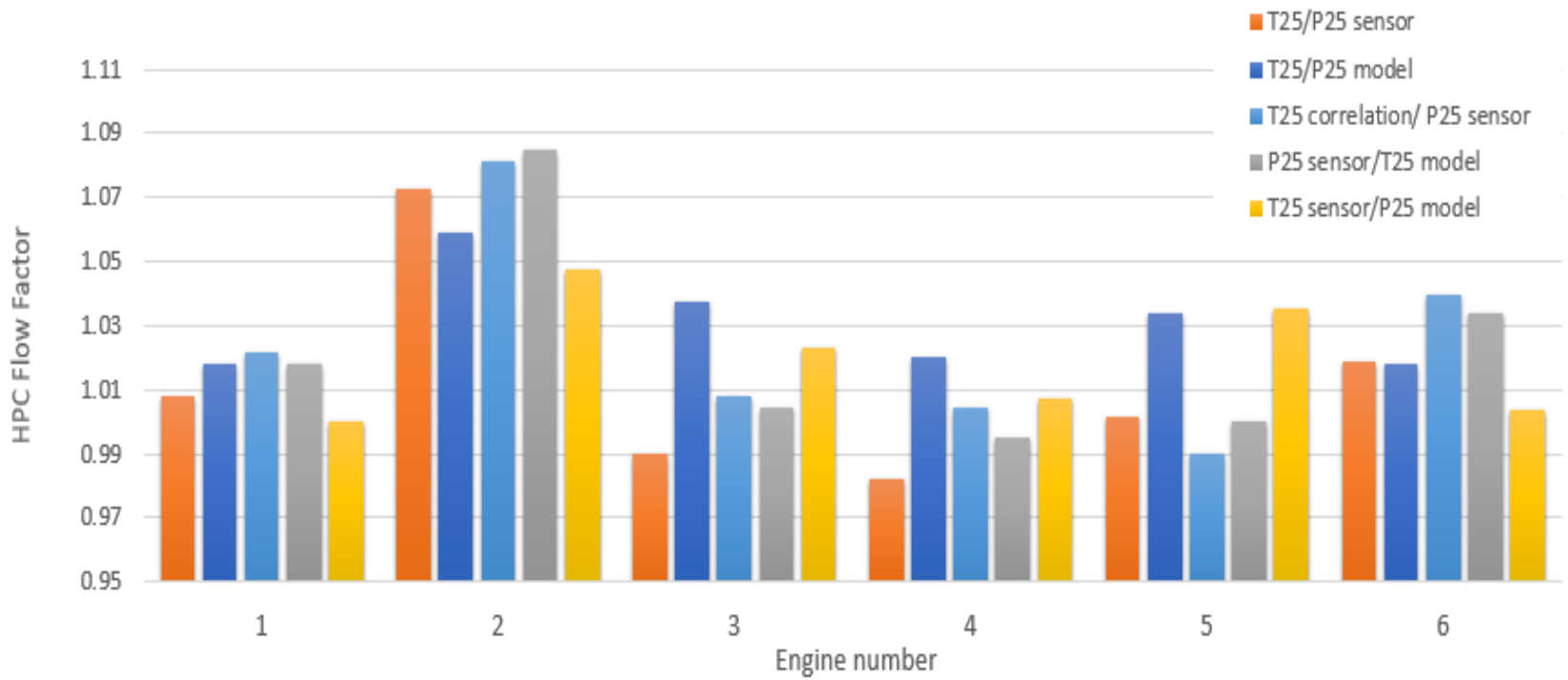

Figure C.12: Comparison of the HPC flowfactor obtained in Gasturb™ for five different scenarios of the T_{25}/P_{25} sensor